

Fractional Conductance in One-Dimensional Systems

by

Rose Davies



A thesis submitted to the
University of Birmingham
for the degree of
DOCTOR OF PHILOSOPHY

School of Physics and Astronomy
College of Engineering and Physical Sciences
University of Birmingham
September 14, 2022

ABSTRACT

This thesis analyses possible origins of fractional conductance in one-dimensional systems. Two complementary approaches that use continuum and finite techniques are presented. The continuum description investigates how Luttinger liquids can, through equilibration with the contacts or backscattering, produce conductance plateaus at fractions of e^2/h . The microscopic perspective uses Wigner chains to concretely understand how whole electrons can be changed into fractional excitations. When only the edges of the system are coupled to the reservoirs, the effect of the coupling can be explicitly solved. The spinful realisation of this model produces resonances with fractional peaks, due to the proportion of configurations that can conduct.

ACKNOWLEDGEMENTS

The acknowledgements section is one of the only places in physics that provides space to centre the sentimental, human contributions without which this thesis would not have been possible. Getting to the final stages of writing a doctoral thesis can only be attributed to the support of a wide-reaching network of colleagues, friends and family.

Firstly, I would like to thank my supervisors, Igor Lerner and Igor Yurkevich, without whom all of these pages would be blank! All the staff of the Birmingham Theory Group have also been invaluable in eventually teaching me to appreciate physics.

All the present and past postgraduate theory students have been consistently helpful with their insight - and patience with my endless questions - that have been vital to the development of this thesis. I would like to especially thank Jacob Spink, Ben McCanna, Manjinder Kainth, Chris Oliver, George McArdle, Dave Perkins, who created a welcoming community in what otherwise could have been a lonely experience.

There are many friends in Birmingham who have shown me that there is more to do here than just physics. To name just a few; Emin Veron, Emily Brereton, Luke Mullins, Emily Morris, Vanessa Gott, Anja Parkes, Emily Doyle, Beatrice Ridge. Without them, and other friends outside of Birmingham - especially Leyla Ury, James Patey, Andrew Reid, Rory Molloy - I would not be the person that I am finally proud of being. For all the support they know that they have given, and support they weren't aware that they were giving, I will always be thankful.

My parents have always given me the best possible chances of succeeding. The foundation that they, and my sisters, have provided is the basis of everything I am today.

Extra special thanks must go to Sophie Hack who helped me make the most of living in Birmingham. She has been a constant reassuring and encouraging presence throughout and I am continually thankful that she took a chance on living with a relative stranger four years ago.

Finally, the most important person to thank is my girlfriend Emma Hall. Another entire thesis could be written on how she has changed my life for the better. It is an honour to have been able to grow together for the past nine years and I could not ask for a more supportive friend and partner. That she has been dedicated enough to actually read every word in this thesis is testament to her boundless capacity to give.

To everyone who has supported me, mentioned or not, I can only hope that I have enriched your life a fraction of the amount you have enriched mine.

CONTENTS

1	Conductance in Ballistic Systems	1
1.1	Length Scales	3
1.2	Low-Dimensional Systems	5
1.3	Fractional Conductance	8
I	Mathematical Requirements	11
2	Quantum Field Theory	13
2.1	Pictures of Quantum Mechanics	14
2.1.1	Interaction Picture	16
2.2	Time Evolving Averages	17
2.2.1	Evolving Two-Point Functions	19
2.2.2	A Time-Ordered Theory	21
2.3	Finite Temperature - Time to Get Complex	22
2.4	Wick's Theorem	25
3	Keldysh Formalism	29
3.1	Keldysh Contour	30
3.1.1	Dyson's Equation	31
3.2	Real-time Expressions	33
3.2.1	Menagerie of Two-Point Functions	34
3.2.2	Langreth's Theorem	36

CONTENTS

3.3	Dyson's Equation Redux	37
4	Luttinger Liquids	39
4.1	One-Dimensional Idiosyncrasies	40
4.2	Tomonaga-Luttinger Model	42
4.3	Bosonisation	45
4.3.1	Including Interactions	48
4.4	Spinful Luttinger Liquids	50
5	Conductance Formalisms	55
5.1	Kubo	56
5.2	Landauer	58
5.2.1	Contact Resistance	63
5.3	Non-Equilibrium	64
5.3.1	Integrating Out Quadratic Fields	66
5.3.2	Real-Time Expression	68
II	Continuum	71
6	Conductance in Luttinger Liquids	73
6.1	Conductance of a Clean Single Channel Luttinger Liquid	74
6.1.1	Infinite Luttinger Liquids	74
6.1.2	Including Reservoirs	77
6.1.3	Equilibrating with Contacts	81
6.2	Impurities in Luttinger Liquids	85
6.3	Multi-channel Luttinger Liquids	88
6.3.1	Shavit and Oreg	90
6.3.2	Calculating the Conductivity	92
6.4	Solitons in Field Theory	95

III Finite	97
7 Wigner Chains	99
7.1 Spinless Model	100
7.1.1 Eigenstates	103
7.1.2 Attaching Contacts	111
7.1.3 Conductance	116
7.2 Spinful Generalisation	120
7.2.1 Eigenstates	121
7.2.2 Attaching Spinful Contacts	122
7.2.3 Conductance	124
7.3 Further Work and Conclusions	128
A Functionals	131
A.1 Functional Calculus	131
A.1.1 Functional Derivatives	131
A.1.2 Functional Gaussian Integration	132
A.1.3 Beyond Quadratic Functionals	135
A.2 Functional Integrals are Quantum Averages	136
A.2.1 Functional Integrals in Quantum Field Theory	137
B Dyson's Expansion	141
C Calculating the Jacobian	143
C.1 Loop Cancellation	144
C.2 The RPA Term	145
D Renormalisation Group	147
E RG Calculations	151
E.1 Weak Local Impurity	151

CONTENTS

E.2	Weak Link	154
E.3	Global Sine-Gordon	156
F	Finite calculations	157
F.1	Finding the $Q = -1/2$ Eigenstates	157
F.2	Green's Function Simplifications	159
References		160

LIST OF FIGURES

1.1	Creating a 2DEG and QPC in a GaAs/AlGaAs heterostructure	6
1.2	Quantisation of conductance in a quantum point contact	7
1.3	Conductance when varying the top gate of a quantum point contact	8
1.4	Fractional conductance in an asymmetrically confined quantum point contact	9
2.1	Time evolution of averages over one operator	18
2.2	Deforming two contours into one	20
2.3	Going from contour time to imaginary time ordering	24
3.1	Keldysh contour	31
4.1	Different values of the Luttinger parameter corresponding to different models	41
4.2	Linearising the Fermi gas dispersion	44
5.1	Partitioning of the system in the Landauer formalism	60
5.2	Channels becoming available to conduct upon decreasing the confinement	61
5.3	Setup of an N channel scattering problem	62
6.1	The spatial dependence of the Luttinger parameter	78
6.2	Types of contact in fractional quantum Hall measurements	82
6.3	RG flows of a single impurity in a Luttinger liquid	87
6.4	Momentum conserving backscattering processes	91
6.5	Conductance for gate voltage sweeps at different temperatures for time symmetric backscattering	95

LIST OF FIGURES

7.1	Demonstrating the difference between boundary conditions for a CDW model	102
7.2	Mapping a configuration of the $Q = 0$ filling to a soliton basis	105
7.3	Configurations in the $Q = -1/2$ subspace	106
7.4	Phase shifts of a $Q = -1/2$ configuration	106
7.5	Mapping to the soliton basis for $Q = -1/2$ configurations	107
7.6	Hopping of solitons between different $Q = -1/2$ configurations	108
7.7	The connection between the basis configurations	108
7.8	Eigenstates of the $Q = -1/2$ filling	110
7.9	The connection of a 1D Wigner chain to reservoirs either side.	112
7.10	Conductance of a 1D spinless chain at different reservoir potentials for different lengths	119
7.11	Calculating the matrix overlaps for \mathcal{G}_{N1} for a given spin configuration	126
7.12	The conductance of a spinful Wigner chain upon varying the chemical potential for a different lengths in the system.	128

CHAPTER 1

CONDUCTANCE IN BALLISTIC SYSTEMS

Modern technology has only been made possible by our understanding of how materials conduct electricity. Transistors have now been produced so abundantly that more transistors are estimated to have been made than there are cells in every living human on the planet [1, 2]. Recent advances of understanding in this field have allowed for increasingly fine control over the transport of electrons. One frontier of research that would improve the capabilities of current computing hardware is the development of devices that allow control over the transport of electron spins. The study of the multiple possible realisations of qubits, that are required for quantum computing, is another area that holds the potential to revolutionise modern technology. The understanding of many of these new devices is based on mesoscopic physics, which accounts for the wave-like nature of particles, and is the area that this thesis explores.

There are two common quantities that are used to encapsulate transport behaviour: the conductance and the conductivity. The conductance is the ratio of the voltage applied across a sample to the current that passes through it. If this varies in a non-linear way, $I(V)$, then the differential conductance is defined,

$$G = \frac{dI}{dV}. \quad (1.1)$$

This is not always the most useful quantity as it often dependent on the size of the sample.

The conductivity is defined to provide an intrinsic variable in common macroscopic applications. For a cross-sectional area A and length of wire L , the conductivity is,

$$\sigma = G \frac{L}{A}, \implies G = \sigma L^{d-2}, \quad (1.2)$$

for generic dimension d . Often the inverse of these quantities, the resistivity ρ and resistance R , are used instead.

This thesis investigates a bizarre phenomenon found when looking at the conductance in certain devices known as quantum point contacts (QPCs) which will be introduced shortly. To describe these experiments and why they are unusual, the transport regime in which the QPC exists needs to be understood. By considering the original model of transport, the reason for these different transport regimes can be seen. For an electron of mass m , charge e , and electron density n in a system, the Drude model produces a conductivity of,

$$\sigma = \frac{ne^2\tau}{m}, \quad (1.3)$$

which introduces the phenomenological scattering time τ that details the amount of disorder in a system. Mobility, μ , is often used to characterise this disorder and is given by $\sigma = en\mu$. This quantity relates the typical drift velocity of the electrons to the applied electric field that is driving the transport. Originally, this treatment considered electrons to be classical particles that elastically scatter off impurities. These impurities randomise the momentum of the electron, with the rate at which these collisions occur being τ^{-1} . Subsequent treatments have managed obtain this formula from both a quantum mechanical [3] and a field theoretical perspective [4] and surprisingly the same result is obtained.

A pertinent question to ask is what will happen as the scattering time increases to infinity and the electron does not scatter - does this cause an infinite conductance? This limit is equivalent to considering a smaller length of system such that the time taken for an electron to travel across the system is smaller than τ , defining the onset of the ballistic regime. It has only been possible to investigate this experimentally in the last 40 years, with the results showing that infinite

conductance is not found and the Drude result no longer holds.

1.1 Length Scales

The transport regime that describes a particular material is defined by the interplay of various length scales that are varied by either the material properties or by changing the applied conditions on the sample. The scales are; the mean free path L_τ , the localisation length l_ξ , the coherence length L_ϕ , system size L , and the Fermi wavelength λ_F [5]. The mean free path determines whether the transport is ballistic or diffusive. Ballistic transport occurs when $L \lesssim L_\tau$, corresponding to an electron traversing the system without scattering. As understood from solid state physics, particles at the Fermi surface are responsible for the transport properties of materials [3]. Therefore, the mean free path is,

$$L_\tau = v_F \tau, \quad (1.4)$$

where $v_F = \hbar k_F$ is the Fermi velocity. For a free electron gas in two dimensions, the relevance of which will be seen shortly, the Fermi wavevector is related to the density of electrons, $k_F = \sqrt[2]{4\pi n}$. The typical density of electrons in metals is $10^{22}/\text{cm}^3$, semiconductors have $10^{19}/\text{cm}^3$, while the quantum point contacts that will be examined have $10^{12}/\text{cm}^3$.

Another important factor is the extent to which the particles responsible for transport are discretised. For lengths below the Fermi wavelength, $\lambda_F = 2\pi/k_F$, the true wave-like nature of the electron is expressed. This length also defines the discreteness of the energy levels of the system, allowing for resonant and discrete behaviour.

The opposite limit to the ballistic regime is that of a ‘bad metal’, when the electron scatters so often it becomes comparable to the Fermi wavelength, $\lambda_F \ll L_\tau$. The criteria, $k_F L_\tau \gg 1$, is where the semiclassical Drude model works. Putting the expression for the Drude conductivity into this separation of length scales gives,

$$\rho \ll 200 \mu\Omega\text{cm} \times \lambda_F (\text{in \AA}). \quad (1.5)$$

This is known as the Ioffe-Regel-Mott criterion [6] which indicates the limits of applicability of the Drude formalism. For resistivities higher than this limit, which correspond to there being many scatterings, a new description is needed which considers the true wave-like nature of the electron.

Interference effects between two particles can still occur on sizes much larger than the Fermi wavelength as long as the phases of particles are related to each other. This stability of the relationship between the phases is the factor that determines whether transport is coherent or incoherent. The length over which they lose their relationship defines the phase breaking length L_ϕ . This scale is independent of the mean free path, as scattering elastically will shift the momentum of a path by a fixed amount, but there is still a definite relation between the two phases [7].

This phase decoherence can be caused by temperature fluctuations, magnetic impurities and electron-electron interactions. Any scattering that is time-dependent will change the phase by an indefinite amount due to the uncertainty in the point in time where the scattering occurred. The temperature fluctuations essentially broaden the quantum states of the system such that they can be excited between each other. When temperature is comparable to the energy spacing, the individuality of the excitations becomes muddled and the phase information is lost. Therefore increasing L_ϕ is often done by reducing the temperature of the system.

The final length of interest is the localisation length, l_ξ , which gives the length over which the wavefunctions of the single particle excitations decay. A large localisation length means the particle will not experience any localisation effects over the entire sample. This length is responsible for metals becoming insulators at low temperatures, when $l_\xi \ll L$. This regime is brought upon by large disorder, so l_ξ is related to L_τ though the precise functional relationship can vary. The coherent nature of the electrons means that incident waves can interfere with waves that are scattered backwards by an elastic collision, resulting in the electrons becoming localised around different lattice sites for a small mean free path.

The diffusive-incoherent classical Drude picture is relevant when the following hierarchy of length scales is found $\lambda_F, L_\phi \ll L_\tau \ll L \ll l_\xi$. Quantum corrections become important

when either λ_F or L_ϕ are comparable to L_τ . Strong localisation occurs when the localisation length is of the order of the mean free path and Fermi wavelength $\lambda_F \sim L_\tau \sim l_\xi \ll L$. The hopping current between these localised states can either be coherent or incoherent dependent on whether l_ξ or L_ϕ is larger [8].

Quantum point contacts exist in the ballistic-coherent transport regime where $L \lesssim L_\phi, L_\tau$. The field of mesoscopics occurs when one of the system lengths becomes comparable to L_ϕ , with a diffusive mesoscopic regime also being possible if $L_\tau \ll L \lesssim L_\phi$. This brief overview of the transport regimes serves as an introduction to the ideas of mesoscopic physics, and will help contextualise the central problems of this thesis. The variety exhibited in these systems is due to the many length scales, one of which must be of the size of the system. It is in the liminality between microscopics and macroscopics that the many of the novel material properties are found.

1.2 Low-Dimensional Systems

To access the ballistic-coherent regime, a system that is clean from impurities must be fabricated and measurements taken at low temperature. This purity is incredibly difficult to achieve. However, a way to reach this behaviour can be guaranteed in low-dimensional systems. Before eventually arriving at the experimental system, physics in low dimensions will first be explored.

In quantum mechanics, and in statistical mechanics, reducing the dimensionality of a system requires some way of freezing out certain degrees of freedom. This occurs when certain eigenstates are energetically inaccessible by temperature fluctuations. This can be done by considering the geometry of a wire where the length in two of the dimensions is a lot smaller than the other. Constricting the electrons by imposing an infinite potential outside the wire geometry leads to the eigenstates,

$$E_{(n_x, n_y, n_z)} = \frac{\pi^2 \hbar^2}{2m} \left(\frac{n_x^2}{d_x^2} + \frac{n_y^2}{d_y^2} + \frac{n_z^2}{d_z^2} \right), \quad (1.6)$$

for integers n_x, n_y, n_z , where m is the mass of the particle and d is the width of the constriction

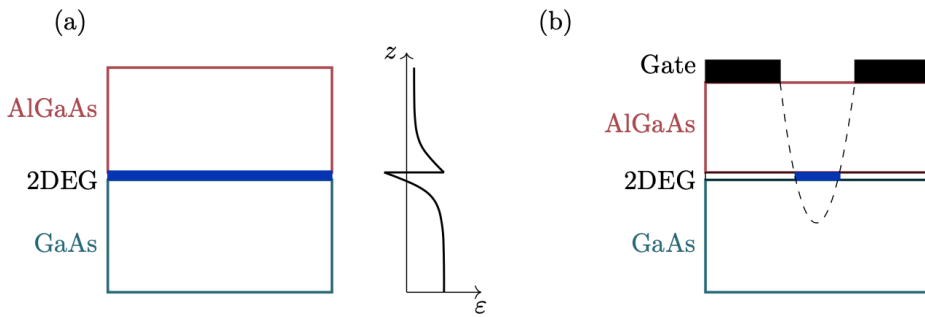


Figure 1.1: Both a QPC and a 2DEG are created near the interface between GaAs and AlGaAs¹. (a) The Fermi level changes in the z direction, with the bending of bands creating a triangular well. (b) Introducing gates on top of the sample allows a parabolic confining potential to constrict the 2DEG into a QPC.

in their respective direction. If d_y is small, then the energetic difference between the $n_y = 1$ and $n_y = 2$ states will be large and no transitions between the states will be possible if temperature is smaller than this gap. Confining electrons to two spatial dimensions creates a two-dimensional electron gas (2DEG).

Creating this infinite confining potential experimentally is difficult, but through some ingenious combination of materials, solid state physics can create one that mimics its effects. Grafting two specific materials together causes the conductance bands to bend in such a way to create a triangular well. This occurs when one of the materials has a larger Fermi level than the other, which then causes electrons to migrate to the lower Fermi energy and leave behind their associated positively charged ions. The build up of charge across the heterojunction prevents all the charges from flooding the lower Fermi energy [5]. This electrostatic field causes the local bending of the bands that form the well, which is shown in Figure 1.1(a).

The current materials of choice are a heterostructure of GaAs/AlGaAs [9], due to the large mobility $\mu = 31 \times 10^6 \text{ cm}^2/\text{Vs}$ possible in these systems [10]. This corresponds to $L_\tau \sim 100 \mu\text{m}$, encroaching upon more everyday length scales. Other methods of creating a 2DEG are possible, with many mesoscopic studies being originally performed on metal–oxide–semiconductor field-

¹The actual QPC used in experiments is more sophisticated than just two materials placed next to each other. In order to achieve the high mobility, there are different layers in the AlGaAs section, including regions of silicon or n-doping. This is to bend the band further upwards on the AlGaAs side to prevent tunnelling from out of the 2DEG. Other realisations use two layers of AlGaAs either side but this schematic understanding will suffice for theorists!

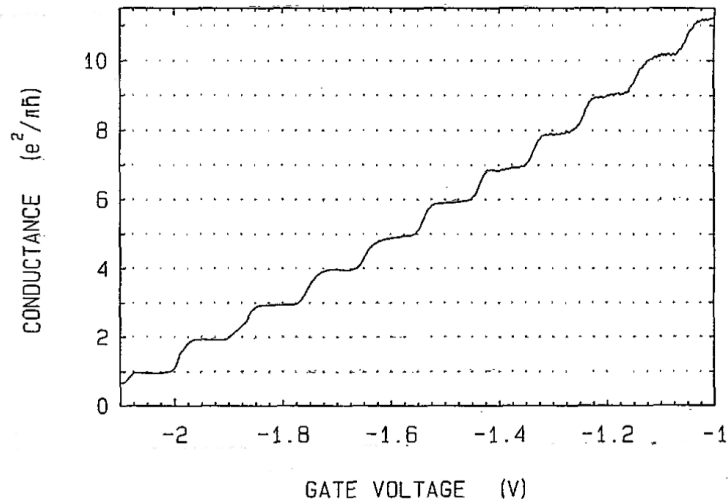


Figure 1.2: The conductance through a quantum point contact is measured against the charging on the side gates of the system. Reprinted from Reference 15.

effect transistor (MOSFET) devices [11]. Precise patterning of wires can allow even metals to access the mesoscopic regime [12], but to obtain the largest mean free paths the heterostructure is the best choice.

Having restricted one direction, the other can be constrained to obtain one-dimensional (1D) behaviour by introducing two contacts, called split gates, either side of the material that can be charged to produce an electrostatic field that will deplete the electrons in the 2DEG layer. The typical spacing of these gates is ~ 250 nm [13]. The squeezing from the side of the sample produces a parabolic potential with its minimum in the centre of the sample, restricting motion to 1D behaviour. This type of experimental system is the quantum point contact [14], with the placement of the gates shown in Figure 1.1 (b).

The transport properties of a QPC can be measured by applying a voltage to the source and drain connected either end of the sample which will cause a current to flow. This conductance can be measured against different chargings of the split gate. At a large negative voltage on the gates, the resulting potential will be strong enough to discourage any current from flowing. Reducing the voltage to zero will remove the restriction and result in two-dimensional behaviour again. Performing this experiment resulted in plateaus appearing at integer values of $2e^2/h$ [15], which has been shown in Figure 1.2. The full reason for this result will be explored in Section 5.2, but it is indicative of 1D physics occurring.

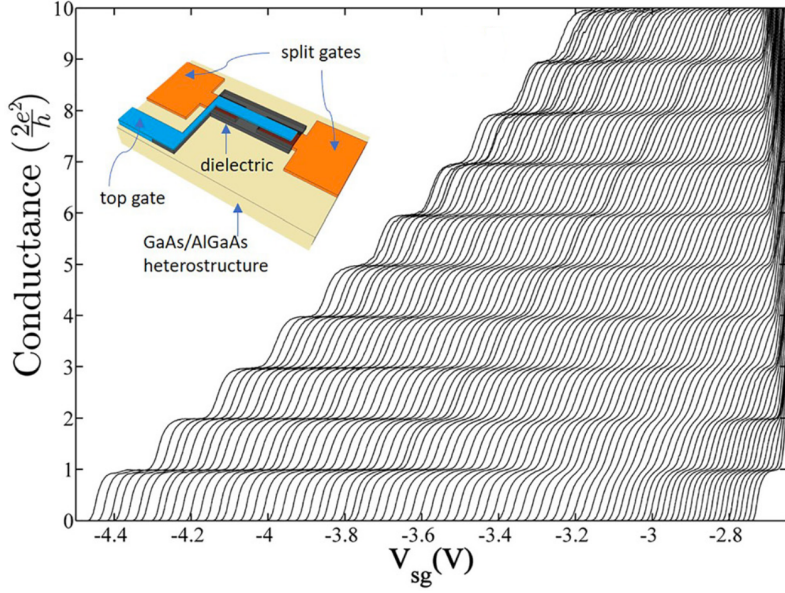


Figure 1.3: The conductance of a QPC against the confining split gate voltage is shown for different chargings of the top gate. The inset figure demonstrates the positioning of the various gates on the underlying heterostructure. Figure taken from Reference 17.

Further refinements of the QPC setup saw a top gate being added. This gate is placed on top of the entire heterostructure with a dielectric buffer, ensuring that the material of the gate does not interact with the confining potential in unintended ways. This allows fine control of the carrier concentration in the 2DEG which, when varied, reveals greater detail on conductance plots as shown in Figure 1.3. There is a small region at a split gate voltage of $V_{sg} = -3.2\text{V}$, in which the previous plateaus at $2e^2/h$ disappear and then reappear. It is in this specific point that the recent experiments have been performed. This region can also be created through asymmetrically biasing the split gates and creating an asymmetric confining potential [16].

1.3 Fractional Conductance

Plateaus are indicative of an underlying quantisation occurring. The previous plateaus occur due to each possible transport channel contributing the quantum of conductance, e^2/h . In Kumar *et al.* [18], multiple different plateaus were found at a plethora of fractional values of the quantum of conductance. Some of these are shown in Figure 1.4, and were expressed through varying

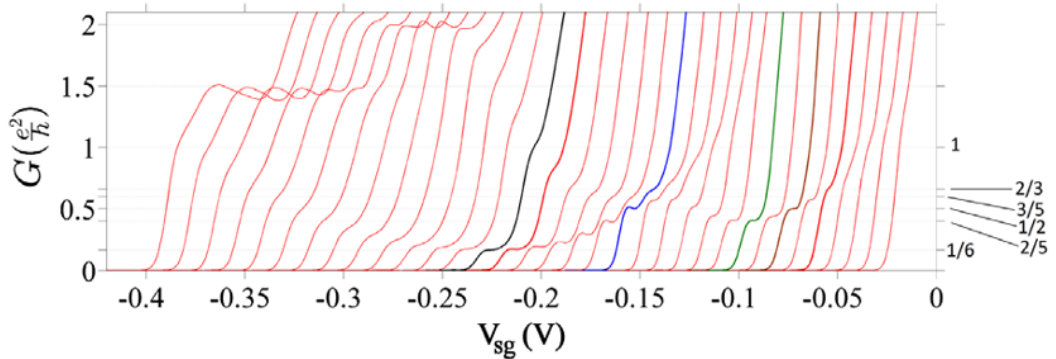


Figure 1.4: The values of the conductance sweeps in side gate potentials are plotted for increasing asymmetry of the confining potentials for each offset plot from left to right. Figure reprinted from Reference 18.

the asymmetry of the confinement.

The fact that plateaus are occurring at fractional values of fundamental constants suggests that somehow there is less charge associated with each transport channel - a fractionalisation of charge! The most prominent fractions occur at $2/5$, $1/2$, $1/6$ with no obvious relation between the fractions. Other similar transport experiments, in a two-dimensional hole gas instead, have seen different fractions [19], notably $1/2$, $1/16$.

These examples are not the first instances of such plateaus in transport measurements, which have also famously been seen to occur in the fractional quantum Hall effect [20]. This was also discovered experimentally in the 2DEG of the GaAs/AlGaAs heterostructure. For this experiment the sample was subjected to a large magnetic field, resulting in plateaus occurring in the Hall conductivity. Of the various plateaus found, the one that occurred at a value of $(1/3)e^2/h$ was explained due to the presence of an excitation that carries the charge of $e/3$ [21]. These Laughlin states apply for all odd denominator fractions that occur. Other fractions, notably $(5/2)e^2/h$, are a lot more subtle [22].

There is also precedent for conductance plateaus in the absence of a magnetic field, which can be seen in the left of Figure 1.4. This plateau around $(1.5)e^2/h$, is known as the 0.7 anomaly² which was observed in early experiments on the system [23]. This feature has been

²This mismatch of naming convention is due to including spin into the quantum of conductance so that it is $2e^2/h$. Even with the doubling, it still does not match, but this is because the value of the plateau can vary. The original experiments used a symmetric confinement to find the eponymous value.

the subject of numerous theoretical work and has many competing explanations.

In this thesis, models that produce fractional conductance in low-dimensional systems will be explored. As such, the thesis is split up into three parts. The first part introduces the multitude of theoretical techniques that are needed to tackle this problem. Chapters 2 and 3 introduce quantum field theory, and build up to the non-equilibrium description of the problem. Chapter 4 introduces Luttinger liquids which will form a basis in how to describe low-dimensional systems in a variety of different situations. Chapter 5 then introduces the techniques to extract the conductance of the system from the mathematical description.

Armed with this theoretical firepower, there will be two parallel developments, one from a continuum perspective and another from a finite perspective. These analyses are split into the final two parts. The continuum part concerns how Luttinger liquids can produce a fractional conductance, focusing on how a description of the contacts or backscattering in multi-channel systems form mechanisms by which a fractional conductance can be produced.

The finite section approaches the problem from a different viewpoint in order to concretely understand how whole particles can turn into fractional excitations. The solitons of a Wigner chain provide the perfect framework in which to see how this transformation occurs. It also results in a different mechanism for producing fractions, where the proportion of conducting configurations in comparison to total configurations controls the conductance. This final chapter contains the bulk of the original research in this thesis.

Part I

Mathematical Requirements

CHAPTER 2

QUANTUM FIELD THEORY

Introducing the ideas of quantum field theory (QFT) in a way that is self-contained is a challenging task: the multiplicity of the subject spills from the seams. For every class of models that can be solved, there are substantially more models that require radically different techniques to extract any information. Condensed matter contains this same multiplicity, with microscopic and phenomenological models inextricably tied together to both provide insight. Through all of these theories, there is a thread that ties them together - a Hamiltonian acting on a Hilbert space of states¹.

Observables are obtained through taking appropriately defined averages of operators and these observables encompass all the information that can be extracted from the theory. Obtaining a complete understanding of the states and averages - and how they evolve in time - is the goal of studying a model. Often this is only possible, however, where the model is so simplistic that it describes nothing! Therefore the techniques developed must be flexible enough to allow information to be extracted, even if a full description of the states is not available.

In this chapter the understanding of how these observables can be calculated will be developed, culminating in the contour-ordered Green's function. Familiarity with second quantised operators and their commutators will be assumed. For the start of this chapter, zero temperature QFT will be considered, where the average of an operator is given by the trace over the

¹High-energy physics does not often concern itself with finding eigenstates but they are still hidden beneath their fundamental Lagrangian approach. This diversity of approaches is precisely why an introduction is so difficult!

normalised eigenstates $|n\rangle$ of the underlying Hamiltonian,

$$\langle \hat{O} \rangle = \sum_n \langle n | \hat{O} | n \rangle.$$

The trace of an operator is independent of basis, so any suitable orthonormal set of states can be chosen. This schematic way of showing the average overlooks a crucial point - that the eigenstates and operators can have time dependence, resulting in a time-dependent observable. There are three common ways of including this dependence into quantum mechanics, which will be introduced in the next section.

2.1 Pictures of Quantum Mechanics

Offloading all of the time dependence onto the states, $|\psi(t)\rangle_S$, is known as the Schrödinger picture. The dynamics of the system are governed by the Schrödinger equation, where $\hbar = 1$, in which application of a time-independent Hamiltonian evolves the states in time,

$$i\partial_t |\psi(t)\rangle_S = \hat{H} |\psi(t)\rangle_S. \quad (2.1)$$

Any quantum state can be expressed in the basis of the eigenvectors of the Hamiltonian, which are stationary states and only change by a phase. This disentangles the matrix aspect of Equation 2.1 into multiple independent problems. The formal solution is the time evolution operator \hat{U} which connects states at different times,

$$|\psi(t)\rangle_S = \hat{U}(t, t_r) |\psi(t_r)\rangle, \quad \hat{U}(t, t_r) \equiv \exp\left\{-i\hat{H}(t - t_r)\right\}. \quad (2.2)$$

The S subscript is dropped for $|\psi(t_r)\rangle$ because this is a state at a given reference time t_r . The operator has the property that any evolution in time can be split up into successive evolutions, $\hat{U}(t_1, t_2)\hat{U}(t_2, t_3) = \hat{U}(t_1, t_3)$. Its conjugate evolves bra states $\langle\psi(t)| = \langle\psi(t')|\hat{U}^\dagger(t, t')$ in a similar way. Requiring that the states are normalised at all points in time means that the evolution must be unitary, and that the conjugate is the inverse of the evolution, $\hat{U}^\dagger(t, t') =$

$$\hat{U}^{-1}(t, t') = \hat{U}(t', t),$$

There is no inherent reason to consider states as the objects that evolve in time. An alternative picture emerges when considering matrix overlaps,

$$\langle \psi(t) | \hat{O} | \psi(t) \rangle_S = \langle \psi(t_r) | \hat{U}^\dagger(t, t_r) \hat{O} \hat{U}(t, t_r) | \psi(t_r) \rangle \equiv \langle \psi(t_r) | \hat{O}_H(t) | \psi(t_r) \rangle$$

where the time dependence can be shifted onto the operators rather than the states. This defines operators for the Heisenberg picture, $\hat{O}_H(t)$, that time evolve the state from the reference time, act with the Schrödinger operator at time t , then evolve back. The dynamics of the operator are described by the Heisenberg equation of motion,

$$\frac{d\hat{O}(t)}{dt} = -i[\hat{O}, \hat{H}(t)]. \quad (2.3)$$

Although this seems like a redundant change of emphasis, the apparatus of many-particle quantum mechanics is built from time-dependent creation and annihilation operators. These operators encode the statistics of the system much more naturally than explicitly considering the (anti)symmetrised state space for the Hilbert space of every particle number.

The time evolution operator can be generalised for a time-dependent Hamiltonian,

$$\hat{U}(t, t_r) = \mathcal{T} \exp \left(-i \int_{t_r}^t d\tau \hat{H}(\tau) \right), \quad (2.4)$$

where \mathcal{T} is the time ordering operator. It denotes that the string of operators within are ordered to have them act by whichever operator is earliest in time, the earliest put to the right. This can be explicitly formulated by using Heaviside functions $\Theta(x)$,

$$\mathcal{T}\{\hat{A}(t_1)\hat{B}(t_2)\} = \theta(t_1 - t_2)\hat{A}(t_1)\hat{B}(t_2) \pm \theta(t_2 - t_1)\hat{B}(t_2)\hat{A}(t_1), \quad (2.5)$$

where the \pm refers to the sign produced by the commutation relations of bosonic or fermionic operators.

Generalising this ordering to a string of n operators requires each of the $n!$ possible combinations of times to be enforced by increasingly intricate Heaviside functions. The derivation of Equation 2.4 is shown in Appendix B. The conjugate of $U(t, t_r)$ will be anti-time ordered, where the latest time operators act first by putting them at the right of the operator string. This is the first encounter with the time ordering operator which arises naturally from solving the Schrödinger equation for a time-dependent Hamiltonian. This ordering of operators turns out to be at the heart of QFT and the concept will be contorted into even more bizarre forms throughout this section.

There are two hurdles with calculating using this machinery built so far; the first is that to calculate anything, the full eigenstates are needed. This is not a simple task, even for a time-independent Hamiltonian. The second issue is that the average of multiple operators acting at different times will be described by a string of time evolution operators with different ordering rules. The aim is to find an ordering rule which applies to the whole expression, regardless of how many operators there are. The process of trying to accommodate for these two things will guide the following section.

2.1.1 Interaction Picture

When the eigenstates are not fully known, the interaction picture is the most convenient way to include the time dependence [24]. It is a halfway house between the previous two pictures, where the operators and states both evolve in time. This complexity appears to have neither benefit of the other pictures, but is crucial to building a robust theory.

The Hamiltonian is split up into two parts, one part for which the eigenstates are known and a second interacting part that depends on time, $\hat{H} = \hat{H}_0 + \hat{V}(t)$. This is the situation throughout physics where we often have an idea of what the rudimentary description should be, with complications being additionally included. This splitting of the Hamiltonian parameterises our ignorance of the full eigenstates into $\hat{V}(t)$.

Mathematically, the idea is to overcompensate in the time evolution of states by the time

evolution that is known. So defining

$$|\psi(t)\rangle_I = e^{i\hat{H}_0(t-t_r)} |\psi(t)\rangle_S, \quad (2.6)$$

and putting this into the Schrödinger equation results in,

$$i\partial_t |\psi(t)\rangle_I = e^{i\hat{H}_0(t-t_r)} \hat{V} e^{-i\hat{H}_0(t-t_r)} |\psi(t)\rangle_I \equiv \hat{V}_I(t) |\psi(t)\rangle_I. \quad (2.7)$$

This gives a new Schrödinger equation that defines a new time evolution operator $\hat{U}_I(t, t_r) = \mathcal{T} \exp(-i \int_{t_r}^t \hat{V}_I(t) dt)$. Ensuring that averages give the same result regardless of picture chosen, all operators must evolve like in the Heisenberg picture but with \hat{H}_0 instead of the full Hamiltonian

$$\hat{O}_I(t) = e^{i\hat{H}_0 t} O e^{-i\hat{H}_0 t}. \quad (2.8)$$

This completes the tour of the pictures of quantum mechanics, each with their merits. The Schrödinger picture often forms the easiest route into quantum mechanics - relying on a wavefunction that describes the system at any point in time, similar to a classical mechanics description but with a new probabilistic object. The Heisenberg representation leads much more naturally into the language of second quantised operators, but it is the interaction picture in which a rigorous perturbation theory can be formulated.

2.2 Time Evolving Averages

The next focus will be on how averages evolve in time which will be independent from the picture chosen. Writing out an average in every picture, where the hat notation of the operators is now dropped,

$$\begin{aligned} {}_S \langle \psi(t) | O_S | \psi(t) \rangle_S &= \langle \psi(t_r) | U^\dagger(t, t_r) O_S U(t, t_r) | \psi(t_r) \rangle =_I \langle \psi(t) | O_I(t) | \psi(t) \rangle_I \\ &= \langle \psi(t_r) | U_I^\dagger(t, t_r) O_I(t) U_I(t, t_r) | \psi(t_r) \rangle. \end{aligned} \quad (2.9)$$

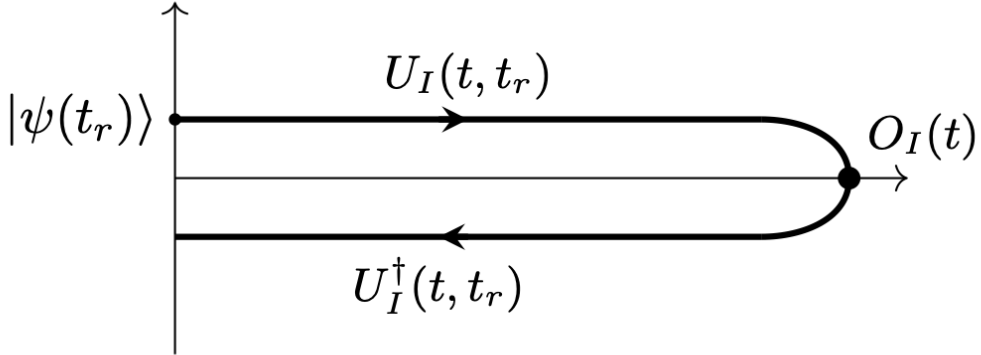


Figure 2.1: An average can be interpreted as evolving an underlying state up to where an operator acts on it and the state is then time evolved back with the inner product taken. The forward and backwards paths have been displaced in the y axis to show the two different directions.

Comparing terms, the full Heisenberg time evolution is related to the interacting time evolution by,

$$U(t, t_r) = e^{-iH_0(t-t_r)} U_I(t, t_r). \quad (2.10)$$

Equation 2.9 can be interpreted as beginning with the reference state and evolving it to time t using $U_I(t, t_r)$ as shown in Figure 2.1.

With this in mind, one of the goals of this section can now be completed for single operator averages. Instead of having time ordering evolving out to time t and anti-time ordering on the way back, all times could be described as existing on a contour in time [25]. Using τ to indicate that these times are now on the contour C of Figure 2.1, which extends from t_r to t and loops back round. This gives for an operator acting at a specific time t ,

$$O_H(t) = \mathcal{T}_C \{ e^{-i \int_C V_I(\tau) d\tau} O_I(t) \}. \quad (2.11)$$

The contour ordering operator, \mathcal{T}_C , orders all operators within to act first at the earliest time along the contour. It has the same form as time ordering but is only in reference to the parameter τ .

terised time on the contour rather than over the full range of time

$$\mathcal{T}_C\{A(\tau_1)B(\tau_2)\} = \theta(\tau_1 - \tau_2)A(\tau_1)B(\tau_2) \pm \theta(\tau_2 - \tau_1)B(\tau_2)A(\tau_1). \quad (2.12)$$

It should now be possible to understand why there was the goal of rewriting the problem in terms of one ordering rule. If there was a small parameter in the interacting part of the Hamiltonian, the exponential in Equation 2.11 can be expanded to give perturbative corrections. All of these corrections obey the same ordering rule so a robust perturbation theory can be formulated. Finding how to actually calculate these contour-ordered correction is examined next chapter. The important thing to see is that everything can be expressed in terms of the same type of object.

2.2.1 Evolving Two-Point Functions

From this point onward, the analysis will only becomes more complicated - as is natural for an introductory chapter. The natural progression is to consider how to express two operators acting at different times. From the previous section, each operator can be described in terms of a contour ordering

$$\begin{aligned} \langle A_H(t_1)B_H(t_2) \rangle &= \left\langle \mathcal{T}_{C_1}\{A(t_1)e^{-i \int_{C_1} d\tau V_I(\tau)}\} \mathcal{T}_{C_2}\{B(t_2)e^{-i \int_{C_2} d\tau V_I(\tau)}\} \right\rangle \\ &= \left\langle \mathcal{T}_{C'}\{A(t_1)B(t_2) \exp\left(-i \int_{C'} d\tau V_I(\tau)\right)\} \right\rangle, \end{aligned} \quad (2.13)$$

where C_1 is the contour of Figure 2.1 that evolves up to t_1 and C_2 evolves up to t_2 assuming that $t_1 > t_2$. This double-peaked contour can be deformed into just one, as shown in Figure 2.2. This can be seen within the maths by writing the ordering explicitly,

$$\langle A_H(t_1)B_H(t_2) \rangle = \langle U_I^\dagger(t_1, t_r) A_I(t_1) \underbrace{U_I(t_1, t_r)}_{U_I(t_1, t_2)U_I(t_2, t_r)} U_I^\dagger(t_2, t_r) B_I(t_2) U_I(t_2, t_r) \rangle. \quad (2.14)$$

The cancellation of the overlapping parts of the contour appears when the full evolution is

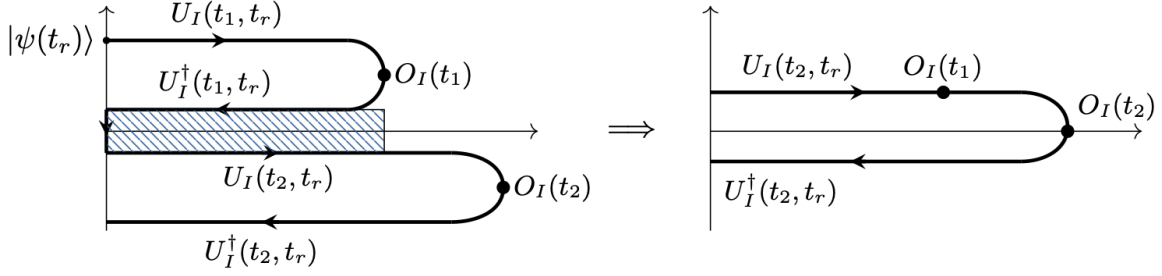


Figure 2.2: The evolution along a complicated double-peaked contour is equivalent to two operators acting on a single peaked contour. This figure demonstrates the case where $t_1 < t_2$, where the shaded box shows the two parts of the contours that cancel out.

split into two parts, which due to the unitarity of the operator cancels the the previous evolution. This overall contour can be therefore deformed to a single contour C' that goes from t_r to t_1 and back again with the operator B acting on the forward evolution branch. The opposite case of $t_1 < t_2$, when the order of operators stays the same, will have a contour that extends to t_2 and the operator A will act during the backwards evolution.

It turns out that although this procedure can be generalised to larger strings of operators, often all that is needed is the two-point averages due to Wick's theorem which will be covered shortly. The newly ordered Equation 2.13 not only describes $\langle A_H(t_1)B_H(t_2) \rangle$ when $t_1 > t_2$, but also $\langle B_H(t_2)A_H(t_1) \rangle$ for $t_1 < t_2$.

The bedrock of QFT, the Green's function, can now be defined. This is the average of a creation and annihilation field operator, with the appropriate bosonic (−) or fermionic (+) commutation relations between them,

$$[\psi(x, t), \psi^\dagger(x', t)]_\pm = \delta(x - x'). \quad (2.15)$$

The contour-ordered Green's function becomes,

$$\left\langle \mathcal{T}\{\psi_H(x, t)\psi_H^\dagger(x', t')\} \right\rangle = \left\langle \mathcal{T}_C\{\psi_I(x, t)\psi_I^\dagger(x', t')e^{-i\int_C d\tau V_I(\tau)}\} \right\rangle = iG_C(x, x'; t, t'). \quad (2.16)$$

It is worth recapping what has been achieved here. The appearance of all of these ordering

operators stems from the time evolution operator containing time ordering. The interaction picture is used due to the possibility of not knowing the full eigenstates. In trying to express the ordering as acting on all operators in the same fashion, contour ordering was introduced.

2.2.2 A Time-Ordered Theory

Having seen all these complicated things about time contours, it is natural to wonder why this rigorous of a treatment is not normally required. Time ordering by itself is actually sufficient for zero temperature QFT, but the full non-equilibrium nature to be explored in the next chapter necessitates this time-contour description.

Moving from contour ordering to time ordering, requires a way to relate the states at the reference time to a time beyond the contour. For averages at zero temperature, the system will always be in the ground state $|GS\rangle$, which may not be fully known. Knowing the evolution of the ground state along the time contour provides all the information required to compute averages.

The reason for switching into the interaction picture is to utilise the fact that there is a solution to a part of the problem, H_0 . It is only when introducing the interaction $V(t)$, that the exact ground state is not known. If there was a time that $V(t^*) = 0$, then there is a complete description of the state at that time. Therefore, consider a system that slowly turns on and off the interacting part [24], such that

$$V(t) = e^{-\epsilon|t|}\tilde{V}(t). \quad (2.17)$$

Changing the value of ϵ allows control over how fast or slow the interactions are turned on. The limit that $\epsilon \rightarrow 0$ corresponds to adiabatically switching on the interactions, where the slow change means that the system will always be in the same ground state. Providing that there are no crossings of energy levels or a phase transition as the interactions are varied, then the Gell-Mann and Low theorem [26] relates the ground states at the different asymptotic times. All the caveats are included simply to ensure that the ground state remains the same ground state after

the infinite time evolution.

The theorem states that the ground state after turning the interactions off at $t = \infty$ is related to the original ground state by a phase, $\langle GS(t = \infty) | GS(t = -\infty) \rangle = e^{i\phi}$. This is proven by expanding the time evolution operator for this specific form of interaction.

By extending the time contour beyond $\max(t_1, t_2)$, using the cancellation from Section 2.2.1, the contour can now stretch from $t = -\infty$ to $t = \infty$ and back again. This contour will have both operators occurring on the section that goes forward in time. The ordered average can be split into a part that orders everything in real time and a final evolution back, $\langle U^\dagger(\infty, -\infty) \mathcal{T}\{A_I(t_1)B_I(t_2)U_I(\infty, -\infty)\} \rangle$. The final evolution back is exactly the phase factor which can be cancelled out by introducing a denominator. Contour ordering only along the forward contour is equivalent to normal time ordering. Therefore the contour average of two operators becomes,

$$\begin{aligned} & \left\langle \mathcal{T}\{\hat{A}_H(t_1)\hat{B}_H(t_2)\} \right\rangle \tag{2.18} \\ &= \frac{\langle GS(t = -\infty) | \mathcal{T}\{A_I(t_1)B_I(t_2) \exp\left(-i \int_{-\infty}^{\infty} dt V_I(t)\right)\} | GS(t = -\infty) \rangle}{\langle GS(t = -\infty) | \mathcal{T} \exp\left(-i \int_{-\infty}^{\infty} dt V_I(t)\right) | GS(t = -\infty) \rangle}. \end{aligned}$$

When time is treated as a real time, instead of the contour-ordered time, a Fourier transform to frequency space can be performed to diagonalise the expression. Often systems have time translational invariance so the two-point average will often depend on $t_1 - t_2$ (which is shown using the cyclic nature of the trace) resulting in only one frequency variable.

2.3 Finite Temperature - Time to Get Complex

The effect of finite temperature is to weight each eigenstate in an average by the Boltzmann factor $e^{-\beta\varepsilon_n}$ for the inverse temperature β . Allowing for variation in particle number is achieved by introducing chemical potential μ and weighting the eigenstates with N particles by $e^{\beta\mu N}$.

The total average schematically then becomes

$$\langle \hat{A}\hat{B} \rangle = \frac{1}{\mathcal{Z}} \sum_n \langle n | \hat{A}\hat{B} e^{-\beta(\hat{H}-\mu\hat{N})} | n \rangle,$$

where the partition function $\mathcal{Z} = \sum_n \langle n | e^{-\beta(\hat{H}-\mu\hat{N})} | n \rangle$ normalises the average and \hat{N} is the number operator. The sum over eigenstates now includes all states with all possible number of particles in those states.

If the operators were time-ordered, it strongly resembles the previous formulation. The main difference is that to obtain the Boltzmann weighting rather than Equation 2.13, time evolution would have to evolve in imaginary time. Writing the factor as $\exp\left(i \int_0^{i\beta} dt(H - \mu N)\right)$, makes this connection explicit. But what does it mean for operators that are defined in real time to be evolving through imaginary time? This question is answered by changing our entire description to be in terms of imaginary time.

Performing a Wick rotation [24] into imaginary time will cause $t \rightarrow i\tau$ for all instances of time. This technique works best for time-independent Hamiltonians, so this form will be assumed for the rest of this section. The Heisenberg time dependence of the operators then becomes,

$$O_H(\tau) = e^{H\tau} O e^{-H\tau}, \quad (2.19)$$

where the reference point is taken as $\tau_r = 0$. Having done this, an analogous interaction picture in imaginary time can be defined relating the time evolution operators in these two pictures

$$e^{-H\tau} = e^{H_0\tau} \mathcal{T}_{C^*} \exp\left(- \int_0^\tau V_I(\tau') d\tau'\right) \quad (2.20)$$

where the contour time ordering now is for imaginary times, denoted by C^* . All the ideas of this chapter can be used again to express the average of two operators,

$$e^{-\beta H} \mathcal{T}_{C^*} \{ A_H(\tau_1) B_H(\tau_2) \} = e^{-\beta H} \mathcal{T}_{C^*} \{ A_I(\tau_1) B_I(\tau_2) \} \exp\left(- \int_{C^*} V(\tau') d\tau'\right). \quad (2.21)$$

Splitting up $e^{-\beta H}$ as in Equation 2.20 reveals a final forward evolution and an remaining

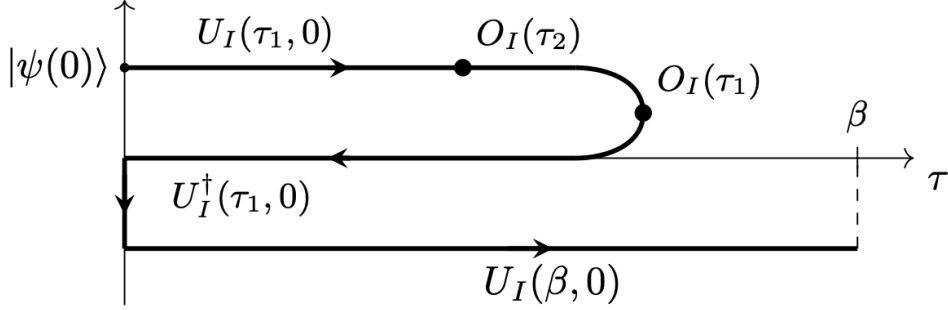


Figure 2.3: The contour followed in imaginary time by the time evolution of the operator $e^{-\beta H} O_I(\tau_1) O_I(\tau_2) |\psi(0)\rangle$ in the case that $\tau_1 > \tau_2$. The contour could be deformed to give just a single line by cancelling the inverse evolution of $U_I^\dagger(\tau_1, 0)$ with the part of $U_I(\beta, 0)$ that goes between 0 and τ_1 .

factor of $e^{-\beta \hat{H}_0}$. This contour is shown in Figure 2.3, and can be deformed into just a single line. The time ordering on this line results in normal time ordering but in imaginary time. Our final expression is therefore,

$$\begin{aligned} & \langle \mathcal{T}_C \{A_H(\tau_1) B_H(\tau_2)\} \rangle \tag{2.22} \\ &= \frac{1}{Z} \sum_n \langle n(\tau = 0) | e^{-\beta H_0} \mathcal{T} \{A_I(\tau_1) B_I(\tau_2) \exp \left(\int_0^\beta V(\tau) d\tau \right) \} | n(\tau = 0) \rangle. \end{aligned}$$

The weighting of the eigenstates is now with respect to the quadratic part of the Hamiltonian, which should be possible to calculate. In order for the averages to not diverge, $\tau_1 - \tau_2 < \beta$. Everything is still in imaginary time though, so the final part is to analytically continue from imaginary time back to real time.

This continuation procedure can be more clearly seen for the imaginary time Green's function, where the two operators of Equation 2.22 are the creation and annihilation field operators seen in Equation 2.16. The spatial index is not affected by switching to imaginary time so can be safely ignored. If the Hamiltonian is time-independent, the Green's function only depends on the difference $\tau \equiv \tau_1 - \tau_2$. Now a curious periodicity in imaginary time appears, with the Green's function being periodic at $\tau = 0, \beta$ if the field operators are bosonic. A fermionic Green's function produces an anti-periodicity at these same points.

This permits a transformation to a Fourier series in terms of the Matsubara frequencies, which have a different form for fermions and bosons

$$\omega_n = \begin{cases} 2\pi n\beta & \text{for bosons} \\ 2\pi\beta(n + \frac{1}{2}) & \text{for fermions} \end{cases}, \quad \text{where } n \in \mathbb{N}. \quad (2.23)$$

In the low temperature limit, the replacement of $\omega_n \rightarrow i\omega$ takes the problem back to real time. If the Green's function has poles or branch cuts in the complex plane, a more complicated continuation may be necessary.

2.4 Wick's Theorem

Returning to the question of why two-point averages can form a basis for an entire theory; this is due to Wick's theorem. It states that the average of a string of contour-ordered creation and annihilation operators with respect to a quadratic Hamiltonian is equal to the sum of the products of the average of only two of these operators² That is to say, for a generic operator c ,

$$\langle \mathcal{T}_C\{c(\tau_n) \cdots c(\tau_1)\} \rangle_{H_0} = \sum_{\text{Pairs}} \prod_{q,q'} \langle \mathcal{T}_C\{c(\tau_q)c(\tau_{q'})\} \rangle_{H_0}, \quad (2.24)$$

where H_0 is there to indicate that these averages are taking place with respect to a quadratic Hamiltonian where the eigenstates are known.

As an example of the pairing, consider the average of a four-point function of bosonic operators, $b(t)$. Bosonic operators are chosen to avoid signs arising when operators are commuted through. The contour ordering and quadratic Hamiltonian notation is dropped here for clarity of the pairing process. The pairing then proceeds in the following way,

²This is true for any of the contours dealt with in the previous section.

$$\langle b^\dagger(t_1)b(t_2)b^\dagger(t_3)b(t_4) \rangle = \langle b^\dagger(t_1)b(t_2) \rangle \langle b^\dagger(t_3)b(t_4) \rangle$$

$$\langle b^\dagger(t_1)b(t_2)b^\dagger(t_3)b(t_4) \rangle = \langle b^\dagger(t_1)b(t_4) \rangle \langle b(t_2)b^\dagger(t_3) \rangle$$

$$\langle b^\dagger(t_1)b(t_2)b^\dagger(t_3)b(t_4) \rangle = \langle b^\dagger(t_1)b^\dagger(t_3) \rangle \langle b(t_2)b(t_4) \rangle$$

To reiterate, each pair of operators in the original expression produces a two-point average that is multiplied into all of the other averages from the pairings for a given configuration. Summing over all configurations gives the full answer, which in this case will be just the sum of these three terms,

$$\begin{aligned} \langle b^\dagger(t_1)b(t_2)b^\dagger(t_3)b(t_4) \rangle &= \langle b^\dagger(t_1)b(t_2) \rangle \langle b^\dagger(t_3)b(t_4) \rangle + \langle b^\dagger(t_1)b(t_4) \rangle \langle b(t_2)b^\dagger(t_3) \rangle \\ &\quad + \langle b^\dagger(t_1)b^\dagger(t_3) \rangle \langle b(t_2)b(t_4) \rangle. \end{aligned} \quad (2.25)$$

Often some of the resulting averages can be ignored. Averages with two annihilation operators will not have any matrix elements connecting them in a quadratic Hamiltonian, so the final term can be set to zero. This is unless the system is superconducting. Wick's theorem will not be proved here as the proof for contour ordering is quite involved [25]. In many places this theorem is shown for time ordering by swapping to normal ordering - where annihilation operators act first [27]. Functional integrals, introduced in Appendix A, also form another path to showing this result.

This chapter has introduced the idea of expressing operators in terms of a contour-ordered interaction picture. This is the most general form of the problem that is designed to deal with models when the eigenstates are not exactly known. Wick's theorem gives a procedure whereby

which larger strings of contour-ordered operators can be ground up into smaller expressions. The detour to relate this contour ordering to the time ordering of zero and finite temperature equilibrium QFT highlights that all techniques here apply equally. It is going from the contour to real time where the difference between the methods appears.

CHAPTER 3

KELDYSH FORMALISM

The tautology of defining non-equilibrium as not being in equilibrium can be made clearer by exploring the conditions that define an equilibrium system [28]. An equilibrium system is described by a unique set of intensive and extensive macroscopic variables that are time independent. Additionally, these variables must not change upon isolating the system from its environment.

Transport experiments present a natural reason to consider non-equilibrium. This is because the experimental realisation consists of measuring current by applying a voltage across the entire sample. When this voltage is applied, the system will have a constant density distribution but isolating the system will cause the density to relax back to the equilibrium Gibbs distribution. The class of systems that have variables that are time-independent apart from when isolated from its surroundings are known as steady states.

Non-equilibrium theories have been the focus of many different sub-disciplines in physics with each discipline requiring different modifications to their underlying theories. The extension of quantum field theory to its full non-equilibrium splendour is encapsulated by the Keldysh formalism. The idea of contour ordering is the nexus of this formalism and additional matrix structure will appear when going back to real time. This matrix structure is what captures the non-equilibrium effects. The advantages of Keldysh above the purely imaginary time Matsubara Green's functions is that time-dependence can be more easily incorporated and the

assumption of the form of distribution (i.e. Fermi-Dirac or Bose-Einstien) is not made.

3.1 Keldysh Contour

The contour-ordered Green's function [29], is written explicitly as

$$G^C(x, t, x', t') = i \frac{\sum_n \langle n(t_r) | \mathcal{T}_K \{ \psi_I(x, t) \psi_I^\dagger(x', t') \exp(-i \int_K V_I(\tau) d\tau) e^{-\beta H_0} \} | n(t_r) \rangle}{\sum_n \langle n(t_r) | \mathcal{T}_K \{ \exp(-i \int_K V_I(\tau) d\tau) e^{-\beta H_0} \} | n(t_r) \rangle}, \quad (3.1)$$

where $\psi_I(x, \tau)$ is a bosonic or fermionic field operator which obeys the canonical commutation relations. The averages are over the eigenstates at the reference time, when there is a full description of the states. The integral over τ is along the Keldysh contour in complex time which is depicted in Figure 3.1 and the ordering \mathcal{T}_K is along this contour.

The contour stretches from our reference time and extends out to infinity, then returns back to our reference time. This forwards and backwards evolution is normally distinguished by the forward branch being offset by $+i\eta$ into imaginary time and $-i\eta$ on the way back. Finally the contour travels along the ‘interaction’ part which extends down to $-i\beta$, including the effects of the temperature like in the Matsubara technique, but without using a Wick rotation. Often the complex part of the contour can be ignored, which reduces down to the contour of the previous chapter. This can be done by taking t_r to be $-\infty$ then the final evolution on the interacting part of the contour will be at $-i \int_{-\infty}^{-\infty-i\beta} V_I(\tau) d\tau$ which will decay rapidly upon going into the complex plane.

The ability to set the reference time to negative infinity is a statement on initial correlations. If the final state is independent of the initial conditions, then any residual correlations must have decayed away. Evolving the state from negative infinity will ensure that the internal scattering time of the interactions will have been exceeded multiple times, washing out any memory of the initial conditions. These assumptions are natural for a steady state solution! The previous section showed how the form of Equation 3.1 was obtained, but now the way that it is used to solve problems will be explored.

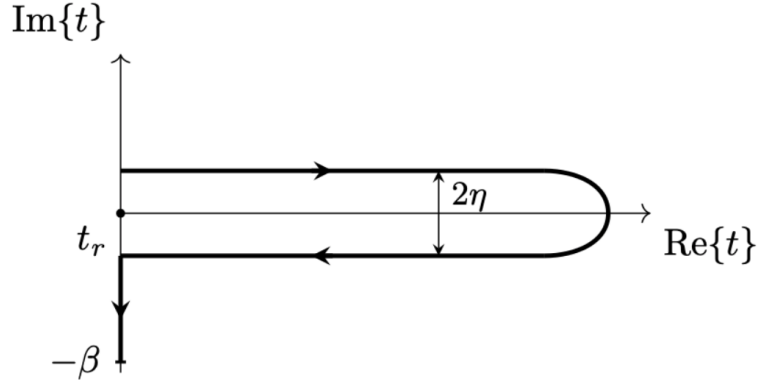


Figure 3.1: The contour through imaginary time, on which the time ordering of Keldysh non-equilibrium technique takes place.

3.1.1 Dyson's Equation

As an instructive example, the interaction part of the Hamiltonian is chosen to be a weak coupling to a classical field $H = H_0 + \lambda \int dx A(x, \tau) \psi^\dagger(x, \tau) \psi(x, \tau)$. The interaction picture will have field operators evolving as $\psi_I(x, \tau) = e^{iH_0(\tau-t_r)} \psi(x) e^{-iH_0(\tau-t_r)}$ and the contour-ordered Green's function, upon expanding the exponential, will be

$$G_C(x, t, x', t') = -i \text{Tr} \left(\mathcal{T}_K \left\{ \psi_I(x, t) \psi_I^\dagger(x', t') \right. \right. \\ \times \left[1 - i\lambda \int_K d\tau_1 \int dx_1 A(x, \tau) \psi_I^\dagger(x_1, \tau_1) \psi_I(x_1, \tau_1) + O(\lambda^2) \right] \left. \right\} \left. \right)_{H_0}. \quad (3.2)$$

The denominator in the original equation can be ignored as without any external operators, evolving the exponential along the forwards and backward part will exactly cancel out with a generic result of Keldysh being that the normalisation in the denominator is equal to 1. Wick's theorem can be applied to the term that is linear in λ , resulting in,

$$G_C(x, t, x', t') = -i \text{Tr} \left(\mathcal{T}_K \left\{ \psi_I(x, t) \psi_I^\dagger(x', t') \right\} \right)_{H_0} \\ - i\lambda \int_K dt \int dx_1 \text{Tr} \left(\mathcal{T}_K \left\{ \psi_I(x, t) \psi_I^\dagger(x_1, \tau_1) \right\} \right)_{H_0} V(x_1, \tau_1) \text{Tr} \left(\mathcal{T}_K \left\{ \psi_I(x_1, \tau_1) \psi_I^\dagger(x', t') \right\} \right)_{H_0}. \quad (3.3)$$

The other possible term allowed from pairing, $\langle \psi(x, t) \psi^\dagger(x', t') \rangle \langle \psi_I^\dagger(x_1, \tau_1) \psi_I(x_1, \tau_1) \rangle$, is

cancelled out by evolving it along the Keldysh contour. This is because one of the averages contains only points along the contour (x_1, τ_1) , without any external operators (x, t) . Without external input, evolution along the Keldysh contour is identically zero. This is the cancellation of vacuum diagrams of equilibrium theory that manifests here in a new way due to setting the denominator to be unity earlier.

Simplifying Notation

Before continuing further, the notation will be condensed as it is unwieldy. The way to multiply Green's functions together to produce another Green's function is by integrating over shared internal variables,

$$A(x, t, x'', t'') = \int dx' dt' B(x, t, x', t') C(x', t', x'', t'') \equiv B(x, t, x', t') \circ C(x', t', x'', t''), \quad (3.4)$$

where this operation is not commutative. Inverses are defined as

$$G^{-1}(x, t, x', t') \circ G(x', t', x'', t'') = \delta(x - x'')\delta(t - t''). \quad (3.5)$$

Introducing the bare Green's function as the average with respect to the quadratic Hamiltonian $G_0(x, \tau, x', \tau') = -i \text{Tr} \left(\mathcal{T}_K \{ \psi_I(x, \tau) \psi_I^\dagger(x', \tau') \} \right)_{H_0}$, the second term in Equation 3.3 becomes $G_0 \circ \tilde{V} \circ G_0$ which defines $\tilde{V}(x, t, x', t') = \delta(x - x')\delta(t - t')\lambda V(x, t)$. This procedure can be iterated to obtain higher and higher orders of perturbation and we can describe this pictorially as an infinite sum of terms. The Green's function can be expressed as an infinite sum of bare Green's functions, which can be expressed iteratively. Suppressing the variables,

$$\begin{aligned} G_C &= G_0 + G_0 \circ \tilde{V} \circ G_0 + G_0 \circ \tilde{V} \circ G_0 \circ \tilde{V} \circ G_0 + \dots \\ G_C &= G_0 + G_0 \circ \tilde{V} \circ G_C, \end{aligned} \quad (3.6)$$

$$\implies G_C^{-1} = G_0^{-1} + \tilde{V}. \quad (3.7)$$

These ideas can be generalised for interactions that are more complicated than just the cou-

pling to a classical field. The expansion of the operator and use of Wick's theorem proceeds in the same way, however many more types of terms are produced. Keeping track of these terms via assigning a diagram to them is the ubiquitous Feynman diagram technique [25], which will not be used extensively in this thesis. The combinatorial process is the same in the equilibrium and non-equilibrium cases due to the equivalence between the ordering rules, therefore all knowledge of equilibrium perturbation theory can be imported into this formalism.

Writing these more complicated terms in the form of 3.6 is possible, and introduces the self-energy Σ which replaces \tilde{V} ,

$$G_C = G_0 + G_0 \circ \Sigma \circ G_C. \quad (3.8)$$

Theoretically Σ can contain an infinite number of terms, but this specificity is not useful. Approximations are therefore usually made to exclude certain types of diagrams that arise in the full perturbative treatment. Self-energy is incredibly useful and encapsulates how the system changes from interactions. How this information is encoded will be understood when the form of Green's functions are looked at.

3.2 Real-time Expressions

There are two equivalent approaches to return to real time; Langreth's rules and introducing matrix structure. The latter is introduced by partitioning the contour into forward and backward evolution [29], allowing a 2x2 matrix to be formed when the operators act on either the top or bottom of the contour. Introducing a new index ψ_T and ψ_B for the top and bottom contour respectively, the matrix Green's function becomes,

$$G_C = \begin{pmatrix} -i \langle \mathcal{T}_C \{\psi_T(t)\psi_T^\dagger(t')\} \rangle & i \langle \mathcal{T}_C \{\psi_T(t)\psi_B^\dagger(t')\} \rangle \\ -i \langle \mathcal{T}_C \{\psi_B(t)\psi_T^\dagger(t')\} \rangle & -i \langle \mathcal{T}_C \{\psi_B(t)\psi_B^\dagger(t')\} \rangle \end{pmatrix}. \quad (3.9)$$

When both operators act on the top of the contour, the time simply increases from $-\infty$ to ∞ , so ordering the operators on this contour is normal time ordering, \mathcal{T} . The same logic applies for when both operators are on the bottom branch except the contour travels backwards in time, producing anti-time ordering $\tilde{\mathcal{T}}$. The diagonal elements only have one possible order as contour ordering forces the operator on the top branch to be on the right, so $G_{TB}^C(t, t') = i \langle \psi_B^\dagger(t') \psi_T(t) \rangle$ and $G_{BT}^C(t, t') = -i \langle \psi_B(t) \psi_T^\dagger(t') \rangle$.

This can be put all into one matrix equation to express the Green's function in real time,

$$\mathbf{G}^C = \begin{bmatrix} -i \langle \mathcal{T} \psi_T(t) \psi_T^\dagger(t') \rangle & -i \langle \psi_B^\dagger(t') \psi_T(t) \rangle \\ -i \langle \psi_B(t) \psi_T^\dagger(t') \rangle & -i \langle \tilde{\mathcal{T}} \psi_B(t) \psi_B^\dagger(t') \rangle \end{bmatrix} = \begin{bmatrix} G^t(t, t') & G^>(t, t') \\ G^<(t, t') & G^{\tilde{t}} \end{bmatrix} \quad (3.10)$$

where we have introduced G -lesser and G -greater alongside the time-ordered and anti-time ordered Green's functions. With a closer inspection of these functions, they can be seen to not be independent. A rotation exists that will cause the matrix to always have one component be zero. The cost of considering non-equilibrium is the introduction of this matrix structure to the problem.

3.2.1 Menagerie of Two-Point Functions

Up to this point, the form that these Green's functions take has been left to the readers imagination. This section will detail all their various representations and the relations between them. The two foundational two-point functions are G -lesser and G -greater, which correspond to the spatial distribution of electrons or holes in the system respectively when $x = x', t = t'$,

$$G^<(x, t; x', t') = i \langle \psi^\dagger(x', t') \psi(x, t) \rangle, \quad G^>(x, t; x', t') = -i \langle \psi(x, t) \psi^\dagger(x', t') \rangle. \quad (3.11)$$

In equilibrium, these functions can be determined using the Fermi (or Bose) distribution when considered in the frequency-momentum basis for systems with spatial and time indepen-

dence,

$$G^<(k, \omega) = \sum_{k, \omega} \frac{1}{e^{-\beta\varepsilon(k, \omega)} + 1}. \quad (3.12)$$

Again it should be stressed that to actually calculate these requires knowledge of the eigenstates of the Hamiltonian. These two functions are also not technically Green's functions but they are often referred to as such. Actual Green's functions satisfy the equation,

$$(i\partial_t - \hat{H})G(x, t; x', t') = \delta(x - x')\delta(t - t') \quad (3.13)$$

which looks like the classical definition of the Green's function for the Schrödinger equation, except for the operator Hamiltonian. Any solution to this differential equation is not uniquely defined and depends on the boundary conditions. There are four boundary conditions that are incredibly useful in physics, which results in four Green's functions,

$$\begin{aligned} G^r(t, t') &= \Theta(t - t') \left(G^>(t, t') - G^<(t, t') \right), \\ G^a(t, t') &= \Theta(t - t') \left(G^>(t, t') - G^<(t, t') \right), \\ G^t(t, t') &= \Theta(t - t')G^>(t, t') - \Theta(t' - t)G^<(t, t'), \\ G^{\tilde{t}}(t, t') &= \Theta(t - t')G^<(t, t') - \Theta(t' - t)G^>(t, t') \end{aligned} \quad (3.14)$$

where spatial dependence will be suppressed as it does not affect the ordering. The theta functions are what produces the delta function so the lesser and greater functions can be then seen to be the solutions to the homogeneous version of Equation 3.13.

These various Green's functions can be shown to satisfy the relations,

$$G^r - G^a = G^> - G^<, \quad G^r = G^t - G^<, \quad G^a = G^t - G^> \quad (3.15)$$

which demonstrates the linear dependence of the four Green's functions. The meaning of the various terms are a little more opaque, but the retarded Green's function shows the response of the electrons to an impulse at $t = t'$ and the advanced Green's function shows this for the holes.

The causal nature of the retarded Green's function means that it has an actual interpretation, rather than the more abstract (contour) time-ordered functions [7]. As we are back in real time a Fourier transform of equation 3.13 can be performed to obtain,

$$G^{r,a}(\omega) = \frac{1}{\omega - \hat{H} \pm i\delta}, \quad G^{t,\tilde{t}}(\omega) = \frac{1}{\omega - \hat{H} \pm i\delta \operatorname{sgn}(\pm\omega)} \quad (3.16)$$

where the form of the infinitesimal δ varies between each one to obtain the boundary conditions on time from Equation 3.14. The effect of the self-energy is often to affect the dispersion as

$$G^r = \frac{1}{\omega - H_0 + \Sigma + i\delta} \quad (3.17)$$

which shifts the energies of the Hamiltonian by Σ . It should be remembered that all these quantities are matrices so despite the seeming simplicity of the equation, most of the work comes in dealing with the matrix aspect. Understanding that the self-energy shifts the energies, the imaginary part of Σ will be seen to create complex energies. The usual oscillatory solutions will now acquire a finite lifetime, which will be proportional to the size of $\operatorname{Im}(\Sigma) = 1/\tau$. The choice of τ here is not accidental as it is the scattering time - describing how long the excitations last before scattering off to a new momentum.

3.2.2 Langreth's Theorem

Langreth's theorems provide a dictionary of how to go from a contour-ordered expression to a real-time one. The proof of these results can be found in Reference 30 and is based on deforming contours, seen in the previous chapter. If the expression is given by $C(\tau, \tau') = \int_K dt_1 A(\tau, t_1)B(t_1, \tau')$, the real time expression for the lesser function will be

$$C^<(t, t') = \int_{-\infty}^{\infty} dt_1 \left(A^r(t, t_1)B^<(t_1, t') + A^<(t, t_1)B^a(t_1, t') \right). \quad (3.18)$$

The real time form of $C^>$ can be found by replacing the lesser by the greater. The retarded function is given by

$$C^r(t, t') = \int_{-\infty}^{\infty} dt_1 A^r(t, t_1) B^r(t_1, t') \quad (3.19)$$

and equivalently for the advanced function where $r \leftrightarrow a$. Having got an expression for all varieties of Green's function, the process can be generalised to a double integral over the product of three contour-ordered functions or higher orders.

There is another form in which contour-ordered functions may appear: as a simple multiplication without the integration, $D(\tau, \tau') = A(\tau, \tau')B(\tau, \tau')$. The corresponding real time lesser function of this becomes,

$$D^<(t, t') = A^<(t, t')B^<(t, t'), \quad (3.20)$$

and changing $<$ for $>$ will again give the greater function. The retarded (and equivalently advanced) function becomes

$$D^r(t, t') = A^<(t, t')B^r(t, t') + A^r(t, t')B^<(t, t') + A^r(t, t')B^r(t, t'). \quad (3.21)$$

This forms our recipe book for how to get from the functions in which there is a formal perturbation theory to functions that correspond to observables.

3.3 Dyson's Equation Redux

To derive some useful formulas, and as a practice of applying Langreth's theorem, a real-time version of the contour-ordered Dyson's equation can be calculated. Suppressing all the indices, Dyson's equation is,

$$G = G_0 + G_0 \circ \Sigma \circ G \quad (3.22)$$

where the self-energy is generically defined. Due to the integration over the internal indices, Equation 3.19 can be used to continue to a retarded or advanced real-time expression,

$$G^r = G_0^r + G_0^r \circ \Sigma^r \circ G^r, \quad G^a = G_0^a + G_0^a \circ \Sigma^a \circ G^a. \quad (3.23)$$

These are reminiscent of the equilibrium case, but new information is contained within the kinetic equation which is the continuation to G -lesser using equation 3.18,

$$G^< = G_0^< + G_0^r \circ \Sigma^r \circ G^< + G_0^r \circ \Sigma^< \circ G^a + G_0^< \circ \Sigma^a \circ G^a. \quad (3.24)$$

Through using $(1 - G_0^r \circ \Sigma^r)^{-1} \circ G_0^r = G^r$ which is obtained from rearranging Equation 3.23, The kinetic equation becomes

$$G^< = G^r \circ (G_0^r)^{-1} \circ G_0^< \circ (1 + \Sigma^a \circ G^a) + G^r \circ \Sigma^< \circ G^a = G^r \circ \Sigma^< \circ G^a, \quad (3.25)$$

where the first term will be zero as the inverse of the retarded free Green's function is the differential operator of Equation 3.13. This will act on $G_0^<$, which is the solution of the homogeneous part, resulting in $(G_0^r)^{-1} \circ G_0^< = 0$ and the cancellation of the first term.

This completes the introductory tour of QFT. Although a detailed description of the perturbative rules has not been shown here, these chapters exemplify how the calculation of these averages, when the full eigenstates are not known, requires this variety of theoretical tools. The perturbative structure is exactly the same in equilibrium and non-equilibrium, The approaches differ in the continuation back to real time. This continuation is trivial for zero temperature QFT, requires analytic continuation for finite temperature Matsubara technique, and introduces a matrix structure for finite temperature non-equilibrium systems.

Green's functions can be found through their definitions when the eigenstates are known. If the eigenstates are not exactly known, Dyson's equation relates the full Green's function to one calculated with the quadratic part of the Hamiltonian which involves the self-energy.

CHAPTER 4

LUTTINGER LIQUIDS

The introduction examined how a system in our inherently three-dimensional world can be restricted to only one. The mathematical formulation of quantum field theory in 1D, does not require such considerations, it is by definition 1D. This chapter will go through the paradigm of 1D physics - the Luttinger liquid which describes the gapless low-energy excitations as a bosonic density wave. Quantum point contacts have experimentally shown behaviour that is consistent with a Luttinger liquid description. This was found by measuring the deviation of the integer conductance plateaus upon increasing temperature [31], therefore this analysis is pertinent to our understanding of the fractional plateaus.

This chapter will first explore how physics is altered in this reduced dimensionality and why conventional descriptions of continuum fermionic systems fail. The process of linearisation is examined to understand why this technique is so widely applicable, which results in a new effective model of the low-lying excitations. This effective model is then converted to the Luttinger liquid description by bosonisation. Additional electron species, in this case spin, will then be included into the description. Most of this chapter draws from Giarmachi's authoritative book on 1D physics [32].

4.1 One-Dimensional Idiosyncrasies

The defining feature of one-dimensional physics is that all motion must be collective. Consider a chain of particles where one particle collides with a neighbouring particle, causing some displacement. The neighbouring particle will then interact with its neighbour and create a cascade of interactions between pairs of particles that travels along the chain - a propagating longitudinal density wave. In higher dimensions, a particle can avoid or lessen a collision by going around other particles. This leads the influence of a disturbance fizzling out over shorter distances in higher dimensions for similar interaction strengths. The requirement to interact in 1D results in all excitations being density fluctuations, which are bosonic and therefore there must be a bosonic description of a fermionic 1D system. Obtaining this description is what bosonisation achieves. Tomonaga [33] was the first to attempt to describe a one-dimensional system in this way, paving the way for the linear model introduced by Luttinger [34] that was grouped into the ‘Luttinger liquid’ collection of models by Haldane [35].

The necessity to consider collective motion elevates the importance of interactions to a system; changing the statistics of particles and amplifying the effect of fluctuations. Quantum fluctuations will have their effect felt over larger distances, resulting long-range order being unable to form even at zero temperature. Statistics upon particle exchange are not only determined from the particle’s inherent statistics, but also from the phase shift from collisions. This means there is a parameter related to the interactions that can be smoothly changed to describe systems with different statistics, shown in Figure 4.1, where the parameter K will get an explicit formulation later.

Throughout this thesis, our interest is in fermionic systems. The underlying solution from which interactions are adiabatically introduced differs for low-dimensional systems. In dimensions larger than two, Fermi liquid theory permits the absorption of electron-electron interactions into a renormalisation of the electron mass in the quadratic Fermi gas dispersion [4]. The Tomonaga-Luttinger model serves as the point from which to introduce interactions in 1D.

One of the reasons that Fermi liquid theory fails in 1D is due to an inherent instability in the description. Considering the susceptibility of an equilibrium system of volume Ω to a static

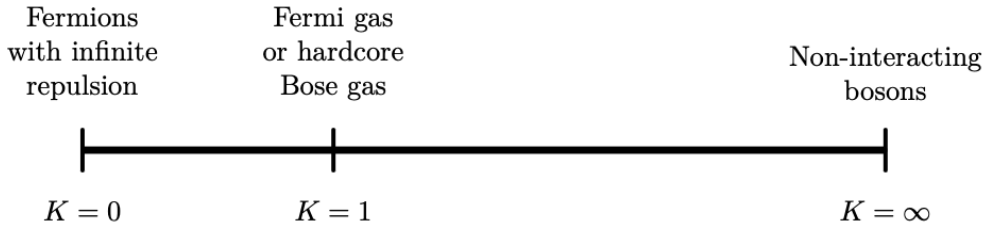


Figure 4.1: Varying the Luttinger parameter changes what underlying model our Luttinger liquid description corresponds to. Certain common models coincide with specific values of K that are shown here.

perturbation of momentum q ,

$$\chi(q) = \frac{1}{\Omega} \sum_k \frac{f(\xi(k)) - f(\xi(k+q))}{\xi(k) - \xi(k+q)}, \quad (4.1)$$

where $f(k)$ is the Fermi function and $\xi(k)$ is the energy measured relative to the Fermi surface. This form follows from an application of Kubo formalism to a perturbation in density, explored in Section 5.1. For a specific k and q that links two points on the Fermi surface, $\xi(k) = \xi(k+q) = 0$ resulting in a divergence in the summand. There are pairs of points in all dimensions where this ‘nesting’ condition is met, but the divergence is smoothed out by the additional factors that appear upon exchanging the sum for an integration, such as $k^{D-1}dk$ when integrating an isotropic distribution in D dimensions.

In one dimension, this divergence is not cancelled and the entire Fermi surface is nested as there are only two points. This means that the system is infinitely susceptible to a perturbation where $q = 2k_F$. A diverging susceptibility is an indication of the original non-interacting ground state being completely different to the interacting one, as any interaction with an infinitesimal $2k_F$ momentum component will result in an infinite response of the system. This will change the underlying description to one that is non-trivially related to the original description. For fermions at half filling on a lattice this instability causes the Peierls transition where pairs of electrons bunch up and double the periodicity of the chain [36]. The system is not just unstable towards this process, as there is a superconducting instability that competes

with the dimerisation. The 1D system is also cursed to never be able to achieve long range order, as mentioned earlier, so these two processes compete and leave the system on the verge of instability.

It will be shown that the elementary excitations of a class of 1D models are density waves of spin and charge. Any fermionic excitation, like creating an additional electron, must necessarily split up into constituent spin and charge components. This spin-charge separation is the simplest example of charge fractionalisation [37], the extension of which are fractionally charged excitations.

4.2 Tomonaga-Luttinger Model

To see how bosonic density excitations could form the low-energy excitations of a fermionic 1D model, first consider a gas of non-interacting electrons. Density fluctuations are particle-hole pairs that destroy a particle at momentum k and create a particle at a new momentum $k + q$, denoted as $c_{k+q}^\dagger c_k$. The dispersion of a Fermi gas measured about the Fermi surface is $\xi(k) = (k^2 - k_F^2)/2m$, so the excitations have an energy of,

$$E_k(q) = \xi(k + q) - \xi(k) = \frac{2qk + q^2}{2m}. \quad (4.2)$$

The average value of the energy $E(q)$ over the region $[k_F - q, k_F]$, and the variation in the energy $\delta E(q) = \max(E_k(q)) - \min(E_k(q))$ in the same segment, can be calculated. This particular region is chosen so that c_{k+q}^\dagger does not act on an already filled state. This gives,

$$E(q) = k_F q / m = v_F q, \quad \delta E(q) = q^2 / m = E(q)^2 / mv_F^2. \quad (4.3)$$

Provided that there is a finite slope at the Fermi level (so $v_F \neq 0$), the average energy of an excitation only depends on the momentum of the particle-hole pair. The variation in energy goes to zero faster than the average energy. Therefore these particles will have a well defined momentum and energy that become long lived as the energy tends to zero. The independence

of Equation 4.3 of the original k means that the mapping to particle-like excitations will hold for all fillings away from the bottom of the band.

Having seen how the density fluctuations are well-defined particles, the Tomonaga-Luttinger model can now be introduced. The energy spectrum is that of a relativistic fermion, travelling at a speed v_F instead of c

$$\varepsilon_q = \eta v_F q \quad \text{where } \eta = \{R = 1, L = -1\}. \quad (4.4)$$

There are two branches of the dispersion that correspond to right movers for positive η and left movers for negative η . An excitation with negative q (so moving to the left) will then have a positive energy, hence the extra minus sign in the dispersion. This directionality causes the branches to act as two different non-interacting fermion species if k_F is large. Then only a large momentum scattering of $2k_F$ would allow a change of direction. In this model, for all possible q to be considered, an infinite number of negative energy states must be introduced that are filled up to a certain energy - much like the Dirac sea.

This model can be seen to represent the low-energy excitations of a Fermi liquid in 1D with electron and hole symmetry. Expanding the dispersion around the two Fermi points of the Fermi surface $k = \pm k_F$, where $q = k - k_F$, gives a dispersion of,

$$\xi_k = \frac{1}{2m}(k - k_F)(k + k_F) = \begin{cases} v_F q, & \text{for } k \approx k_F, \\ -v_F q, & \text{for } k \approx -k_F. \end{cases} \quad (4.5)$$

This expansion is only valid if $k_F \gg q$. For fluctuations caused by temperature, this condition becomes $T \ll \epsilon_F$. Although the increase to the infinite number of electrons in the Tomonaga-Luttinger model is unphysical, it will not affect the low-energy behaviour. The exclusion principle means that in order for electrons at a large negative energy to be able to contribute, they must be excited above the Fermi surface. This would cost a lot of energy and so the original approximation of low energies would be violated. Figure 4.2 shows this process of linearisation.

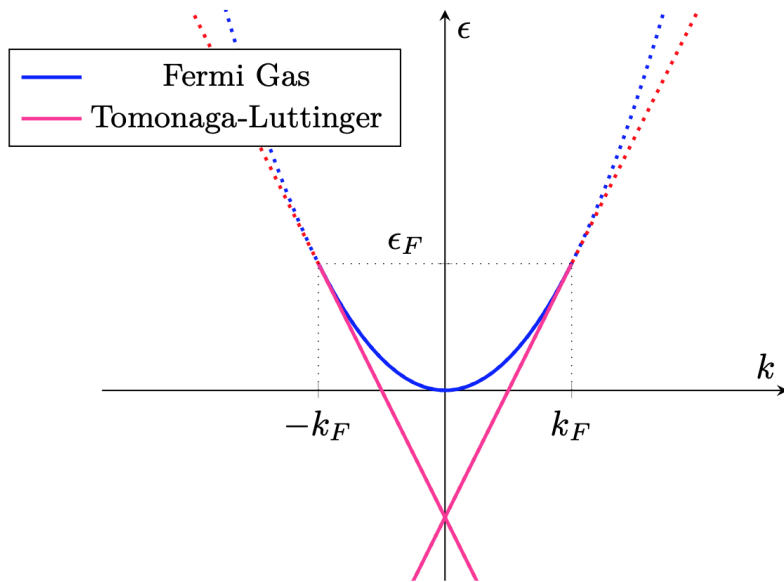


Figure 4.2: Linearising the Fermi gas dispersion about the Fermi points results in the two linear branches of the Tomonaga-Luttinger model. The solid lines indicate that the states are occupied and the dashed lines are unoccupied states, with the occupation in the Tomonaga-Luttinger model extending to $\epsilon \rightarrow -\infty$.

The reason for this extension to a Dirac sea is that the model has a complete, infinite dimensional Hilbert space with an energy spectrum that is unbounded from above. To have an exact mapping from fermions to bosons this must be the case as bosons can infinitely occupy a single mode.

There are various different ways of mapping this model onto a bosonic one: through functional [38], operator [39] or phenomenological methods [35, 40]. The operator route is often used as there is an exact Fock space operator identity [41], though the phenomenological pathway provides a lot of intuition as to what the bosonic fields correspond to. Most of the thesis focuses on treating Luttinger Liquids using functional integrals, which are introduced in Appendix A, therefore functional bosonisation will be introduced.

4.3 Bosonisation

The action of the Tomonaga-Luttinger model without interactions is,

$$S_0 = S_L + S_R = \sum_{\eta} \int dx dt \bar{\psi}_{\eta}(x, t) i \partial_{\eta} \psi_{\eta}(x, t), \quad \partial_{\eta} = \partial_t + \eta v_F \partial_x, \quad (4.6)$$

where there are separate fermion fields for the different chiralities. The dispersion of Equation 4.3 is linear in momentum and therefore gains a single spatial derivative along with the usual pq term from the action. To reiterate that this description is equivalent to the low-energy model of the quadratic model, consider the chiral fields $\psi_{\eta}(x, t)$. These fields can be derived from the fields of the quadratic dispersion by considering the general Fourier transform of the field $\psi(x, t)$ and removing a factor of $e^{ik_F x}$ to get in the vicinity of $k = \pm k_F$,

$$\begin{aligned} \psi(x, t) &= e^{ik_F x} \psi_R(x, t) + e^{-ik_F x} \psi_L(x, t), \\ \psi_{\eta}(x, t) &= \int_{-\infty}^{\infty} \frac{d\omega}{2\pi} \int_{\eta k > 0}^{\infty} \frac{dk}{2\pi} e^{i(k - \eta k_F)x - i\omega t} \psi_{k,\omega}. \end{aligned} \quad (4.7)$$

Therefore $\psi_{\eta}(x, t)$ will only have slow oscillating components when $k \sim k_F$.

The density operator becomes split into chiral components,

$$\rho = \psi^{\dagger} \psi = \rho_R + \rho_L + e^{2ik_F x} \psi_L^{\dagger} \psi_R + e^{-2ik_F x} \psi_R^{\dagger} \psi_L, \quad \text{where } \rho_{\eta} = \psi_{\eta}^{\dagger} \psi_{\eta}. \quad (4.8)$$

The cross terms contain an rapidly oscillating component that will cause the term be negligible for any integration over space, such as the one in the action. This cannot be ignored if a large momentum scattering interaction $2k_F$ is relevant.

Now the foundational equation of bosonisation is introduced, which is a mapping between the fermionic field and a bosonic field $\theta_{\eta}(x, t)$,

$$\psi_{\eta} = \chi e^{i\theta_{\eta}(x, t)}, \quad \bar{\psi}_{\eta} = \chi e^{-i\theta_{\eta}(x, t)}, \quad (4.9)$$

where χ is a global Majorana field, included to ensure the proper anticommutation of fermionic

fields while commuting with the bosonic fields¹. Majorana fields have the property that they are their conjugate, so $\bar{\chi} = \chi$. The anticommutation implies that $\chi^2 = 0$. Naively substituting this transformation into the action results in Equation 4.6 becoming zero due to both $\chi^2 = 0$ and $\partial_x \chi = 0$ with the latter caused by the global nature of the Majorana field. In all methods of bosonisation, there are spurious zeroes that occur that upon closer inspection, have a finite value. When using functional bosonisation, this is a manifestation of the QFT anomaly. The way to obtain a non-zero action is to look at the measure of the partition function when changing variables [42]. The anomaly arises as the symmetry of the classical action under this chiral transformation $\psi_\eta \rightarrow \psi_\eta e^{i\eta\theta_\eta}$ (suppressing the variables of the fields from now on) is not obeyed by the Jacobian of the transformation, which affects the measure $\mathcal{D}\psi_\eta$ in the partition function.

To understand how this symmetry is preserved in the measure, consider the gauge transformation $\psi_\eta \rightarrow \tilde{\psi}_\eta e^{i\theta}$ on the action, where not using Majorana fields means the action does not vanish. The transformed action becomes,

$$\tilde{S} = \int dx dt \tilde{\psi}_\eta (i\partial_\eta + \partial_\eta \theta_\eta) \tilde{\psi}_\eta. \quad (4.10)$$

The partition functions $\mathcal{Z}_\eta = \int \mathcal{D}\psi_\eta e^{iS_\eta}$ for the original and transformed action can be calculated as the fields are quadratic in the action. The relation of these to each other defines the Jacobian of the transformation,

$$\mathcal{Z}_\eta = J_\eta \tilde{\mathcal{Z}}_\eta, \implies J_\eta = \frac{\det(g_\eta^{-1})}{\det(g_\eta^{-1} + \partial_\eta \theta_\eta)}, \quad (4.11)$$

where g_η^{-1} is the inverse of the Green's function for the equation of motion,

$$i\partial_\eta g_\eta = \delta(x - x')\delta(t - t'). \quad (4.12)$$

¹There is some subtlety about choosing the prefactor to be a Majorana field [41]. From an operator perspective, this factor here should also reduce/raise the number of fermions in the system by one, amounting to a shift in k_F . In the thermodynamic limit, this shift is very small so can be ignored. When calculating averages that have an equal number of creation and annihilation operators, the raising and lowering operator take us back to the original particle number subspace and can therefore be left out. This is why despite seeming crucial to this derivation, they do not appear again in this thesis.

Upon using the ubiquitous linear algebra identity, $\ln(\det(A)) = \text{tr}(\ln(A))$ for a matrix A , Equation 4.11 can be seen as a disguised exponential and therefore as a contribution to the action. Upon performing the trace over the Green's functions, the Jacobian becomes,

$$\ln(J_\eta) = -\frac{i\eta}{4\pi} \text{Tr}(\partial_\eta \theta_\eta \partial_x \theta_\eta). \quad (4.13)$$

The derivation of this result is presented in Appendix C. Defining new fields $\theta = (\theta_L - \theta_R)/2$ and $\phi = (\theta_L + \theta_R)/2$, the action which is determined fully by the Jacobian becomes,

$$\begin{aligned} S_0 &= \frac{1}{4\pi} \int dx dt \partial_L \theta_L \partial_x \theta_L - \partial_R \theta_R \partial_x \theta_R \\ &= \frac{1}{2\pi} \int dx dt \partial_t \theta \partial_x \phi + \partial_t \phi \partial_x \theta - v_F (\partial_x \theta)^2 - v_F (\partial_x \phi)^2. \end{aligned} \quad (4.14)$$

Integrating one of the first two terms by parts and then performing the functional integral over one of the fields gives two possibilities for the action, dependent on what field was integrated out². The bosonised action is,

$$S_0 = \frac{1}{2\pi v_F} \int dx dt (\partial_t \theta)^2 - v_F^2 (\partial_x \theta)^2, \quad (4.15)$$

$$= \frac{1}{2\pi v_F} \int dx dt (\partial_t \phi)^2 - v_F^2 (\partial_x \phi)^2. \quad (4.16)$$

This dual representation allows whatever action is most convenient to be used. The distinction here seems academic, but upon including interactions the two actions will have different forms. In trying to obtain a representation of the density in this new bosonised form, the anomaly once again rears its ugly head, as $\rho_\eta = \bar{\psi}_\eta \psi_\eta$ will be zero upon using Equation 4.9. The antidote this time is to introduce a source field prior to bosonisation, which when differentiated gives the density. Carrying it through the derivation, the density becomes,

$$\rho_\eta = \frac{\eta}{2\pi} \partial_x \theta_\eta, \quad \Rightarrow \quad \rho = -\frac{1}{\pi} \partial_x \theta. \quad (4.17)$$

²Any contribution from the quadratic functional integral that is integrated out will be cancelled out by the denominator in an average and therefore can be forgotten.

This issue can also be resolved by point splitting the fields and being more careful in the limit that the fields are evaluated in the same point [43]. From the continuity equation, the current can be found to be,

$$\partial_t \rho = -\partial_x j, \quad j = \frac{1}{\pi} \partial_t \theta. \quad (4.18)$$

If this bosonisation procedure was performed with operators, it can be found the the operator fields θ and $\partial_x \phi$ are conjugate variables and satisfy the canonical commutation relations with an extra factor of π .

4.3.1 Including Interactions

The strength of this technique is in how it simplifies interactions. It has just been shown that, surprisingly, a kinetic term that is quadratic in fermionic fields is also quadratic in bosonic fields. For terms that are quartic in the fermionic fields, it is obvious that this can be expressed by two bosonic fields. The interaction term in a generic fermionic model is

$$S_{int} = \int dx dx' dt dt' \bar{\psi}(x, t) \psi(x, t) V(x, x'; t, t') \bar{\psi}(x', t') \psi(x', t) \sim \int dx dt \rho^2(x, t). \quad (4.19)$$

The ‘g-ology’ formalism of interactions in the Tomonaga-Luttinger model is obtained through setting the interactions to be instantaneous and only upon contact, $V(x, x'; t, t') \sim \delta(x-x')\delta(t-t')$. This strongly screened Coulomb approximation manages to retain a lot of the underlying physics despite its apparent restriction. This interaction, however, is not modelled as entirely featureless with a different weighting being given to the terms that appear upon substituting Equation 4.8 into the interacting action,

$$S_{int} = \int dx dt g_4(\rho_L^2 + \rho_R^2) + g_2 \rho_2 \rho_4 + (g_1 \psi_L^\dagger \psi_R \psi_R^\dagger \psi_L + g_3 e^{4ik_F x} \psi_L^\dagger \psi_R \psi_L^\dagger \psi_R + \text{h.c.}), \quad (4.20)$$

where the $e^{2ik_F x}$ terms are averaged out. The g_3 term can be relevant if there is umklapp scattering from the presence of a lattice - this is the cause of the Peierls distortion. In the spinless case,

where just one fermionic species is considered, g_1 is a rearrangement of g_2 and can therefore be absorbed into the definition of the g_2 terms. When performing the spinful analysis in the next section, this cannot be completely absorbed.

Away from specific fillings of a lattice, there will be no relevant umklapp scattering so the interaction just becomes the first half of Equation 4.20. Using the equivalent density for the bosonic fields in Equation 4.17, the action becomes,

$$S_{int} = \int dx dt \frac{g_4}{4\pi^2} ((\partial_x \theta_L)^2 + (\partial_x \theta_R)^2) - \frac{g_2}{4\pi} \partial_x \theta_L \partial_x \theta_R. \quad (4.21)$$

Performing the same substitution as before where $\theta_L = \theta + \phi, \theta_R = \phi - \theta$ gives a final action of

$$S = \frac{1}{2\pi} \int dx dt 2\partial_x \phi \partial_t \theta - \left(v_F + \frac{g_2}{2\pi} + \frac{g_4}{2\pi} \right) (\partial_x \theta)^2 - \left(v_F + \frac{g_4}{2\pi} - \frac{g_2}{2\pi} \right) (\partial_x \phi)^2. \quad (4.22)$$

Commonly, the coefficients of the gradient terms are defined using variables ν and K where

$$\begin{aligned} \nu K &= v_F + \frac{g_2}{2\pi} + \frac{g_4}{2\pi}, & \frac{\nu}{K} &= v_F + \frac{g_4}{2\pi} - \frac{g_2}{2\pi} \\ \implies K &= \sqrt{\frac{2\pi v_F + g_4 - g_2}{2\pi v_F + g_4 + g_2}}, & \nu &= v_F \sqrt{\left(1 + \frac{g_4}{2\pi v_F}\right)^2 - \left(\frac{g_2}{2\pi v_F}\right)^2}. \end{aligned} \quad (4.23)$$

The action can then be integrated out to give,

$$S = \frac{K}{2\pi\nu} \int dx dt \left((\partial_t \phi)^2 - \nu^2 (\partial_x \phi)^2 \right) \quad (4.24)$$

$$S = \frac{1}{2\pi\nu K} \int dx dt \left((\partial_t \theta)^2 - \nu^2 (\partial_x \theta)^2 \right). \quad (4.25)$$

Finally, we have obtained an explicit formula for the Luttinger parameter K that was introduced conceptually at the start of the chapter. The above form means that for g_4 and g_2 being positive constants, as they should be for a fermionic model, then $K \leq 1$. This confirms what was previously stated in Figure 4.1, that fermionic models correspond to this region of K . This

action can be expressed in terms of an inverse Green's function by integrating by parts,

$$S = \frac{1}{2\pi\nu K} \int dx dt \theta \left(\partial_t^2 - \nu^2 \partial_x^2 \right) \theta = \frac{1}{2} \int dx dt \theta(x, t) G^{-1}(x, x', t, t') \theta(x' t'). \quad (4.26)$$

The field dependencies have appeared again to make it clear that this expresses the inverse Green's function in position and real time. From this form, all the other Green's functions can be found through computing the Fourier transforms. This will be done in Chapter 6 in order to calculate the conductance through the system.

The overall effect of this renormalisation on the spectrum is that the dispersion becomes $\varepsilon_q = \eta\nu q$, where ν has replaced v_F . In this final form the reason for the dual actions can be seen as the interaction parameter K is inverted in the two different representations. This means that if the parameter is large in one representation, we can use the dual to express our action in such a way that the parameter is small and a perturbative expansion can be found.

4.4 Spinful Luttinger Liquids

Including the electron's spin into the non-interacting Tomonaga-Luttinger model simply doubles the degrees of freedom with 4 types of fermion, one for each chirality and spin. Each of these can be bosonised by,

$$\psi_{\eta\sigma} = \chi_\sigma e^{i\theta_{\eta\sigma}}, \quad (4.27)$$

where $\sigma = \{\uparrow, \downarrow\}$. Following the same procedure of calculating the Jacobian gives the kinetic part of the action as,

$$S_0 = \frac{1}{2\pi v_F} \sum_\sigma \int dx dt (\partial_t \theta_\sigma)^2 - v_F^2 (\partial_x \theta_\sigma)^2, \quad (4.28)$$

with the new fields $\theta_\sigma = \theta_{L\sigma} - \theta_{R\sigma}$, $\phi_\sigma = \theta_{L\sigma} + \theta_{R\sigma}$. The density is then generalised as

$$\rho_{\eta\sigma} = -\frac{\eta}{2\pi} \partial_x \theta_{\eta\sigma}, \quad \rho_\sigma = -\frac{1}{\pi} \partial_x \theta_\sigma. \quad (4.29)$$

The full electron-electron interaction is a generalisation of Equation 4.19, where the density fluctuations of a particular spin species will influence other density fluctuations. Splitting the field of each spin into the left and right chiral components gives an interaction term that can be split up into the different possible pairings of chirality. The terms are,

$$S_{int} = S_1 + S_2 + S_4 \sim \int dx dt \sum_{\substack{\eta_1 \eta_2 \eta_3 \eta_4 \\ \sigma_1 \sigma_2}} \psi_{\eta_1 \sigma_1}^\dagger \psi_{\eta_2 \sigma_1} \psi_{\eta_3 \sigma_2}^\dagger \psi_{\eta_4 \sigma_2}, \quad (4.30)$$

$$S_4 = \int dx dt \sum_{\sigma, \eta} g_{4\perp} \rho_{\eta\sigma} \rho_{\eta\bar{\sigma}} + g_{4||} \rho_{\eta\sigma} \rho_{\eta\sigma}, \quad (4.31)$$

$$S_2 = \int dx dt \sum_{\sigma} g_{2\perp} \rho_{L\sigma} \rho_{R\bar{\sigma}} + g_{2||} \rho_{L\sigma} \rho_{R\sigma}, \quad (4.32)$$

$$S_1 = \int dx dt \sum_{\sigma} g_{1||} \psi_{L\sigma}^\dagger \psi_{R\sigma}^\dagger \psi_{L\sigma} \psi_{R\sigma} + g_{1\perp} \psi_{L\sigma}^\dagger \psi_{R\bar{\sigma}}^\dagger \psi_{L\bar{\sigma}} \psi_{R\sigma} + \text{h.c.}, \quad (4.33)$$

where the introduction of \perp and $||$ is to denote whether the interaction is between different spins or the same spins respectively. The umklapp terms that should appear with g_3 are again ignored. Mirroring the spinless case, $g_{1||}$ can be rearranged to give a contribution of the form $g_{2||}$. However, $g_{1\perp}$ contains interactions between different spin species and cannot be formulated in terms of densities.

Ignoring the $g_{1\perp}$ term for the moment, the g_2 and g_4 spinful terms have terms that mix the θ_\uparrow and θ_\downarrow fields. A rotation is therefore made to diagonalise the Hamiltonian, which introduces charge and spin fields,

$$\begin{aligned} \theta_\rho &= \frac{1}{\sqrt{2}}(\theta_\uparrow + \theta_\downarrow), & \theta_\sigma &= \frac{1}{\sqrt{2}}(\theta_\uparrow - \theta_\downarrow), \\ \phi_\rho &= \frac{1}{\sqrt{2}}(\phi_\uparrow + \phi_\downarrow), & \phi_\sigma &= \frac{1}{\sqrt{2}}(\phi_\uparrow - \phi_\downarrow). \end{aligned} \quad (4.34)$$

With these definitions, and the patience to perform some algebra, both the g_2 and g_4 terms can be absorbed into a quadratic description. The g_1 term however results in a different kind of term upon bosonising,

$$\bar{\psi}_{L\uparrow} \bar{\psi}_{R\downarrow} \psi_{L\downarrow} \psi_{R\uparrow} \sim e^{-i(\theta_{L\uparrow} + \theta_{R\downarrow} - \theta_{L\downarrow} - \theta_{R\uparrow})} = e^{-2i\sqrt{2}\theta_s}. \quad (4.35)$$

Adding this to its Hermitian conjugate gives a final action,

$$S = \frac{1}{2\pi\nu_\rho K_\rho} \int dx dt (\partial_t \theta_\rho)^2 + \nu_\rho^2 (\partial_x \theta_\rho)^2 + \frac{1}{2\pi\nu_\sigma K_\sigma} \int dx dt (\partial_t \theta_\sigma)^2 + \nu_\sigma^2 (\partial_x \theta_\sigma)^2 + \int dx dt 2g_{1\perp} \cos(2\sqrt{2}\theta_\sigma). \quad (4.36)$$

The ν_a and K_a parameters, where $a = \{\rho, \sigma\}$, are given by,

$$K_a = \sqrt{\frac{2\pi v_F + g_{4a} - g_{2a}}{2\pi v_F + g_{4a} + g_{2a}}}, \quad \nu_a = v_F \sqrt{\left(1 + \frac{g_{4a}}{2\pi v_F}\right)^2 - \left(\frac{g_{2a}}{2\pi v_F}\right)^2}, \quad (4.37)$$

for $g_{2a} = g_{1\parallel} - g_{2\parallel} \pm g_{2\perp}$, $g_{4a} = g_{4\parallel} \pm g_{4\perp}$,

where ρ corresponds to the positive sign choice and σ for the negative. Note that the action could be equivalently described with ϕ_ρ instead of θ_ρ which amounts to using the form of Equation 4.24 with the new spinful Luttinger parameters.

Now the spin and charge fields are completely decoupled and unaffected by each other's dynamics. This is the spin-charge separation mentioned at the beginning of the chapter and presents an example of fractionalisation. The spin sector however now contains a curious cosine term. This will have no affect on the charge transport but will obviously result in different behaviour for the spins. Terms of this form will be explored further in Chapter 6.

A final side note is that all of this analysis relied on bosonising the full Tomonaga-Luttinger model with its infinite spectrum but many systems have a finite bandwidth. To mimic this in the bosonic fields, a factor of $(2\pi\alpha)^{-1/2}$ where α is related to the bandwidth is introduced to the bosonisation formula as well as a restriction on the momentum integrals of Equation 4.7 to the bandwidth.

This concludes the introduction to Luttinger liquids. The transport properties of both the spinless and spinful model will be explored in Chapter 6. The great strength of this model is in its applicability to a variety of situations, not just the QPC. Carbon nanowires [44] and chains of gold atoms [45] can be fabricated and they produce results that are consistent with a Luttinger liquid being the underlying description. The fractional quantum Hall effect contains a chiral

Luttinger liquid, which will also be explored in Chapter 6. Signatures of this state have been experimentally verified [46]. A large class of materials display more general 1D behaviour, when the cosine terms modifies the pure Luttinger liquid action [39]. The past few decades have shown that 1D physics is not only the theorist's playground, but the experimentalist's too.

CHAPTER 5

CONDUCTANCE FORMALISMS

The variety of regimes of transport that were covered in the opening chapter suggests that a diverse range of mathematical approaches are needed to extract the conductance. The three microscopic techniques that will be discussed in this chapter are the Kubo, Landauer, and non-equilibrium Green's function (NEGF) formalisms. The Kubo technique is the most theoretically direct way of finding the conductivity, where the current due to an applied electromagnetic field is calculated perturbatively. The conductivity, by definition, relates these two quantities. The difficulty comes from mathematically computing the response to the perturbation.

The Landauer formalism is based on how current is passed through mesoscopic systems experimentally. It introduces additional concepts to keep the calculation tractable rather than mathematical approximations of the Kubo formalism. Complicating the conceptual understanding allows the calculation to become that of a scattering problem. In the most simple cases, finding the conductance is no more complicated than the quintessential quantum mechanics problem of finding the transmission of an incident particle on a potential barrier. The final technique is the NEGF formalism where the entire system is included in the description by using the Keldysh technique. However, the accuracy of the description comes at the price of the analytical results becoming harder to extract.

5.1 Kubo

At the heart of the Kubo formalism is the fluctuation-dissipation theorem (FDT). This deep underlying relation between the fluctuations of a system at equilibrium and the method by which the system dissipates excess energy allows the full non-equilibrium description to be avoided. Dissipation is interlinked with conductivity, as the scattering of electrons from their original path is what causes a finite conductivity. If electrons do not get scattered, an electric field would infinitely accelerate the particles. This would produce an infinite current from an infinitesimally weak applied field and an infinite conductance.

The current in the Kubo formalism is induced by a perturbing electric field. Conceptually, this is equivalent to putting a sample of material into an electromagnetic cavity and looking at the absorption of the field in the cavity due to the presence of the sample [6]. Obtaining the frequency-dependent response is natural for this formalism. The proof of the FDT will now be presented, following Reference 28. Using the FDT depends on the perturbing field being weak, therefore the linear response $R(x, t)$, to an external perturbation $P(x', t')$ defines the general susceptibility χ ,

$$R(r, t) = \int dr' \int dt' \chi(r, r', t, t') P(r', t') + O(P^2), \quad (5.1)$$

for sufficiently weak perturbation. If there is time and translational invariance, then the susceptibility will depend on the difference in space and time $\chi(r - r', t - t')$. This allows the transformation to a diagonal basis of a single momentum k and frequency ω so that,

$$R(k, \omega) = \chi(k, \omega) P(k, \omega). \quad (5.2)$$

Any response that is at a different frequency to the perturbing field indicates non-linear behaviour, where the Kubo formalism is no longer applicable. A macroscopic response in quantum mechanics will be the expectation of some single particle operator, X , that has an expansion in terms of the eigenstate fields, $R(r, t) = \sum_{ij} \langle \bar{\psi}_i(r, t) X_{ij} \psi_j(r, t) \rangle$. The action of the system will include the perturbation $P(r, t)$, locally coupled to the single particle operator

that responds to the perturbation,

$$S[\bar{\psi}, \psi, P, A] = S_0[\bar{\psi}, \psi] + \sum_{ij} \int dr \int dt \bar{\psi}_i(r, t) X_{ij} \psi_j(r, t) [P(r, t) + A(r, t)], \quad (5.3)$$

where $A(r, t)$ is a source field. The expectation value of operator becomes

$$R(r, t) = -\frac{\delta}{\delta A(r, t)} \ln(Z[P, A]) \Big|_{A=0}, \quad \text{where } Z[P, A] = \int \mathcal{D}\bar{\psi} \mathcal{D}\psi e^{iS[\bar{\psi}, \psi, P, A]}. \quad (5.4)$$

For a weak perturbing field, the logarithm of the partition function can be expanded to linear order in $P(r, t)$,

$$\ln(Z[P, A = 0]) = \ln(Z[P]) \Big|_{P=0} + \int dr' \int dt' \frac{\delta \ln(Z[P])}{\delta P(r', t')} \Big|_{P=0} P(r', t'). \quad (5.5)$$

The first term in the expansion will be independent of P . Without the perturbation, the average of the operator is zero (or can be shifted to be zero) so only the first order term needs to be included. The response becomes,

$$R(r, t) = - \int dr \int dt \frac{\delta^2}{\delta A(r, t) \delta P(r, t)} \ln(Z[P, A]) \Big|_{A=P=0} P(r, t). \quad (5.6)$$

Comparing this equation to the definition of the susceptibility in Equation 5.1 gives an equation for the susceptibility. Using the chain rule, it becomes,

$$\chi(r, r', t, t') = -\frac{1}{Z[P, A]} \frac{\delta^2}{\delta A(r', t) \delta P(r', t')} Z[P, A] \Big|_{A=P=0}. \quad (5.7)$$

Performing the functional derivative shows that the susceptibility is related to the four-point function $\langle X(r, t)X(r', t') \rangle$. When the expectation value of X is shifted to zero, the four-point function can be directly related to the fluctuations,

$$\chi(r, r', t, t') = \langle (X(r, t) - \langle X \rangle)(X(r', t') - \langle X \rangle) \rangle, \quad (5.8)$$

which is the statement of the FDT. The susceptibility characterises how the system disperses the perturbation and it has been related to the fluctuations of an operator about its average.

To derive the exact expression for the response to an applied electric field, we need to account for the fact that it is actually the vector potential that couples to the action. In this case, the perturbation and source term of Equation 5.3 are the same field. The current in response to a constant electric field is given by,

$$j(x, t) = \int dx' dt' \chi(x, x', t, t') \partial_t A(x', t'), \quad \Rightarrow \quad \sigma_\omega(x, x') = \frac{\chi_\omega(x, x')}{\omega}. \quad (5.9)$$

A choice of gauge for the A field can be chosen that eliminates the scalar potential from the description. The calculation of this average is often not simple, as perturbative methods have to be used for a non-quadratic action. In this thesis, perturbative methods are not used because the Luttinger liquid action is quadratic.

One consideration to bear in mind is that the susceptibility must be causal. The system cannot respond to a perturbation before it has been applied, therefore the external field in the future should not affect the response. This alters the integral limits in Equation 5.1 and 5.9 to be only for $t' < t$. The retarded current-current correlator is therefore the actual susceptibility, but as seen in Chapter 3, a perturbation theory can only be built from contour-ordered expressions. Therefore the calculation of the average is done with the contour-ordered contribution and then is analytically continued to real-time.

5.2 Landauer

The Landauer formalism appeals to the setup of transport experiments in order to avoid the full non-equilibrium description. In contrast to the Kubo technique - where the definition of current across the system came from using a perturbing electric field with no reference to how this field is generated - the Landauer formalism [47] centres how the external circuit causes a potential difference across the sample. The rallying cry of this formalism is ‘conductance is transmission’ which concisely states its main result. It is intuitively appealing that the conductance of a

sample can be understood as a scattering problem. Indeed, scattering problems had been used to describe the behaviour of tunnel junctions as early as 1930 [48]. The introduction of the concepts within this formalism, however, provide a more conclusive understanding as to why this approach works in many other cases.

The crucial concept that is introduced is the reservoirs between which our sample of material lies [7, 49]. These reservoirs can freely exchange electrons to and from the wire without changing the internal state of the reservoir¹, with the energy required to extract an electron being the chemical potential. This feature also appears in the non-equilibrium description and corresponds to experiment where the wire is connected to an external circuit and particle number in the sample is not conserved. Current will only flow when the chemical potential of the reservoirs either side of the sample are different. If the chemical potentials are equal, any current one way will be exactly cancelled by current flowing in the opposite direction. It is this spatial difference of potential energy boundary conditions that self-consistently induces an electric field across the sample, as opposed to the fundamental external electric field of the Kubo formalism.

These reservoirs (or contacts) are connected to leads which funnel a wavepacket into the sample. The leads are waveguides with quantised transverse modes, where the quantisation behaves in the same way as the low-dimensional systems considered in Chapter 1.2. Essentially this replaces the full open system description of the reservoirs with a scattering problem for the leads and wire system. This partitioning of the system is shown in Figure 5.1. A scattering description is where an incident particle, prepared infinitely far away, hits a potential barrier. It will either pass through and continue infinitely past the sample with a possible additional phase, or reflect back. The potential in the direction of motion in the leads is flat and particles will only encounter a barrier, and possibly reflect, when reaching the sample. The leads are also assumed to perfectly eject the particle into a reservoir - known as a reflectionless contact.

This final reflectionless assumption means that the right moving electrons in the left lead can only originate from the left reservoir and vice versa for the left moving electrons in the right lead. The problem is now in terms of the scattering of these asymptotic solutions (also

¹This requirement is interchangeable with considering the reservoirs to be infinite.

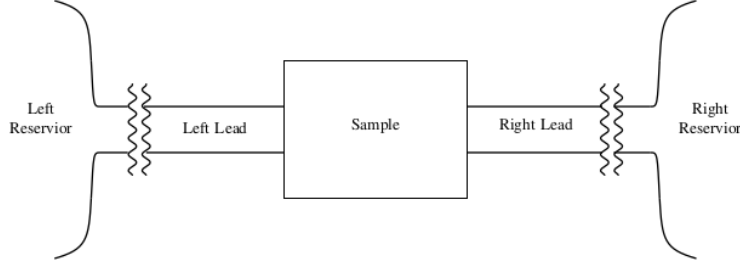


Figure 5.1: The partitioning of the system into reservoirs, leads and sample that forms the basis of the Landauer formalism.

called channels or modes) by the sample. To understand the maths used, we will begin with the perfectly transmitting one-channel case. As the system is in a steady state, the current can be measured through any slice of the system, as the current through the slice is independent of the chosen site of the slice.

In a single channel there are a continuum of states in the unconstrained direction of the system, so any quantity needs to be averaged over these states. The current is then the difference in the averaged velocity for the right and left channels,

$$I = q \int dk \langle \psi_{L,k} | v | \psi_{L,k} \rangle - \langle \psi_{R,k} | v | \psi_{R,k} \rangle. \quad (5.10)$$

These states originate from the reservoirs that are described by a free Fermi gas, $|\psi_{L,k}\rangle$, with dispersion $\epsilon = k^2/2m$ and charge e . The velocity of these states is given by the group velocity $v = \frac{d\epsilon}{dk}$. Changing the integration to be over energy introduces the density of states, $g(\epsilon) = \frac{1}{2\hbar\pi} \frac{dk}{d\epsilon}$, where an extra factor of a half occurs as the dispersion is split up into positive and negative momentum. The current becomes,

$$I = \int d\epsilon g(\epsilon) \frac{d\epsilon}{dk} (|\psi_{L,\epsilon}|^2 - |\psi_{R,\epsilon}|^2). \quad (5.11)$$

The energy dependence of both the density of states and velocity cancel out exactly. As the states are injected into the leads by the reservoirs, the probability of the states being occupied will be given by the Fermi-Dirac distribution for their respective chemical potentials. In the

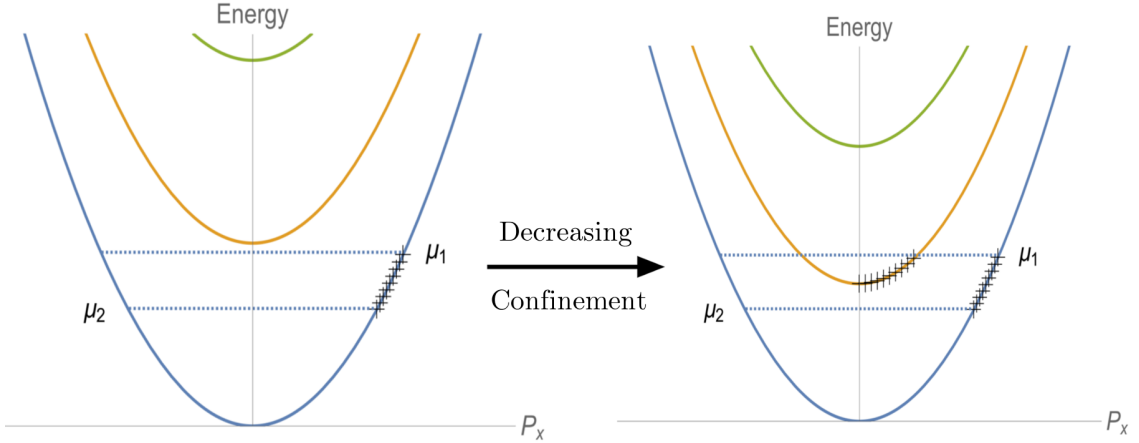


Figure 5.2: Decreasing the size of the transverse confinement allows more channels to become energetically accessible at the energies set by the Fermi levels of the reservoirs.

ballistic case where there is no potential barrier, this results in,

$$I = \frac{e}{h} \int d\epsilon f(\epsilon - \mu_L) - f(\epsilon - \mu_R), \quad (5.12)$$

a form which makes apparent the importance of differing chemical potentials. If $\mu_L = \mu_R$, then the two Fermi functions completely cancel out, which results in no current flowing. If a voltage difference is applied to left reservoir then $\mu_L = \mu + eV$. In the linear bias regime, the Fermi functions can be expanded in terms of V to give,

$$I = \frac{e}{h} \int d\epsilon \frac{df}{d\epsilon} eV, \quad \Rightarrow \quad G = I/V = \frac{e^2}{h}. \quad (5.13)$$

This is the quantisation of conductance. The final step is possible because the derivative of a Fermi function is a delta function at zero temperature. At finite temperatures, there is a broadening of this peak. The discrete steps that occur in experiments correspond to the fact that there are multiple modes. Each contributing mode imparts e^2/h as different eigenstates are orthogonal, so the calculation above will contain the sum over the modes.

Not all modes, however, are energetically accessible. Transverse quantisation is often modelled with a quantum well that has eigenstates of $E_n = \hbar^2 \pi^2 n^2 / 2mL_y^2$. Upon increasing the

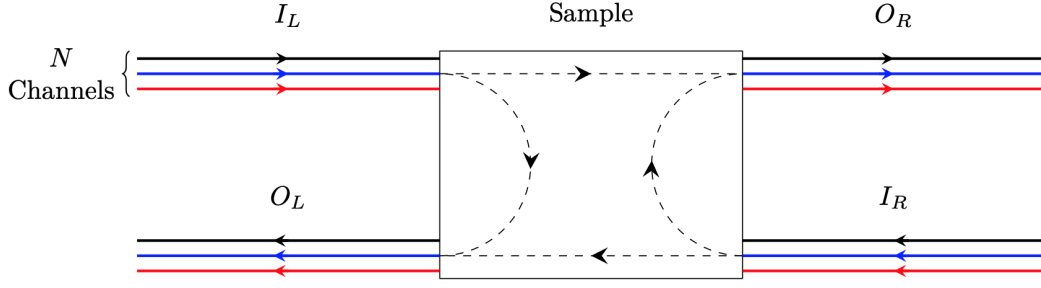


Figure 5.3: The N incoming channels from the left/right of the sample are connected to the outgoing channels on the left and right of the sample. The incoming channels either side are not related to each other due to the requirement of the contacts to be reflectionless.

size of the constriction L_y , the energy difference between the modes will decrease. The energy of a certain mode can then drop beneath the Fermi energy of the reservoirs and suddenly become accessible to the electrons for the same chemical potentials. This is the cause of the steps in conductance, depicted in Figure 5.2. This argument is more explicitly shown by Lesovik *et al.* [50] to explicitly show why the quantum point contacts used in experiments show the same features as this idealised case.

The more general case is when multiple modes impinge upon the sample and have a probability of being reflected. This is described by a scattering matrix S , which encapsulates the problem that is displayed graphically in Figure 5.3

$$\begin{pmatrix} O_L \\ O_R \end{pmatrix} = \begin{pmatrix} \mathbf{r} & \mathbf{t} \\ \mathbf{t}' & \mathbf{r}' \end{pmatrix} \begin{pmatrix} I_L \\ I_R \end{pmatrix}, \quad (5.14)$$

where $I_{\{L,R\}}$ is a N dimensional vector of the incoming particles in the left or right leads and $O_{\{L,R\}}$ are the outgoing solutions. The $N \times N$ matrices \mathbf{r} , \mathbf{t} encode how the solutions transform after scattering with the sample. Requiring that probability is conserved means that $S^\dagger S = \mathbb{1}$. In terms of the reflection and transmission matrices, this requirement states that,

$$\sum_{n'} |r_{nn'}|^2 + |t'_{nn'}|^2 = 1, \quad (5.15)$$

for any n where n, n' index the $N \times N$ matrix. Each channel in the system must either reflect or transmit. Often there is time-reversal symmetry so the complex conjugate of the scattering matrix, which swaps positive and negative momenta, gives another valid description of the system. From this, it follows that $S = S^T$ and $\mathbf{t} = \mathbf{t}'$.

To find the current, the idea of steady states having current that is not spatially dependent is used. Choosing to evaluate the current on the left of the sample gives,

$$\begin{aligned} I &= e \int dk \langle I_L | v | I_L \rangle - \langle O_L | v | O_L \rangle \\ &= e \int dk \langle I_L | v | I_L \rangle - \langle I_L | v \mathbf{r}^2 | I_L \rangle - \langle I_R | v \mathbf{t}^2 | I_R \rangle, \end{aligned} \quad (5.16)$$

as scattering states on the left and right side are orthogonal. Using Equation 5.15 the two I_L terms can be combined. Swapping to an energy integral and imputing the probability that the modes are occupied gives the famous Landauer result,

$$I = e \int d\epsilon \text{Tr} \left[\mathbf{t}(\epsilon) (f_L(\epsilon) - f_R(\epsilon)) \right]. \quad (5.17)$$

The trace enforces the sum over the different contributing modes. In the spinful case there are two modes, spin up and spin down, that will be decoupled from each other in the reservoirs. When the voltage across the sample is the same for both spins, and they are both perfectly transmitted, there will be a conductance of $2e^2/h$. The presence of the transmission matrix allows fractions of the conductance to appear.

5.2.1 Contact Resistance

The form of the Landauer formula in Equation 5.17 is not the only version of this formula. Another form existed that predicted infinite conductance across a 1D sample, exactly the issue brought up at the start of this thesis. The resolution of these competing equations was found by the multi-terminal Landauer-Büttiker formalism [51], which can derive both forms and was interpreted by Imry [6].

The idea is that for the two-terminal conductance measurement, the voltage is deep within the contacts and not in the leads. The voltage drop, and therefore the dissipation, in the ballistic regime occurs at the interface of the leads and the higher-dimensional contacts. Although the contacts are reflectionless, this does not preclude electrons from being reflected when trying to enter the leads. This ‘filtering out’ of many electrons in the contacts to a few in the leads is the source of resistance - measuring the voltage within the leads will not include this. The multi-terminal geometry can reproduce the infinite result with voltage probes actually measuring the voltage in the sample.

The explicit value of the resistance can be found through using the Landauer formula $G^{-1} = h/2e^2 M$, where M is the number of transport channels. The resistance decreases with the number of modes participating in transport, which is why the effect only matters at the quantum level. The resistance for a single mode is approximately $12.9k\Omega$. In a ballistic system with a few modes, any description of two-terminal conductance must explicitly take into account the contacts. This idea will be used when calculating the conductance through a Luttinger liquid in the next chapter.

5.3 Non-Equilibrium

The previous two sections explored ways to side-step the full non-equilibrium description. Now the coupling to the leads will be explicitly considered, removing the need to introduce leads that transmit perfectly. This section follows work done by Meir and Wingreen [52, 53] to develop an expression for the current through a generic interacting 1D region. Unlike this chapter thus far, where intuition where intuition and concepts were introduced, this section is purely an exercise in QFT fluency.

The system under consideration shares many features with the Landauer setup but does not contain the leads, with the reservoirs now directly tunnelling into the system. The sample will now be taken to not have a continuum of states but a discrete spectrum, meaning we are dealing with a quantum dot. Firstly, the Hamiltonian of the system needs to be split up into these

different sections,

$$\begin{aligned}
 H &= H_{reservoir}^L + H_{dot} + H_{reservoir}^R + H_{tun} \\
 &= \sum_k \epsilon_k^L c_{L,k}^\dagger c_{L,k} + \sum_q E_q d_q^\dagger d_q + \sum_k \epsilon_k^R c_{R,k}^\dagger c_{R,k} \\
 &\quad + \sum_{k,q} V_{L,q,k} (c_{L,k}^\dagger d_q + d_q^\dagger c_{L,k}) + V_{R,q,k} (c_{R,k}^\dagger + d_N^\dagger c_{R,k}).
 \end{aligned}$$

The operators $c_{\alpha,k}$, where $\alpha = \{L, R\}$, destroy an electron in the left/right reservoirs with a momentum k . Assuming that the leads are given by a Fermi gas (or liquid with a renormalised mass/charge) results in ϵ_k^α being a quadratic dispersion. The other set of operators, d_q , describe creating and destroying electrons in the sample, expressed in terms of their eigenvalues q . For the moment, spinless fermions will be considered but this formalism can be generalised to more channels.

Tunnelling into the system occurs with an electron in the α reservoir with momentum k becoming the eigenstate q in the dot. The strength of that hopping is given by $V_{q,k}^\alpha$. The current can be defined from the continuity equation to be the quantum average of the time derivative of the number of electrons, $J_\alpha \equiv -e \langle \dot{N}_\alpha \rangle$. The number of fermions in the α reservoir is $N_\alpha = \sum_k c_{\alpha,k}^\dagger c_{\alpha,k}$. Using the Heisenberg equation of motion, where $\hbar = 1$,

$$\begin{aligned}
 J_\alpha &= -ie \langle [H, N_\alpha] \rangle \\
 &= -ie \left\langle \sum_{k',q} [V_{q,k'}^\alpha (c_{\alpha,k'}^\dagger d_q + d_q^\dagger c_{\alpha,k'}), \sum_k c_{\alpha,k}^\dagger c_{\alpha,k}] \right\rangle = ie \sum_{k,q} V_{q,k}^\alpha (\langle c_{\alpha,k}^\dagger d_q \rangle - \langle d_q^\dagger c_{\alpha,k} \rangle).
 \end{aligned}$$

The only non-zero commutator of N_α will be with the tunnelling part of the Hamiltonian as c commutes with d and $[N_\alpha, c_{L,k}^\dagger c_{L,k}] = 0$. Using functional integration to express these averages, the quantum Hamiltonian is changed into an action with classical fields ψ_k, ϕ_q where

$|\psi_{\alpha,k}\rangle = e^{\psi_{\alpha,k} c_{\alpha,k}^\dagger} |0\rangle$ and $|\phi_q\rangle = e^{\phi_q d_q^\dagger} |0\rangle$. This results in an action of,

$$S[\psi, \phi] = S_{res}^L + S_{wire} + S_{res}^R + S_{tun}, \quad (5.18)$$

$$S_{res}^\alpha = \int_K dt \int_{K'} dt' \sum_k \bar{\psi}_{\alpha,k}(t) g_{\alpha,k}^{-1}(t, t') \psi_{\alpha,k}(t'), \quad (5.19)$$

$$S_{wire} = \int_K dt \int_{K'} dt' \sum_q \bar{\phi}_q(t) X_q^{-1}(t, t') \phi_q(t'), \quad (5.20)$$

$$S_{tun} = \sum_{\alpha, k, q} \int_K dt V_{q,k}^\alpha (\bar{\psi}_{\alpha,k}(t) \phi_q(t) + \bar{\phi}_q(t) \psi_{\alpha,k}(t)). \quad (5.21)$$

The time integral is taken along the Keldysh contour as the system is not guaranteed to be in equilibrium. The Green's functions of the isolated reservoirs and dot are given by g and X respectively. The Green's functions can be expressed as averages over parts of the action,

$$ig_{\alpha,k}(t, t') = \langle \psi_{\alpha,k}(t) \bar{\psi}_{\alpha,k}(t') \rangle_{S_{res}^\alpha}, \quad iX_q(t, t') = \langle \phi_q(t) \bar{\phi}_q(t') \rangle_{S_{wire}}. \quad (5.22)$$

Introducing a source field into the action allows the current to be expressed as a derivative with respect to this source field,

$$\begin{aligned} J_\alpha &= \frac{1}{\mathcal{Z}} \int \mathcal{D}\psi \mathcal{D}\phi \sum_{k,q} \frac{ieV_{q,k}^\alpha}{\hbar} (\bar{\psi}_{\alpha,k} \phi_q - \bar{\phi}_q \psi_{\alpha,k}) e^{iS} \\ &= \frac{1}{\mathcal{Z}} \frac{\delta}{\delta A_\alpha} \int \mathcal{D}\psi \mathcal{D}\phi \exp \left(iS + \sum_\alpha \int_K dt A_\alpha(t) j_\alpha(t) \right) \Big|_{A_\alpha=0} \end{aligned} \quad (5.23)$$

$$\text{where } j_\alpha(t) = \sum_{k,q} ieV_{q,k}^\alpha (\bar{\psi}_{\alpha,k}(t) \phi_q(t) - \bar{\phi}_q(t) \psi_{\alpha,k}(t)), \quad \mathcal{Z} = \int \mathcal{D}\psi \mathcal{D}\phi e^{iS}.$$

5.3.1 Integrating Out Quadratic Fields

One of the most useful features of functional integrals is that an effective description of the problem can be obtained by integrating out quadratic fields. As the dot is the object that is of most interest, the two reservoir actions will be integrated out. Performing the integral of the left

reservoir first and denoting part of the action as I ,

$$\begin{aligned} I &= \int \mathcal{D}\psi^L \exp\left(i(S_{res}^L + S_{tun}^L) + \int_K dt A_L(t) j_L(t)\right) \\ &= \int \mathcal{D}\psi^L \exp\left(iS_{res}^L + i \sum_{k,q} \int_K dt V_{L,q,k} (\bar{\psi}_{L,k} \phi_q (1 + eA_L) + \bar{\phi}_q \psi_{L,k} (1 - eA_L))\right). \end{aligned}$$

Shifting the fields in the following way,

$$\begin{aligned} \psi_{L,k}(t') &\rightarrow \psi_{L,k}(t') - \sum_q V_{L,q,k} \int dt_1 g_{L,k}(t_1, t') \phi_q(t_1) (1 - eA_L(t_1)) \\ \bar{\psi}_{L,k}(t) &\rightarrow \bar{\psi}_{L,k}(t) - \sum_q V_{L,q,k} \int dt_2 g_{L,k}(t, t_2) \bar{\phi}_q(t_2) (1 + eA_L(t_2)) \end{aligned}$$

allows the usual quadratic action functional integral formula of Equation A.3 to be used. A change of the position of the minimum does not affect the Gaussian integral result so I becomes,

$$\begin{aligned} I &= \int \mathcal{D}\psi_L e^{iS_{res}^L} \\ &\times \exp\left(-i \sum_{k,q,q'} \int dt \int dt' V_{L,q,k} V_{L,q',k} \bar{\phi}_q(t) (1 + eA_L(t)) g_{L,k}(t, t') \phi_{q'}(t') (1 - eA_L(t'))\right). \end{aligned}$$

The exact same process can be repeated using $\psi_{R,k}$ and A_R to give a similar result where $L \rightarrow R$, with both contributions being multiplied together. The fields in the partition function \mathcal{Z} also need to be integrated out, which won't involve adding a source field,

$$\begin{aligned} \mathcal{Z} &= \int \mathcal{D}\phi e^{iS_{wire}[\phi]} \int \mathcal{D}\psi_L e^{i(S_{res}^L[\psi_L] + S_{tun}^L[\psi_L, \phi])} \int \mathcal{D}\psi_R e^{i(S_{res}^R[\psi_R] + S_{tun}^R[\psi_R, \phi])} \\ &= \int \mathcal{D}\phi e^{iS_{wire}} \exp\left(- \sum_{\alpha, q, q', k} iV_{q,k}^\alpha V_{q',k}^\alpha \int dt \int dt' \bar{\phi}_q(t) g_{\alpha,k}(t, t') \phi_{q'}(t')\right) \\ &\quad \times \int \mathcal{D}\psi_L e^{iS_{res}^L[\psi_L]} \int \mathcal{D}\psi_R e^{iS_{res}^R[\psi_R]} \\ &= \int \mathcal{D}\phi e^{iS_{eff}} \int \mathcal{D}\psi_L e^{iS_{res}^L[\psi_L]} \int \mathcal{D}\psi_R e^{iS_{res}^R[\psi_R]}. \end{aligned} \tag{5.24}$$

The integrals over ψ_L and ψ_R will cancel out in the numerator and denominator of the current

expression. This leaves us with just the effective action,

$$S_{eff} = S_{wire} - \int_K dt dt' \sum_{\alpha, q, q', k} V_{q, k}^\alpha V_{q', k}^\alpha \bar{\phi}_q(t) g_{\alpha, k}(t, t') \phi_{q'}(t). \quad (5.25)$$

Performing the functional derivative in Equation 5.23 with the new action from integrating out the fields gives,

$$\begin{aligned} J_\alpha(t_1) &= \frac{1}{\mathcal{Z}'} \int \mathcal{D}\phi e^{iS_{wire}} \left(-i \sum_{q, q', k} V_{q, k}^\alpha V_{q', k}^\alpha \int dt \int dt' \right. \\ &\quad \times e \bar{\phi}_q(t) g_{\alpha, k}(t, t') \phi_{q'}(t') \delta(t - t_1) - e \bar{\phi}_q(t) g_{\alpha, k}(t, t') \phi_{q'}(t') \delta(t' - t_1) + O(A) \Big) \\ &\quad \times \exp \left(-i \sum_{\alpha, q, q', k} \int dt \int dt' V_{q, k}^\alpha V_{q', k}^\alpha \bar{\phi}_q(t) \left(1 + e A_\alpha(t) \right) g_{\alpha, k}(t, t') \phi_{q'}(t') \left(1 - e A_\alpha(t') \right) \right) \Big|_{A_\alpha=0} \\ &= -\frac{ie}{\mathcal{Z}'} \int \mathcal{D}\phi \left(\sum_{k, q, q'} V_{q, k}^\alpha V_{q', k}^\alpha \int dt \bar{\phi}_q(t_1) g_{\alpha, k}(t_1, t) \phi_{q'}(t) - \bar{\phi}_q(t) g_{\alpha, k}(t, t_1) \phi_{q'}(t_1) \right) e^{iS_{eff}/\hbar}, \end{aligned} \quad (5.26)$$

where $\mathcal{Z}' = \int \mathcal{D}\phi e^{iS_{eff}/\hbar}$.

5.3.2 Real-Time Expression

With the reservoir fields now integrated out, the self-energy is defined as $\Sigma_{\alpha, qq', k}(t, t') \equiv V_{q, k}^\alpha V_{q', k}^\alpha g_{\alpha, k}(t, t')$. Equation 5.26 contains averages of terms that are bilinear in the field ϕ over an effective action that includes these reservoirs. The new Green's function, $iG_{qq'}(t, t') \equiv \langle \phi_q(t) \bar{\phi}_{q'}(t') \rangle_{S_{eff}}$, describes the effective excitations of the system in the presence of the reservoirs that scatter from eigenstate q' to q . The current expression can be written as,

$$J_\alpha(t_1) = e \sum_{k, q, q'} \int_K dt G_{qq'}(t_1, t) \Sigma_{\alpha, qq', k}(t, t_1) - \Sigma_{\alpha, qq', k}(t_1, t) G_{qq'}(t, t_1). \quad (5.27)$$

The sum over q, q' is the same as taking the trace when the states are expressed in an eigenstate basis. This allows some of the indices to be dropped to give,

$$J_\alpha(t_1) = e \sum_k \text{Tr}_{qq'} \left[\int_K dt \mathbf{G}(t_1, t) \boldsymbol{\Sigma}_{\alpha, k}(t, t_1) - \boldsymbol{\Sigma}_{\alpha, k}(t_1, t) \mathbf{G}(t, t_1) \right]. \quad (5.28)$$

This expression is still over the Keldysh contour which now needs to be continued to a real-time expression. Using Langreth's theorem from Equation 3.18 and Fourier transforming gives the final expression of,

$$J_\alpha = e \sum_k \text{Tr}_{qq'} \left[\int_{-\infty}^{\infty} \frac{d\omega}{2\pi} \mathbf{G}^r(\omega) \boldsymbol{\Sigma}_{\alpha,k}^<(\omega) + \mathbf{G}^<(\omega) \boldsymbol{\Sigma}_{\alpha,k}^a - \boldsymbol{\Sigma}_{\alpha,k}^r(\omega) \mathbf{G}^<(\omega) - \boldsymbol{\Sigma}_{\alpha,k}^<(\omega) \mathbf{G}^a(\omega) \right] \quad (5.29)$$

$$= e \sum_k \text{Tr}_{qq'} \left[\int_{-\infty}^{\infty} \frac{d\omega}{2\pi} \Delta \mathbf{G}(\omega) \boldsymbol{\Sigma}_{\alpha,k}^<(\omega) - \mathbf{G}^<(\omega) \Delta \boldsymbol{\Sigma}_{\alpha,k}(\omega) \right], \quad \text{where } \Delta A \equiv A^r - A^a. \quad (5.30)$$

This expression is very general and difficult to manipulate any further without first making assumptions about the form of the coupling to the leads. In quantum dots, especially for the Coulomb blockade regime, a resonant-level model is used where the coupling to only one of the eigenstates is considered [30, 54]. Often, in order to proceed further, the kinetic equation derived in the Keldysh chapter is used to re-express $G^<$. The current in the reservoirs can also be taken to be equal in magnitude but in opposite directions and can be related using $J_L = (J_L - J_R)/2$. This allows some simplifications to be made in certain cases.

To summarise the arduous process to arrive at Equation 5.30, the current in the reservoirs is first expressed by using the continuity equation. An effective description of the isolated system that includes the effect of the reservoirs is then found. Although somewhat difficult in practice, the Green's function can then be calculated. The self-energy term contains both the coupling to the reservoirs and the Green's function of the reservoirs. Having found both of these terms, their retarded, advance, and lesser versions are found by analytically continuing from the Keldysh contour. The self-energy can all be found for all versions as the reservoirs are in equilibrium. Finding the different types of Green's function for \mathbf{G} is harder, as they are linked through the kinetic equation. Taking the trace over all modes then gives the current, from which the conductance can be found.

These three ways of calculating conductance; Kubo, Landauer, and NEGF, will be used in the following chapters of this thesis. Although this chapter has often viewed them as contrasting, these methods are flexible enough to be modified to account for their weaknesses. As an example, the Kubo formula could be rewritten using an action along the Keldysh contour which would encapsulate non-equilibrium effects. Considering the action as varying spatially would allow reservoirs to be accounted for in the Kubo formula too, which will be undertaken in Chapter 6.1.2. Even the Landauer formalism can be

CHAPTER 5. CONDUCTANCE FORMALISMS

generalised to the interacting case and described in terms of Green's functions and self-energy terms that couple to the leads. Choosing which formalism to use is more a question of taste than necessity.

Part II

Continuum

CHAPTER 6

CONDUCTANCE IN LUTTINGER LIQUIDS

Having extensively detailed many different techniques, our attention must now be laser focused on finding 1D models that can have a fractional two-terminal conductance. This chapter will focus on conductance through Luttinger liquids: an obvious place to start from due to the applicability of the model to many different physical situations.

The first task is to understand how an infinite Luttinger liquid conducts. Contacts will then be attached either side of a Luttinger liquid wire, in the knowledge that they dominate the behaviour in the ballistic regime. This compliments the original debate on relevance of contacts in the Landauer formalism, now encompassing interacting electrons. The nature of the coupling to the contact will be explored by showing that the equilibration between the Luttinger liquid and reservoir is what controls whether the conductance is fractional or not.

Manipulating the contacts is not the only way in which to generate interesting transport behaviour, as the presence of an impurity completely changes the transport properties. The behaviour of a single impurity on the conductance will be investigated in detail next, as this calculation will form a foundational basis for the more complex situations that will be considered going forwards. This requires the use of the renormalisation group (RG) technique which is introduced in Appendix D.

Furnished with the knowledge of how one channel is affected by an impurity, we can consider impurities in multi-channel Luttinger liquids. For certain impurities, a fractional conductance will be achieved

by completely reflecting a portion of the affected channels. There is a wealth of theoretical papers analysing the response of Luttinger liquids to different types of backscattering or impurities [55, 56, 57], but our attention will be focused on a recent paper by Shavit and Oreg [58] that claims that this backscattering mechanism is the cause of the fractional plateaus observed in experiment.

6.1 Conductance of a Clean Single Channel Luttinger Liquid

6.1.1 Infinite Luttinger Liquids

As an introduction to the application of conductance techniques, the conductance of an infinite Luttinger liquid will be found using the Kubo formula developed in the Section 5.1. The first thing required is to include the electromagnetic potential into the Luttinger liquid action, which will be carried out by considering the Hamiltonian and using minimal coupling. The Hamiltonian can be obtained through performing the usual Legendre transformation on the action where $\Pi = \delta S / \delta(\partial_t \theta)$. The two quantities are related¹ as,

$$S = \int dt dx \mathcal{L}(\theta(x, t), \partial_t \theta(x, t)) = \int dt dx \left(\Pi(x, t) \partial_t \theta(x, t) - \mathcal{H}(\theta(x, t), \Pi(x, t)) \right). \quad (6.1)$$

The Hamiltonian with the shift will be, suppressing the field dependencies,

$$H(\Pi, \theta) = \int dx \frac{\nu K}{2\pi} (\pi \Pi - eA)^2 + \frac{\nu}{2\pi K} (\partial_x \theta)^2, \quad (6.2)$$

where minimal coupling causes $\Pi \rightarrow \Pi + eA/\pi$. The factor of π comes from actually performing the substitution on the derivative of the phase field that is the conjugate to the density θ , $\partial_x \phi = \pi \Pi$. This can now be put back into the action $S[A, \Pi, \theta]$ by introducing the $\Pi \partial_t \theta$ term again. In imaginary time, this

¹A technical point is that there is some subtlety about going between the formalisms as a specific time point is chosen, and hence the disappearing of the time integral in the Hamiltonian formulation. As it is only a brief detour, these will be not dealt with explicitly - plus the Hamiltonian is a constant of the motion anyway!

6.1. CONDUCTANCE OF A CLEAN SINGLE CHANNEL LUTTINGER LIQUID

term will become $i\Pi(x, \tau)\partial_\tau\theta(x, \tau)$. The response can be calculated using Equation 5.7, which gives,

$$\begin{aligned}\chi(x, x', \tau, \tau') &= -\frac{1}{Z} \frac{\delta^2}{\delta A \delta A} \int \mathcal{D}\theta e^{-S[A, \Pi, \theta]} \Big|_{A=0} \\ &= \frac{1}{Z} \int \mathcal{D}\theta \frac{\delta}{\delta A} \left[\frac{e\nu K}{\pi} (\pi\Pi - eA) e^{-S[A, \Pi, \theta]} \right] \Big|_{A=0} \\ &= -e^2 \nu^2 K^2 \langle \Pi(x, \tau) \Pi(x', \tau') \rangle_{S[A=0, \Pi, \theta]} + \frac{e^2 \nu K}{\pi} \delta(x - x') \delta(\tau - \tau'),\end{aligned}\quad (6.3)$$

where the field dependencies have been put back in on the final line. The delta functions occur due to the second functional derivative acting on the field $A(x', t')$ in the coefficient of the exponential of the action. This term is known as the diamagnetic part as it can be traced back to the A^2 term that is produced by minimal coupling, which results in a contribution to the current that is proportional to the field. This is in contrast to the paramagnetic part, which is the current at $A = 0$ and is the first term in Equation 6.3.

The average can be calculated [32] by introducing a source field,

$$\begin{aligned}\langle \Pi(x, \tau) \Pi(x', \tau') \rangle_{S[\Pi, \theta]} &= \frac{1}{Z} \frac{\delta^2}{\delta B \delta B} \int \mathcal{D}\Pi \mathcal{D}\theta \exp \left(-S[\Pi, \theta] + \int dx d\tau \Pi(x, \tau) B(x, \tau) \right) \\ &= \frac{1}{Z'} \frac{\delta^2}{\delta B \delta B} \int \mathcal{D}\theta \exp \left(\frac{1}{2\pi\nu K} \int dx d\tau (i\partial_\tau\theta + B)^2 - \nu^2 (\partial_x\theta)^2 \right) \\ &= -\frac{\langle \partial_\tau\theta(x, \tau) \partial_\tau\theta(x', \tau') \rangle}{\pi^2 \nu^2 K^2} + \frac{1}{\pi\nu K} \delta(x - x') \delta(\tau - \tau').\end{aligned}\quad (6.4)$$

This results in a susceptibility of,

$$\chi(x, x', \tau, \tau') = \frac{e^2}{\pi^2} \langle \partial_\tau\theta(x, \tau) \partial_\tau\theta(x', \tau') \rangle_{S[\theta]}. \quad (6.5)$$

This cancellation of the diamagnetic part should be expected as the original model has a linearised fermionic spectrum, which upon minimal coupling will only generate terms linear in A . This cancellation is true for all non-superconducting electronic states, although the proof gets more involved than the natural cancellation presented here. It generically occurs in Fermi liquids because of the analyticity properties when continuing the paramagnetic term back to real time [28]. An alternative operator approach in Luttinger liquids is shown by Shankar, where integration by parts acts on the time-ordering operator to cancel the diamagnetic term [59].

The susceptibility above has been calculated in imaginary time. The final result should be in real-time and must be causal as was explained in Chapter 5.1. The imaginary-time Matsubara frequencies, $\bar{\omega}$,

must be continued to the retarded two-point average by setting $i\bar{\omega} \rightarrow \omega + i\delta$. The conductivity can be found through dividing the calculated susceptibility by $\bar{\omega}$ giving,

$$\sigma(x, x'; \bar{\omega}) = \frac{e^2}{\bar{\omega}\pi^2} \int_0^\beta d\tau \langle \partial_\tau \theta(x, \tau) \partial_\tau \theta(x', 0) \rangle e^{i\bar{\omega}t}. \quad (6.6)$$

Performing integration by parts twice, the conductivity becomes related to the two-point correlator of the θ fields,

$$\sigma(x, x'; \bar{\omega}) = -\frac{e^2 \bar{\omega}}{\pi^2} \int_0^\beta d\tau \langle \theta(x, \tau) \theta(x', 0) \rangle e^{i\bar{\omega}t} = -\frac{e^2 \bar{\omega}}{\pi^2} G_{\bar{\omega}}(x, x'). \quad (6.7)$$

The action of a Luttinger liquid is quadratic in the fields, so this correlator is the Green's function of the action that has been Fourier transformed into frequency. In general, the Luttinger parameters ν, K can vary in space so the Green's function of a Luttinger liquid must satisfy,

$$\left(-\partial_x \frac{v(x)}{\pi K(x)} \partial_x + \frac{\bar{\omega}^2}{\pi v(x) K(x)} \right) G_{\bar{\omega}}(x, x') = \delta(x - x'). \quad (6.8)$$

There is a sign change from what would be expected from Equation 4.26 due to the rotation into imaginary time. When the parameters do not vary in space, there is translational invariance. A Fourier transform can then be taken to obtain,

$$G(q, \omega) = \left[\frac{1}{(\bar{\omega} - i\nu q)(\bar{\omega} + i\nu q)} \right] \pi \nu K \implies G(x - x'; \bar{\omega}) = \frac{-\pi K}{2\bar{\omega}} e^{-i\bar{\omega}|x-x'|/\nu}, \quad (6.9)$$

where a contour integral has been performed to go from momentum to position space. The conductivity reduces to,

$$\sigma(x, x'; \bar{\omega}) = \frac{e^2 K}{2\pi} e^{-i\bar{\omega}(x-x')/\nu}. \quad (6.10)$$

The continuation back to real-time of the conductivity can be performed without any issues $i\bar{\omega} \rightarrow \omega + i\delta$, due to the cancellation of the diverging part.

To find the conductance from the conductivity, the total current must be found. This is defined to be,

$$I(x, t) = \int_0^L dx' \int \frac{d\omega}{2\pi} e^{i\omega t} \sigma_\omega(x, x') E_\omega(x'). \quad (6.11)$$

where ω without the bar corresponds to the frequency of the perturbing electric field. A static electric

field over the entire system will be given by $E_\omega(x) = 2\pi\delta(\omega)\partial_x V(x)$, where the factor of 2π eliminates the one that comes with the now redundant Fourier transform. This results in,

$$I(x) = \frac{Ke^2}{2\pi} (V(L) - V(0)). \quad (6.12)$$

This reproduces the quantum of conductance e^2/h (as the scaling $\hbar = 1$ or $h = 2\pi$ has been used throughout) renormalised by the Luttinger parameter. The situation, however, is more complex than this infinite translationally invariant result suggests, with the analysis requiring the inclusion of the process by which the system changes from higher dimensions into 1D.

6.1.2 Including Reservoirs

When applying the Landauer result to ballistic transport, the importance of the contacts was stressed. The infinite Luttinger liquid cannot incorporate contacts, so a finite length of Luttinger liquid will now be investigated.

There are multiple ways of imbuing the effects of the reservoirs into the mathematics. One of the most popular ways was pioneered by Maslov and Stone [60], and Ponomarenko [61]. They consider a spatially varying Luttinger parameter because the reservoirs are modelled as a 1D Fermi gas, which corresponds to $K = 1$. Despite the instability of a Fermi gas in 1D, which was explained in Chapter 4.1, this is permitted as the reservoirs are higher-dimensional which stabilises the state. The inflow of particles into the sample will be on one line, with particles off this line being reflected at the contact, so the modelling as 1D captures this aspect. The system is split into three regions; two outside regions where $K_L = 1$, and the wire that connects these that has a Luttinger parameter of K_W . If an adiabatic connection between the parts is assumed, the parameter will then change sharply at the boundaries of the section. The spatial variation of the Luttinger parameters is displayed in Figure 6.1.

This spatial variation results in the conductance not being renormalised by the interactions. Due to the breaking of translational invariance by the spatial dependence of the parameters, Equation 6.8 now has to be fully solved to show this lack of renormalisation. Away from $x = 0, x', L$, the parameters are all constants and the differential equation is homogeneous,

$$\partial_x \frac{v(x)}{K(x)} \partial_x G_{\bar{\omega}}(x, x') = \frac{\bar{\omega}^2}{v(x)K(x)} G_{\bar{\omega}}(x, x'), \quad (6.13)$$

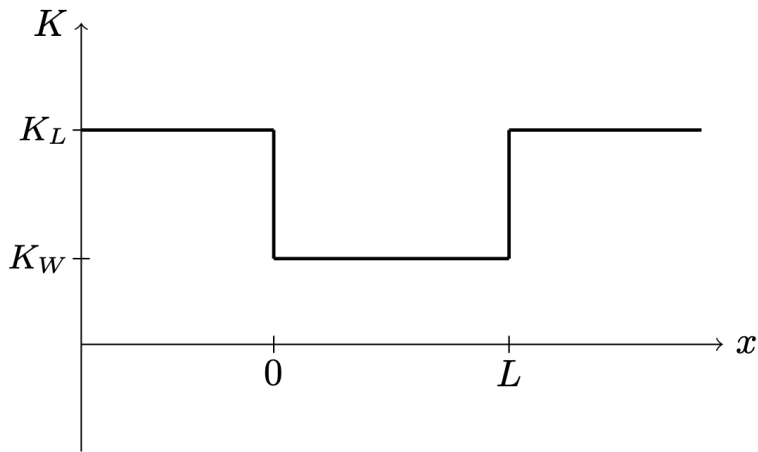


Figure 6.1: The Luttinger parameter is made to vary spatially, to reach a value of $K_L = 1$ in the contacts and K_W in the wire which is chosen to be for $0 \leq x < L$.

which has solutions of $G_{\bar{\omega}}(x, x') \sim e^{\pm \bar{\omega}x/v(x)}$. In the definition of current in Equation 6.11, x' is only considered in the wire. Therefore there will be four different regions in x for a fixed x' to consider; the two Green's functions in the wire and reservoir where $x < x'$ and the two on the right where $x > x'$. The total Green's function is,

$$G_{\bar{\omega}}(x, x') = \begin{cases} Ae^{\bar{\omega}x/v_L}, & x \leq 0, \\ Be^{\bar{\omega}x/v_W} + Ce^{-\bar{\omega}x/v_W}, & 0 < x \leq x', \\ De^{\bar{\omega}x/v_W} + Ee^{-\bar{\omega}x/v_W}, & x' < x \leq L, \\ Fe^{-\bar{\omega}x/v_L}, & x > L, \end{cases} \quad (6.14)$$

where the diverging solutions are left out. The constants in the above equation are determined by the boundary conditions, although they will only be constant for a specific value of x' - changing x' will change the ‘constants’. One of the boundary conditions that specify these ‘constants’ is that the Green’s function must be continuous everywhere. Any discontinuity would be expressed with a step function, which would result in the derivatives of delta function appearing on the right hand side of Equation 6.8. Therefore $G_{\bar{\omega}}(x, x')$ will be continuous at $x = 0, x', L$.

The boundary condition on the derivatives can be found by integrating Equation 6.8 over a small

width 2δ . For $y = \{0, x', L\}$,

$$\int_{y-\delta}^{y+\delta} dx \left(-\partial_x \frac{v}{\pi K} \partial_x + \frac{\bar{\omega}^2}{\pi v K} \right) G_{\bar{\omega}'}(x, x') = \int_{y-\delta}^{y+\delta} \delta(x - x'). \quad (6.15)$$

Considering that the $\bar{\omega}^2$ term on the left hand side is continuous, the $\delta \rightarrow 0$ limit will have no contribution from that term. The boundary condition on the derivatives becomes,

$$\left[\frac{v(x)}{\pi K(x)} \partial_x G(x, x') \right]_{y=0}^{y=0} = \begin{cases} 0 & \text{for } y = 0, L \\ 1 & \text{for } y = x' \end{cases}. \quad (6.16)$$

Solving the problem

Substituting the full problem into the boundary conditions at $x = 0, L$, results in the following equations,

$$\begin{aligned} A &= B + C, & F &= D e^{\bar{\omega}L(1/v_K+1/v_L)} + E e^{-\bar{\omega}L(1/v_K-1/v_L)} \\ \frac{K_W}{K_L} A &= B - C, & \frac{K_W}{K_L} &= E e^{-\bar{\omega}L(1/v_K-1/v_L)} - D e^{\bar{\omega}L(1/v_K+1/v_L)}. \end{aligned}$$

To be mathematically safe, the constants E, D could be redefined to include their $\bar{\omega}$ dependent coefficients but they will all tend to unity as in the d.c. limit², $\bar{\omega} \rightarrow 0$. Therefore, they shall be ignored, but a full treatment at finite frequencies must include these terms. These now give,

$$B = -C\tilde{K}, \quad E = -D\tilde{K}, \quad \text{where } \tilde{K} = \frac{1 + \frac{K_W}{K_L}}{1 - \frac{K_W}{K_L}}, \quad (6.17)$$

which defines the two functions inside the wire either side of the point $x = x'$,

$$y_L = C(e^{-\bar{\omega}x/v_W} - \tilde{K}e^{\bar{\omega}x/v_W}), \quad y_R = D(e^{\bar{\omega}x/v_W} - \tilde{K}e^{-\bar{\omega}x/v_W}). \quad (6.18)$$

Joining up two solutions with a discrete step in the derivative is done by evaluating y_L, y_R and their

²The precise limit here is $\omega \rightarrow 0$, and the continuation to $\omega + i\delta$ should be performed first. But as seen in the infinite case, these limits are equivalent.

derivatives at $x = x'$. This gives,

$$G_{\bar{\omega}}(x, x') = \frac{1}{W(x)} \Big|_{x=x'} \left(\theta(x' - x) y_L(x) y_R(x') + \theta(x - x') y_R(x) y_L(x') \right),$$

$$W(x) = \frac{v_W}{\pi K_W} (y'_L(x) y_R(x) - y'_R(x) y_L(x)).$$

The Wronskian $W(x')$ becomes $-2\bar{\omega}CD(1 - \tilde{K}^2)/\pi K_W$ when the solutions are substituted in. The numerator contains the sum of exponentials that depend on $\pm x \mp x'$. Again appealing to the $\bar{\omega} \rightarrow 0$ limit allows the exponentials to be ignored to give,

$$G_{\bar{\omega} \rightarrow 0}(x, x') = -\frac{\pi K_W (1 - \tilde{K})^2}{2\bar{\omega} (1 - \tilde{K}^2)} = -\frac{\pi K_L}{2\bar{\omega}}. \quad (6.19)$$

In the d.c. limit, the Green's function becomes independent of both x, x' and the dependence of K_W cancels out. The conductance becomes,

$$G = K_L e^2 / 2\pi. \quad (6.20)$$

The order of the $\omega \rightarrow 0$ and $q \rightarrow 0$ limits is what causes the difference between this result and that of Equation 6.12. This is because there is a finite size associated with the frequency ω which corresponds to the distance travelled by an excitation in time $1/\omega$ [32]. This distance is $L_\omega = v/\omega$ and a finite system that has an applied static field corresponds to $L \ll L_\omega$. In obtaining Equation 6.20, the finite length of the Luttinger liquid section was not taken to infinity at any point, therefore the $\omega \rightarrow 0$ limit was performed first. In the derivation of Equation 6.12, the integral over q was performed before the ω integral, meaning that the $q \rightarrow 0$ limit was taken first and the opposite regime, $L \gg L_\omega$, is considered.

Incorporating the effects of the reservoirs by spatially modulating the Luttinger parameter, is a popular method due to its numerical applicability. Safi and Schultz [62] presented an alternative view of the problem by looking at multiple reflections of a wavepacket incident upon this spatial variation of parameters, generalising the Landauer approach for interacting systems. Kuwabata [63] developed a more physical understanding, considering that the conductance of e^2/h was due to the renormalisation of the voltage drop. This complements the approach that Egger and Grabert took [64, 65] in which the effects of the reservoirs amount to boundary conditions on the displacement field of the Luttinger liquid.

6.1.3 Equilibrating with Contacts

Despite the reasoning of the previous section, there is a way to obtain fractional two-terminal conductance in a Luttinger liquid but it requires the contacts to fully equilibrate with the Luttinger liquid. This can be seen by relaxing our strict adherence to 1D systems and considering the fractional quantum Hall effect in 2D. A chiral Luttinger liquid, where the two directions of movers are spatially separated, lives on the edge of a sample in the fractional quantum Hall state [46, 66]. The presence of gapless modes on the edge of the sample is guaranteed due to the bulk-boundary correspondence in topological condensed matter.

Due to the spatial separation of the directions, the description is not exactly the Luttinger liquid action that we are used to, but can be derived from it. Starting from the Hamiltonian, the transformation

$$\tilde{\phi}_R = K\theta - \phi, \quad \tilde{\phi}_L = K\theta + \phi, \quad (6.21)$$

can be seen to decouple the problem into new ‘left’ and ‘right’ movers [67]. The density of these fields can be defined to give a Hamiltonian,

$$H = \frac{\pi\nu}{K} \int dx \tilde{\rho}_L^2 + \tilde{\rho}_R^2, \quad \tilde{\rho}_{R,L} = \pm \frac{1}{2\pi} \partial_x \tilde{\phi}_{R,L}. \quad (6.22)$$

If the fields were being treated as operators, they would now commute between each other. All fields with a tilde over them should now be understood as operators. The commutation relation of the fields is given as,

$$[\tilde{\phi}_\eta(x), \tilde{\phi}_{\eta'}(x')] = \delta_{\eta\eta'} i\pi K \text{sgn}(x - x'), \quad \Rightarrow \quad \tilde{\Pi}_\eta = -\frac{1}{2\pi K} \partial_x \tilde{\phi}_\eta. \quad (6.23)$$

The conjugate momenta can be calculated from the commutation relation. The commutation between the types of movers means that, when the Heisenberg equation of motion is used to find the time dependence of these densities, they only depend on their respective field. These modes propagate without any notice of the other. The equation of motion is in the form of a continuity equation,

$$\partial_t \tilde{\rho}_{R,L} \pm \nu \partial_x \tilde{\rho}_{R,L} = 0, \quad \Rightarrow \quad J_{R,L} = \nu \tilde{\rho}_{R,L}. \quad (6.24)$$

To calculate the current of these new states, we again use the continuity equation to obtain, $J_{R,L} =$

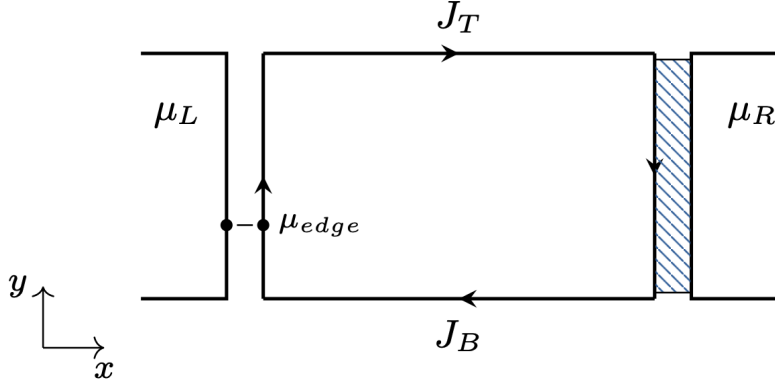


Figure 6.2: This figure depicts the way that contacts couple to the chiral edge mode of the fractional quantum Hall state in the Hall bar geometry. The two types of contacts are defined by how many points along the sides connect the system to the reservoir - either there is a single point where this occurs or there is a continuum of them. The various quantities used in the derivation are placed in their appropriate location.

$\pm \partial_t \tilde{\phi}_{R,L}/2\pi$. Setting $\delta H = - \int dx e \mu \tilde{\rho}_L$, the current can be calculated from using the Heisenberg equation of motion on $\tilde{\phi}_L$ which produces,

$$J = \frac{eK}{2\pi} \mu. \quad (6.25)$$

This would result in the renormalised conductance, which is expected as there is no Fermi reservoirs to change the result from the one obtained for an infinite Luttinger liquid. However, as was seen in the previous section, the addition of reservoirs can completely change the behaviour.

For a Hall bar geometry, the 2DEG electron gas is a rectangle that is connected to reservoirs on the shorter sides of the rectangle. The 1D current flows around the edge of the system in a direction determined by the applied magnetic field. Therefore the L, R notation will be dropped as only one direction is considered. Two different types of contacts with the reservoir will be considered - single points and a continuum of contacts [68, 69]. The setup of the system is shown in Figure 6.2, with both possible types of coupling shown.

To model the injected current, a term can be added to the continuity equation,

$$\partial_t n + \partial_x j = I_c, \quad (6.26)$$

where I_c denotes the contributions from particles tunnelling into the edge. The operator that creates a particle in the chiral Luttinger liquid is given by the bosonisation formula for the chiral field $e^{i\tilde{\phi}}$. The effect of this operator on the number of particles can be calculated through the commutator,

$$[\tilde{\rho}(x), e^{i\tilde{\phi}(x')}] = [-K \int^x dx_1 \tilde{\Pi}(x_1), e^{i\tilde{\phi}(x)}] = -Ke^{i\tilde{\phi}(x)}. \quad (6.27)$$

Acting all the terms on a generic state with n particles of charge e , shows that $e^{i\tilde{\phi}}$ removes eK of charge from the system. Due to the ‘mixing up’ of the interactions and fermionic field in Equation 6.21, the fields now describe fractional charges. Equivalently, $e^{-i\tilde{\phi}}$ inserts a charge of eK into the system. Whether these fractional charges are quantum mechanically sharply defined as fractional particles or whether this represents a splitting of the probabilities is a subtle question due to the gapless nature of the excitations [70]. For our purposes, the distinction is not important so it is left as a side note.

The operator $e^{-i\tilde{\phi}/K}$ will therefore insert a whole fermion into the system. This restricts what values of K correspond to a model of the edge excitations of a fractional quantum Hall state by requiring that $e^{-i\tilde{\phi}/K}$ must anti-commute with itself. This results in the requirement that $1/K$ must be an odd integer [46].

Therefore the tunnelling operator, acting a point y along the edge of the sample, will be given by,

$$\hat{I}_c = -t_0 \psi(y) e^{-i\phi(y)/K} \delta(y) + \text{h.c.}, \quad (6.28)$$

where $\psi(y)$ destroys an electron in the reservoir. This non-linear operator cannot be put into the continuity equation as it is, but an averaged version which will be a good approximation in the $t_0 \rightarrow 0$ incoherent tunnelling limit, can be used in the continuity equation.

The average tunnelling contribution becomes the contact conductance, G_c , multiplied by the voltage drop upon entering the edge. The chemical potential at the edge can be calculated by rearranging the previously calculated current, $j = Ke\mu/2\pi$. The contribution from the tunnelling at each contact $\{y_i\}$ will be,

$$I_c = \sum_i \delta(y_i) G_c \left(\mu_{L,R}(y_i) - 2\pi j(y_i)/eK \right). \quad (6.29)$$

In the case of a single contact either side, the continuity equation can be integrated from 0 to W for both edges in contact with the reservoirs, where W is the width of the sample. This results in two

equations that both contain the difference between current at the top and bottom of the sample. On the left side, the current becomes,

$$\int_0^W \partial_y J(y) = J_T - J_B = G_c \left(\mu_L - \frac{hJ_B}{eK} \right). \quad (6.30)$$

Finding a similar equation for the right contact allows the total current $I = J_T - J_B$ to be found as,

$$I_{point} = \frac{\frac{G_c}{2}(\mu_L - \mu_R)}{1 - \frac{G_c h}{eK}}, \quad (6.31)$$

where the h dependence has been put back in. The limit that the contact conductance is small, $G_c \ll e/h$, reproduces the unrenormalised conductance result of the previous section. This condition will often be satisfied as the contact resistance is inversely proportional to the number of modes.

Considering the conductance per unit length $\sigma_c = G_c/W$, the continuity equation now can be solved via an integrating factor to give the generic result for both reservoirs,

$$I_{cont}(y) = \frac{eK}{h}(\mu_L - \mu_R) + (J(0) + (\mu_L - \mu_R)eK/h)e^{-\frac{eK}{h\sigma_c}y}. \quad (6.32)$$

If $y \gg h\sigma_c/eK$, then the second term will be negligible and the renormalised conductance of the infinite Luttinger liquid will be found. The difference in the fractional quantum Hall case and the usual Luttinger liquid comes down to whether the $\tilde{\rho}$ mode is directly coupled to in the contacts. Even if they are directly coupled, an equilibration of these modes to the chemical potentials of the reservoirs is also required for a fractional conductance to be obtained.

This concludes the analysis of a clean Luttinger liquid, where the nature of the contacts is the determining factor of whether the conductance is renormalised by the interactions in a system. Not all systems can enjoy the luxury of being free from all scattering, so the effect of backscattering and impurities on the conductance will be examined for the remainder of the chapter. The detour to chiral Luttinger liquids will now be abandoned in preference of our previous formulation of action.

6.2 Impurities in Luttinger Liquids

In the conventional Drude picture of transport, impurities are what generate the dissipation of energy contained within the finite conductance. A natural question to ask is what happens when impurities are embedded into a Luttinger liquid. This was the main investigation of the preeminent Kane and Fisher paper [71], which analyses the RG flow of the impurity strength. The renormalisation group technique is one of the most important developments in modern physics but the introduction to it has been relegated to Appendix D in this thesis.

Consider a scattering potential V_0 that only exists at $x = 0$ in a spinless Luttinger liquid. The potential will locally bias the density at a single point, contributing to the action as,

$$\mathcal{L}_{imp} = V_0 \rho(x = 0, t) = V_0 \left(\psi_L^\dagger \psi_L + \psi_R^\dagger \psi_R + \psi_L^\dagger \psi_R + \psi_R^\dagger \psi_L \right) \Big|_{x=0}. \quad (6.33)$$

After splitting up this density into left and right movers, the forward scattering terms that contain the same chirality can be absorbed into a redefinition of the Luttinger parameter. The scattering of $2k_F$ changes the directionality of the movers. When combined with its Hermitian conjugate, it produces a cosine term when bosonised. This results in the Luttinger liquid action changing into the local sine-Gordon model,

$$S = \frac{1}{2\pi\nu K} \int dx dt \left((\partial_t \theta)^2 - \nu^2 (\partial_x \theta)^2 \right) + 2 \int dt V_0 \cos(\theta(x = 0, t)). \quad (6.34)$$

A RG analysis can be performed to perturbatively determine the effect of a weak impurity at the relevant energy scales, leading to the RG flow equation of the backscattering strength,

$$V_0(b) = b^{1-K} V_0, \quad (6.35)$$

for b being the size of the slice of momentum space that has been integrated out. The momentum slice could be taken to be infinitesimal to get a differential equation, but that is not necessary for our purposes. This result, along with the rest of the RG calculations, are shown more explicitly in Appendix E. Under n iterations of the RG (until a low-energy cutoff such as temperature or length of system has been reached), the strength of the impurity at that energy will be multiplied by $b^{n(1-K)}$. Therefore if $K > 1$, then V_0 will become smaller with decreasing energy. The term is then RG irrelevant and can be ignored at low temperatures.

In the opposite case, $K < 1$, the strength of the impurity will increase at lower energies and the interaction is then RG relevant. Both of these cases will produce power law corrections to various quantities for a finite infrared cutoff. In the zero temperature case for an infinite Luttinger liquid, there is no low-energy cutoff and the RG flow will iterate indefinitely. The impurity strength will then become either infinitely large or vanishingly small. A large impurity strength violates the original assumption that the impurity is weak and therefore the whole perturbative RG process breaks down.

The contrasting case of weak tunnelling, which is equivalent to a very strong impurity, can be analysed in a similar way. Using the dual action in terms of ϕ , the effect of large impurities can be understood. This gives an RG flow equation of,

$$t(b) = b^{1-\frac{1}{K}} t_0 , \quad (6.36)$$

where t is the strength of the tunnelling and t_0 is the unrenormalised hopping. Performing the same analysis as before, the $K > 1$ regime results in the hopping matrix becoming larger with successive renormalisation. If $K < 1$ then t will tend to zero and can be ignored.

Phase Diagram of Conductance

Having established two complimentary descriptions, the behaviour of the whole system can be interpolated. Figure 6.3 shows the the RG flows of the respective parameters to small or large coupling. By positioning the two parameters as contrasting limits, the RG flows can be seen to be pointing in the same direction. This suggests that the two descriptions can be joined up to give a complete continuous phase diagram. For $K < 1$, any impurity will drastically affect the system and for an infinite wire at zero temperature, any strength impurity will eventually flow to the case where the hopping is reduced to zero. For $K > 1$, the opposite is true: no matter how strong the impurity is, there will be no effect on the zero temperature transport. Furusaki and Nagaosa investigated an impurity in a spatially varying Luttinger liquid where the reservoirs are explicitly taken into account [72]. They found that the unrenormalised conductance is still obtained in the static limit but distinct non-universal features that depend on interaction K can be seen in the system's response to finite ω perturbations.

The analysis of impurities in a Luttinger liquid was explored in detail because it forms the blueprint of how to approach multi-channel Luttinger liquids. The basic idea is that channels with an impurity can be assumed to perfectly reflect incoming modes, opening up a gap in the spectrum. Channels without

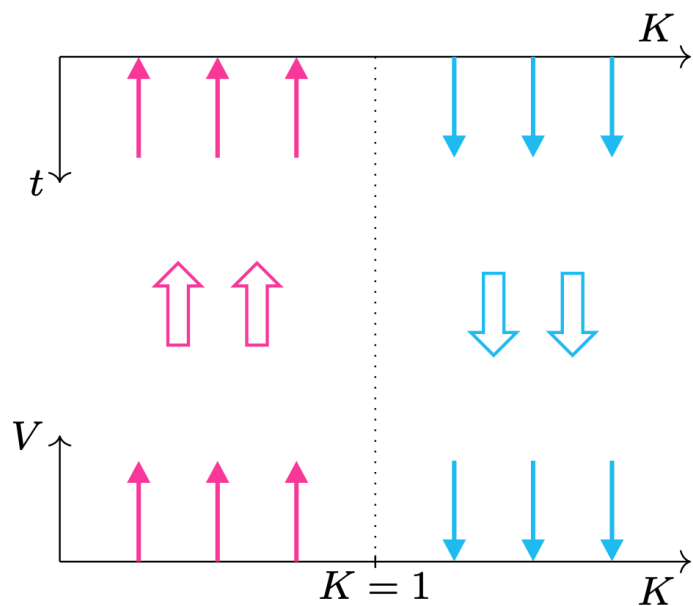


Figure 6.3: The RG flows are represented by filled arrows. Considering the single impurity problem for $K < 1$, they flow to stronger impurity strength V and weaker tunnelling for t . The opposite case is found for $K > 1$ and by continuity, shown by the outlined arrows, both regions can be joined to give the entire picture. The flows are faster the further away they are from $K = 1$, meaning that the low-energy behaviour will be reached faster for stronger interactions.

an impurity successfully carry the current through the system. The interplay of these processes causes a transmission-like effect resulting in a fraction of the conductance contributing.

6.3 Multi-channel Luttinger Liquids

A large body of scholarship has built up with the aim of understanding how many-channel Luttinger liquid behave, specifically when different types of scattering mechanisms are inserted into the system. An overarching model for two channels is one in which the spinful Luttinger Liquid Hamiltonian has a global sine-Gordon term [73],

$$H = \int dx \frac{\nu_\rho}{2\pi} \left(\frac{1}{K_\rho} (\partial_x \phi_\rho)^2 + K_\rho (\partial_x \theta_\rho)^2 \right) + \frac{\nu_\sigma}{2\pi} \left(\frac{1}{K_\sigma} (\partial_x \phi_\sigma)^2 + K_\sigma (\partial_x \theta_\sigma)^2 \right) - \int dx \lambda \cos(\sqrt{2}(n_{\rho-}\theta_\rho + n_{\rho+}\phi_\rho + n_{\sigma-}\theta_\sigma - n_{\sigma+}\phi_\sigma)) \quad (6.37)$$

where each n is a different possible integer. The naming convention comes from θ_ρ being the sum of spins but the difference between chiralities, hence the subscript $-$ in $n_{\rho-}$. The choice to use the Hamiltonian instead of the action is due to the cosine term containing higher orders of both fields, which means that functional integration cannot be performed. When only $n_{\sigma-} = 2$ is non-zero, then this matches up with Equation 4.36 and corresponds to the $g_{1\perp}$ term, which was ignored in Chapter 4.4. Note that here the cosine term extends throughout the system unlike the local version of Equation 6.35.

The origin of the cosine term comes from bosonising a generic backscattering operator, which will be expressed as a combination of the $\bar{\psi}_{\eta\sigma}, \psi_{\eta\sigma}$ fields. Each field will be bosonised to give an exponential containing different amounts of $\theta_{L\uparrow}, \theta_{L\downarrow}, \theta_{R\uparrow}, \theta_{R\downarrow}$. This specifies a vector which can be transformed to the charge-spin basis by using a matrix form of Equation 4.34,

$$\begin{pmatrix} \theta_\rho \\ \theta_\sigma \\ \phi_\rho \\ \phi_\sigma \end{pmatrix} = \frac{1}{2\sqrt{2}} \begin{pmatrix} 1 & 1 & -1 & -1 \\ 1 & -1 & -1 & 1 \\ 1 & 1 & 1 & 1 \\ 1 & -1 & 1 & -1 \end{pmatrix} \begin{pmatrix} \theta_{L\uparrow} \\ \theta_{L\downarrow} \\ \theta_{R\uparrow} \\ \theta_{R\downarrow} \end{pmatrix}. \quad (6.38)$$

This global cosine term can cause a gap to open in the spectrum, pinning the field to be such that the argument of the cosine is zero. The reason that a gap opens will be shown shortly and occurs when the

cosine term is RG relevant. Any orthogonal sectors to this will remain gapless. This will obviously result in different behaviour than the purely gapless Luttinger liquid. Not all possible backscattering terms are permitted as they must conserve charge which implies that $n_{\rho+} = 0$.

Beginning the analysis with different fermionic models results in different values for the integers. Nanowires with an external rotating magnetic field [74] will couple different spins by $\bar{\psi}_{R\uparrow}\psi_{L\downarrow}$. This leads to $n_{\rho-} = 1, n_{\sigma+} = 1$ [75]. This field can naturally arise in GaAs/AlGaAs 1D systems, though the lattice of nuclear spins interacting with the conducting fermions of the Luttinger liquid by the RKKY interaction and tending to helical order [76]. Rashba nanowires occur when the Rashba spin orbit interaction and a magnetic field combine to make a back scattering process of $(\bar{\psi}_{R\uparrow}\psi_{L\uparrow})^n \bar{\psi}_{L\downarrow}\psi_{R\uparrow}(\bar{\psi}_{R\downarrow}\psi_{L\downarrow})^n$ relevant. This corresponds to $n_{\sigma+} = 1, n_{\rho-} = 2n + 1$ for integer n [57, 77]. This is a generalisation of the rotating field which corresponds to the $n = 0$ limit of the Rashba nanowire. There are multiple possible relevant scatterings because the chemical potential of the bands can be tuned to make different processes be momentum conserving.

The result of the cosine term is to open up a gap in the spectrum. This can be shown through a semiclassical analysis of the problem that can be performed if λ is large compared to the contributions from the rest of the action. To see this, return back to Equation 4.36 which has a gapless θ_ρ that allows that part to be safely ignored. A large cosine term, $\lambda \rightarrow \infty$, will pin the value of the field to have the argument be zero, $\theta_\sigma = \pi(n + 1/2)$, as any fluctuations from the minimum will be penalised by a large contribution to the action. The field could be pinned to any value of the minima. Expanding about one of these minima to quadratic order,

$$\begin{aligned} S_\sigma &= \frac{1}{2\pi\nu_\sigma K_\sigma} \int dx dt (\partial_t \theta_\sigma)^2 + \nu_\sigma^2 (\partial_x \theta_\sigma)^2 + \frac{\lambda}{2} \int dx dt 8\theta_\sigma^2 \\ &= \frac{1}{2\pi\nu_\sigma K_\sigma} \frac{1}{\beta V} \sum_{k,\omega_n} \left(\omega_n^2 + \nu_\sigma^2 k^2 + 8\pi\nu_\sigma K_\sigma \lambda \right) \theta_\sigma^*(k, \omega_n) \theta_\sigma(k, \omega_n), \end{aligned} \quad (6.39)$$

where the constant contribution from the expansion and shifting of the fields can be ignored. For simplicity, translational invariance is assumed which allows the Fourier transform of the fields to be performed. The dispersion then can be read off as being,

$$\omega = \pm \sqrt{\nu_\sigma^2 k^2 + 8\pi\nu_\sigma K_\sigma \lambda}, \quad \Delta = \sqrt{8\pi\nu_\sigma K_\sigma \lambda}. \quad (6.40)$$

The gap Δ is the finite amount of energy required for an excitation at $k = 0$. The requirement for backscattering to be strong is not as restrictive as it seems, as an RG analysis of this term can be performed. If the term is RG relevant, then at low temperatures even a small original backscattering strength could renormalise to a regime in which the semiclassical analysis is appropriate. The size of the gap is proportional to the coupling, so will also become larger under successive renormalisation. The RG flow equation for the cosine operator, when an infinitesimal slice of momentum space is integrated out, is

$$\frac{d\lambda}{dl} = \lambda(l)(2 - D) = \lambda(2 - 2K_\sigma) \quad (6.41)$$

where D is the scaling dimension of the operator, and is equal to $2K_\sigma$. This is also derived in Appendix E. The difference between this and Equation 6.35 is the factor of two which comes from the number of dimensions being rescaled. Previously the cosine term acted at a single point, so only the time integral had to be rescaled but now both time and space have to be rescaled. This term will be relevant if $K_\sigma < 1$.

This analysis of backscattering terms can be generalised to more than just two channels which involves being more careful with the rotation of fields [56]. The problem becomes increasingly complex for more than two channels but progress can be made for certain models, such as Hsu *et al.* who tackle two spinful bands [78] with a rotating magnetic field.

6.3.1 Shavit and Oreg

To make this analysis more concrete, our attention will turn to a recent paper from Shavit and Oreg [58]. Here a two band system, which is not specified to be spin but will be notated as such for consistency with previous sections, is tuned in order to make intraband scattering between chiralities become momentum conserving. The scattering operator is

$$(\bar{\psi}_{R\uparrow}\psi_{L\uparrow})^n(\bar{\psi}_{L\downarrow}\psi_{R\downarrow})^m \sim e^{-in\theta_{R\uparrow}+in\theta_{L\uparrow}-im\theta_{L\uparrow}+im\theta_{\downarrow}}. \quad (6.42)$$

Using the rotation as defined in Equation 6.38, this corresponds to $n_{\rho-} = n - m, n_{\sigma-} = n + m$, where n, m are both integers. If the Fermi wavevector of the different bands is given by $k_{F\uparrow}, k_{F\downarrow}$, then this process will conserve momentum when $nk_{F\uparrow} \approx mk_{F\downarrow}$ which amounts to adjusting the chemical potentials of each band. This allows a wide range of fractions to materialise and notably also allows this backscattering to occur when the system is time-reversal symmetric - so without a magnetic

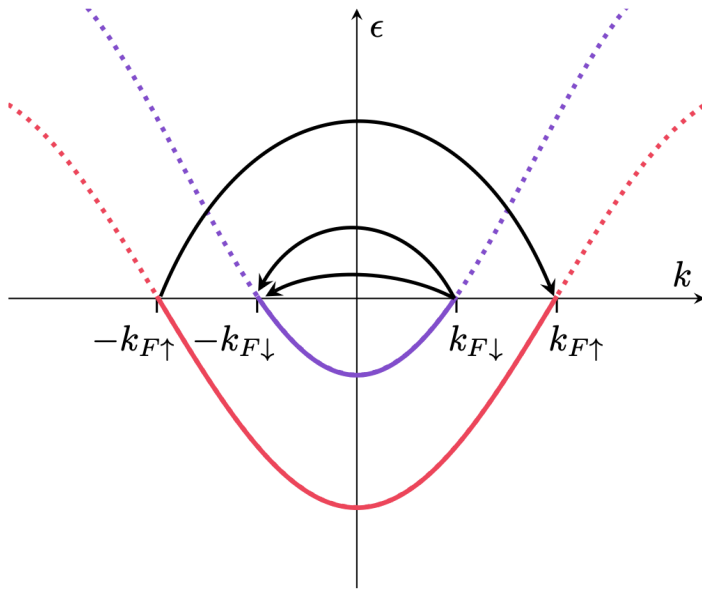


Figure 6.4: A momentum conserving backscattering process is shown for a two-channel system. The solid lines represent occupied states that are filled up to a chemical potential and the dotted lines show the unoccupied states. Two scatterings from right to left chiralities in one band counteract a single backscattering process in the other band in the opposite direction.

field! Umklapp scattering can also be considered within this formalism by having a negative n or m as $(\psi_R^\dagger \psi_L)^{-|n_1|} \equiv (\psi_L^\dagger \psi_R)^{|n_1|}$, which is a scattering in the other direction. This will conserve momentum for $nk_{F\uparrow} + mk_{F\downarrow} \approx \pi N$ for integer N . Figure 6.4 demonstrates one of the possible realisations of these scattering process when $n_1 = 1, n_2 = 2$.

Now the RG relevance of this operator can be calculated by considering the coupling strength of the operator, λ , as a small parameter. The scaling dimension of this operator, to be used in the generic RG flow equation of Equation 6.35, is

$$D = (n^2 + m^2) \frac{K_\rho + K_\sigma}{2} - nm(K_\rho - K_\sigma). \quad (6.43)$$

This result is also derived in Appendix E. If $D < 2$, then the operator is relevant and this condition can be satisfied for sufficiently strong repulsive interactions. As seen earlier, a gap will open up in the sector, $\theta_g \equiv (n\theta_1 + m\theta_2)/A$, while being gapless for $\theta_f \equiv (m\theta_1 - n\theta_2)/A$ for $A = \sqrt{n^2 + m^2}$.

At low temperatures, θ_g will be completely inaccessible for low-energy excitations. All current in these channels will be completely backscattered, while all current in ϕ_f will be mostly unobstructed. The rotation of the Luttinger liquid Hamiltonian to these new fields however does create a mixed term of

the form $\partial_x \theta_g \partial_x \theta_f$, which only causes a slight renormalisation of the gap.

6.3.2 Calculating the Conductivity

For a system that is smoothly connected to the reservoirs, the ideas of Landauer can be applied to define a scattering matrix in terms of the chiral fields for each spin species. Taking the time derivative of these fields, evaluated at $\pm\infty$, gives incoming and outgoing currents,

$$I_{\eta,\sigma} = \frac{e}{2\pi} \partial_t \theta_{\eta\sigma} \Big|_{x=\eta\infty}, \quad O_{\eta\sigma} = \frac{e}{2\pi} \partial_t \theta_{\eta\sigma} \Big|_{x=-\eta\infty}. \quad (6.44)$$

The incoming current will be the vector $(I_{L\uparrow}, I_{L\downarrow}, I_{R\uparrow}, I_{R\downarrow})^T = (\mathbf{I}_R, \mathbf{I}_L)^T$. Assuming time-reversal symmetry and the conservation of current, the incoming and outgoing chiral vectors can be related by the 2×2 scattering matrix,

$$\begin{pmatrix} O_L \\ O_R \end{pmatrix} = \begin{pmatrix} T & 1-T \\ 1-T & T \end{pmatrix} \begin{pmatrix} I_L \\ I_R \end{pmatrix}. \quad (6.45)$$

In contrast to the naming conventions of introductory Landauer section, the indices L, R , reference the direction of the movers, not the side of the sample.³. In the limit that the backscattering becomes infinitely strong under successive renormalisation, the θ_g field will be completely gapped and the θ_f field will be gapless. Therefore, there is no current in the gapped sector and perfect transmission in the orthogonal sector,

$$\frac{e}{2\pi} \partial_t \theta_g = 0, \quad \frac{e}{2\pi} \partial_t \theta_f \Big|_{x=-\infty} = \frac{e}{2\pi} \partial_t \theta_f \Big|_{x=\infty}. \quad (6.46)$$

The gapped boundary conditions become,

$$\frac{1}{A} (nI_{L\uparrow} + mI_{L\downarrow} - nO_{R\uparrow} - mO_{R\downarrow}) = 0, \quad n\frac{1}{A} (O_{L\uparrow} + mO_{L\downarrow} - nI_{R\uparrow} - mI_{R\downarrow}) = 0. \quad (6.47)$$

Defining the vector $\mathbf{n}^T = \frac{1}{A}(n, m)$, allows the transmission matrix of Equation 6.45 to be used to

³Because of the conflicting notation, the results of the Landauer section cannot be recklessly applied. This spirit of the calculation is the same but the trace of the transmission matrix as defined here is not equal to the conductance.

simplify the boundary conditions,

$$\mathbf{n}^T T(\mathbf{I}_L - \mathbf{I}_R) = 0, \quad \mathbf{n}^T T(\mathbf{I}_R - \mathbf{I}_L) = 0, \quad \Rightarrow \quad \mathbf{n}^T T = (0, 0). \quad (6.48)$$

Turning to the gapless sector boundary condition, the vector $\mathbf{m}^T = \frac{1}{A}(n, -m)$ is similarly defined to produce,

$$\mathbf{m}^T(1 - T)(\mathbf{I}_L - \mathbf{I}_R) = \mathbf{m}^T(1 - T)(\mathbf{I}_R - \mathbf{I}_L), \quad \Rightarrow \quad \mathbf{m}^T(1 - T) = 0. \quad (6.49)$$

Realising that the vectors \mathbf{n} and \mathbf{m} are actually orthogonal to each other and have been normalised all along, the following solution

$$T = 1 - \mathbf{n}\mathbf{n}^T = \begin{pmatrix} 1 - n^2/A^2 & nm/A^2 \\ nm/A^2 & 1 - m^2/A^2 \end{pmatrix}, \quad (6.50)$$

can be seen to satisfy both conditions.

Having found the transmission matrix, the total current will be

$$J = \begin{pmatrix} 1 & 1 \end{pmatrix} \cdot (\mathbf{I}_L - \mathbf{O}_R) = \begin{pmatrix} 1 & 1 \end{pmatrix} \cdot (T\mathbf{I}_R - T\mathbf{I}_L). \quad (6.51)$$

Setting the incoming current to be at a voltage V on the right, and zero voltage on the left. In this vector form, this is $\mathbf{I}_L = (0 \ 0)^T$ and $\mathbf{I}_R = e^2 V (1 \ 1)^T$. The dimensionless conductance therefore becomes,

$$g = \frac{J}{Ve^2} = \begin{pmatrix} 1 & 1 \end{pmatrix} \cdot \begin{pmatrix} 1 - n^2/A^2 & nm/A^2 \\ nm/A^2 & 1 - m^2/A^2 \end{pmatrix} \begin{pmatrix} 1 \\ 1 \end{pmatrix} = \frac{(n + m)^2}{n^2 + m^2}. \quad (6.52)$$

This is the crucial result of Shavit and Oreg's paper: the appearance of fractional values of conductance g [58]. The fractions that appear are determined by the number of backscatterings and require the strong coupling limit to be taken. The system will be time-reversal symmetric if $n + m$ is even. Remembering that setting m to $-m$ treats the corresponding umklapp processes, fractions less than e^2/h are possible,

$$g_{um} = \frac{(n - m)^2}{n^2 + m^2}. \quad (6.53)$$

The smallest possible fraction that is time-reversal symmetric occurs for $n = 1, m = 3$. Plugging these values into the conductance formula, gives, $g = \frac{2}{5}$.

This derivation of conductance from the conditions imposed by backscattering opening a gap in the spectrum and causing no current to flow can be generalised to N channels quite easily. The result is that the conductance for N channels is

$$g = \mathbf{1}_N^T (1 - \mathbf{n} \mathbf{n}^T) \mathbf{1}_N = N - \frac{(\sum_i n_i)^2}{\sum_i n_i^2}. \quad (6.54)$$

The choice to use a scattering description to obtain the conductance may seem a little odd as it is not clear whether the excitations of the Luttinger liquids (rotated ones at that) persist in the reservoir where the voltage is measured. Other papers that dealt with helical Luttinger liquids, which corresponds to $|m| = |n + 1|$ in this model, use different analysis which produce similar results. Meng *et al.* [77] explicitly solve for the current-current correlator in a spatially varying helical Luttinger liquid, as introduced in Chapter 6.1.2. Refermionisation - the opposite of bosonisation - is an exact mapping that is possible at a specific value of K [79]. This technique is used to give an exact solution that the complements the RG results that provides a description of a large area in parameter space. Assev, Loss and Klinovaja [55] analyse the sine-Gordon action of the helical wire by using the semiclassical dilute soliton gas approximation. This captures the tunnelling that is ignored in the strong coupling limit, with the conductance being found through using the Kubo formula. Solitons will be explained in most detail over the rest of this thesis. All of these other methods have reified this fractional result.

Shavit and Oreg performed this refermionisation to obtain finite temperature and length behaviour, and the similarity between their results and experiment is striking. Their results are shown in Figure 6.5. However, there are a limited number of fractions that can occur, even for systems that break time-reversal invariance. For processes involving $n = 1$ and $m = -2$, the fraction is found to be $1/5$ through Equation 6.52. Other fractions can appear, but require more total scatterings. The larger the number of scatterings, the smaller the original value of λ and the longer it takes for RG to reach the strong coupling regime.

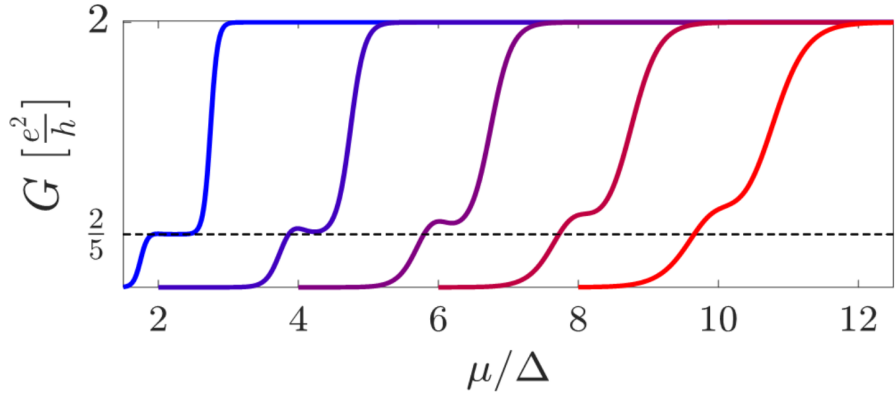


Figure 6.5: The conductance as a function of the chemical potential, and therefore the gate voltage, is plotted. Δ is the size of the gap opened by the backscattering. The different plots correspond to the conductance at different temperatures, increasing from left to right. Originally from Reference 58.

6.4 Solitons in Field Theory

The opening of gaps that was discussed in the previous section suggests that there is interesting behaviour that is missed by the gapless Luttinger liquid analysis at the start of the chapter. Therefore to end the continuum section, some results from QFT that describe solutions in the gapped sector will be discussed [80].

Fractional charge is not unique to Luttinger liquids, with the first model to display such unique behaviour being introduced by Jackiw and Rebbi [81]. They showed that a double well potential will have a classical solution, known as a soliton, that connects the two minima. These solutions satisfy the boundary condition of the field being in different minima at $x = \pm\infty$. Solitons have non-trivial topology as it costs an infinite amount of energy to change between the different possible boundary conditions, disconnecting sectors of solutions. The solitons of the model carry a fractional charge of $e/2$. To make these solutions fully quantum, the oscillations around this classical solution are quantised. These can then be excited and the soliton solution brought into the full quantum theory [82].

Su, Schrieffer and Heeger [83] discovered that this behaviour can occur in a condensed matter context while studying a model for poly-acetylene. This model has a degenerate ground state where there is an alternation of double and single bonds. For periodic boundary conditions, the degeneracy is between the double bonds being between the even and odd numbered sites or vice versa. Rotating the system by a single position transforms the solutions between each other. This degeneracy will be explored in a finite context in the next chapter.

Further analysis of solitons, that was forward by Goldstone and Wilczek, found that charges of $1/n$ could be obtained [84]. The distinction between the fractional charges in the chiral Luttinger liquid and the solitons is that the former are gapless excitations while solitons occur in gapped systems. The quick analysis of the cosine backscattering term in the previous section showed that gaps can appear in Luttinger liquid models. Multiple degenerate minima are present due to the cosine potential and solitons will describe transport in this gapped regime.

However, the question of whether these fraction charges manifest in the conductance measurements remains unclear. Some papers suggest that solitons do cause fractional conductance [85, 86], but the process by which they obtain these results is suspect. In remerging the entire system, including the Fermi gas reservoirs, the boundary conditions are changed. As learnt in Chapter 6.1.2, the behaviour of the reservoirs is crucial to the fractional conductance results, so changing their value will naturally affect the conductance.

This chapter has examined the conductance of Luttinger liquids and found that the connection to the reservoirs is crucial in determining whether the conductance is fractional or not. Deviating from the purely gapless multi-channel Luttinger liquid behaviour can provide a mechanism by which a fractional conductance can occur. There are multiple ways of realising the necessary backscattering, including one which shows time-reversal symmetric backscattering as being possible. This reflects a certain proportion of channels and produces a fractional transmission. This recreates experimental behaviour for the $2/5$ fraction, but other fractions are not accounted for.

Finally, solitons were briefly introduced in continuum field theory as the transport mechanism when the spectrum is gapped. These have been hiding in the gaps created by impurity backscattering in a Luttinger liquid. The transport of fractionally charged excitation will be the main focus of the final chapter, where solitons will be realised in a finite system and their conductance properties analysed.

Part III

Finite

CHAPTER 7

WIGNER CHAINS

The bulk of literature on fractional conductance in 1D systems comes from continuum field theories as explored in the previous chapter. This coming chapter investigates whether these results can occur in a discrete theory. Discrete here means, unlike papers that consider fermionic ladders [87], the energy spectrum is taken to be discrete and not a continuum in the direction along the wire. This discreteness of charge has been the focus of work on quantum dots in the Coulomb blockade regime [88]. In the continuum part of the thesis, it was mentioned that solitons carry a fractional charge. This chapter investigates the transport properties of solitons through defining a discrete microscopic model.

The movement of domain walls in a charge density wave (CDW) are described by solitons. A discrete analogue of this state is a Wigner crystal where a lattice is formed of mutually repelling electrons¹. The CDW phase occurs in a Luttinger liquid for long-range Coulomb interaction or when certain backscattering terms are relevant. These terms can be generated by the presence of a lattice that is commensurate with the average electron spacing, $1/2k_F$ [32]. Commensurate fillings mean that the g_3 backscattering term in the Luttinger liquid description becomes relevant and opens a gap in the charge sector. The filling of the lattice, $1/n$, defines the number of degenerate minima and therefore the fractional charge. Direct visualisation of the spatial separation of electrons has been managed in carbon nanotubes [89, 90].

Upon increasing the interactions between the electron further in a quasi-one-dimensional system, a zig-zag Wigner crystal is predicted to occur [91, 92]. This is when two lines of the chain move away to minimise the repulsion, resulting in the fermions alternating their position in the confined direction. The

¹There is more subtlety about this correspondence in dimensions higher than one. This is due to the finite number of discrete crystalline solutions possible, compared to the freedom to describe any spatial modulations in continuum.

fractional conductance plateaus observed in experiment [18] occur in this weak-confinement, strong-interaction regime. Other experiments have managed to confirm the presence of this phase in QPC devices through either the conductance properties [93] or electron focusing techniques [94]. Therefore an analysis of transport through a single Wigner chain is a pertinent problem to study.

This chapter is split into the spinless and spinful analyses, where both parts follow the same process to get the conductance near the resonance. The Hamiltonian of the discrete system is introduced first and the eigenstates at certain fillings found. The next step is to introduce the system to two reservoirs either side and utilise the NEGF formalism to find an expression for the current. Finally, the Green's functions for the isolated wire will be calculated to obtain a description of the conductance near the eigenstates of the finite system.

On investigation, the spinless case reifies the Maslov-Stone result - that interactions do not affect the two-terminal conductance. The conductance is found to be a series of Breit-Wigner resonant peaks that reach a maximum of the quantum of conductance. The width of these peaks do, however, depend on the microscopics of the system and exhibit different behaviour as the length of the system changes. The spinful case shows a splitting of these peaks and a reduction of their maximum values to fractions of e^2/h , despite expecting the conductance to double.

7.1 Spinless Model

A finite model that produces a Wigner crystal is described by the Hamiltonian,

$$H = -t \sum_i (d_i^\dagger d_{i+1} + d_{i+1}^\dagger d_i) + U_1 \sum_i n_i n_{i+1}, \quad (7.1)$$

where operator d_i^\dagger creates a spinless fermion on site $i \in \{1, 2, \dots, L-1\}$ in a chain of L sites. The number operator n_i will be either zero or one for each site. The usual 1D tight binding hopping term is present. It gains an energy t upon a fermion changing sites, which encourages hybridisation of the configurations into the usual cosine bands. The other term is an energetic cost to occupy two neighbouring sites.

This differs from other models used in the literature [95, 96] where their interaction term is,

$$I \sum_i \left(d_i^\dagger d_i - \frac{1}{2} \right) \left(d_{i+1}^\dagger d_{i+1} - \frac{1}{2} \right). \quad (7.2)$$

This particular form of the interaction is used because it maps onto the XXZ Heisenberg model through the Jordan-Wigner transformation, which can be solved using the Bethe Ansatz. Aside from an irrelevant constant shift of the energy, there is an additional onsite contribution, $-I/2 \sum_i (n_i + n_{i+1})$, in comparison to Equation 7.1. For periodic boundary conditions, the site indices will now include $i = L$ and contains the periodicity $L + 1 \equiv 1$. Performing the sum of the additional onsite term leads to an equal energy shifting of $-I$ for every fermion in the system. A lot of the literature focuses on rings of CDWs where this periodicity is enforced. These two interaction terms then encapsulate the exact same physics.

The Hamiltonians no longer match when the system has open boundary conditions. In this case, the sum in the onsite term only ranges from 1 to $L - 1$, which results in a difference between the energetic shifting of the bulk and edge sites. In configurations containing occupied bulk states, $i \neq 1, L$, the states will undergo a $-I$ energy shift. The configuration with occupied edges sites, $i = 1, L$, only have one term in the sum and are shifted by $-I/2$. This asymmetry between the bulk and edge of the chain can result in a soliton being bound to the edge of the system for $I > 2t$.

There is also a difference in how the occupations of the lattice hybridise with each other when different boundary conditions are applied. To understand why this is, consider the ground states in the $t = 0$ limit, which reduces the problem to arranging the fermions so that no two are next to each other. Half filling, for even L and periodic boundary conditions, leads to a ground state where either the even or odd sites are occupied. This is contrasted with open boundary conditions at half filling where there are $L/2 + 1$ states with zero energy. Figure 7.1 displays this difference.

Upon reintroducing hopping, such that $t \ll U_1$, the previously degenerate states will hybridise with each other to utilise the reduction in energy that hopping between sites provides. For open boundary conditions, the number of these states that can hybridise will linearly increase with the size of the system. This results in an energy band that does not happen for CDW rings, which will be frozen into one of the configurations.

Having explored why the boundary conditions and choice of Hamiltonian should produce different results, we will now stick to open boundary conditions and the Hamiltonian defined in Equation 7.1. As

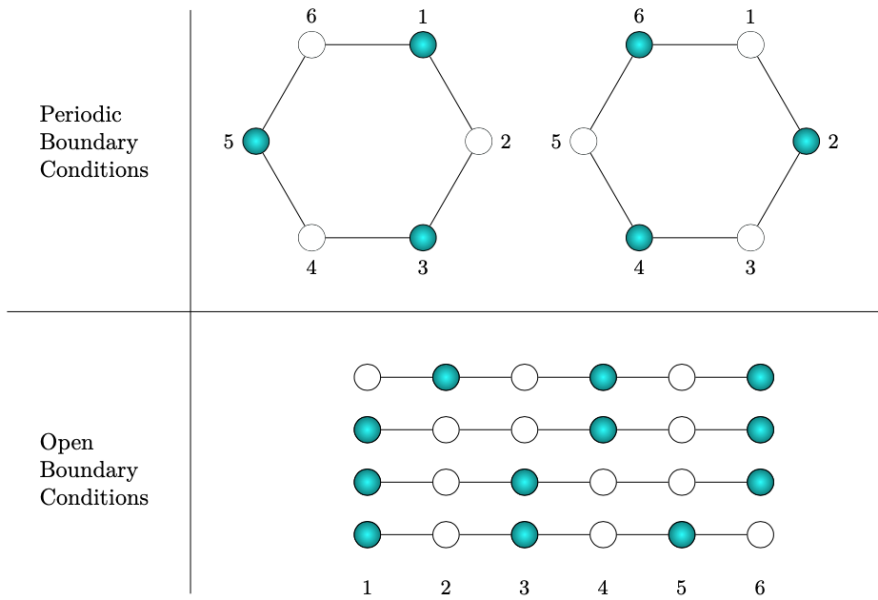


Figure 7.1: Showing the different possible zero-energy configurations in the $t = 0$ classical limit for different boundary conditions where the blue dots are the occupied sites

the details of the eigenstates depend on the filling, the filling parameter is introduced as,

$$Q = n_e - \frac{L}{2}, \quad (7.3)$$

where n_e is the number of fermions. Q will be either an integer or half-integer, dependent on whether there are an even or odd number of sites. It will be positive or negative depending on being above or below half filling. The aim is to find the conductance through this system when connected up to contacts, which for the NEGF formalism requires the Green's function of the isolated system. As the system is isolated, the number of fermions in the system is a good quantum number and so the first task is to solve for the eigenstates for different fillings of the system.

To analytically find the eigenstates of the system, the limit $U_1 \rightarrow \infty$ is taken which will project out any occupations that contain neighbouring fermions from our state space. Before this projection, our state space in the n particle subspace will be given by all the ways of arranging n fermions on a chain of length L .

The parameter L_S , which describes the total possible number of fermions before there must be two

neighbouring fermions, is given by,

$$L_S = \begin{cases} \frac{L+1}{2}, & \text{when } L \text{ is odd} \\ \frac{L}{2} + 1, & \text{when } L \text{ is even.} \end{cases} \quad (7.4)$$

Any state with more than L_S fermions will then be associated with an infinite energy in the limit and become energetically inaccessible for states to hybridise with. For the subspaces with L_S fermions in or fewer, some of the configurations of the fermions on the chain will be projected out. This reduces the total number of states in these subspaces and it is in these reduced subspaces that the Hamiltonian will be solved.

7.1.1 Eigenstates

The most simple filling to understand is the $Q = 1/2$ filling where only one configuration exists.

$$|Q = 1/2\rangle = |\times - \times - \cdots - \times\rangle = \prod_{i=0}^{\frac{L-1}{2}} d_{2i+1}^\dagger |0\rangle. \quad (7.5)$$

The string $\times - \times \cdots$ represents the occupation of the sites with \times denoting a fermion occupying that site. Any other configuration of fermions will have neighbouring fermions and therefore an infinite energy cost, which would have been projected out by the $U_1 \rightarrow \infty$ limit. This state will be a zero-energy eigenstate of the system, as there are no other states in the subspace for it to hybridise with and all possible hops of the fermions will take us to a state with neighbouring fermions.

For other fillings that will be considered, there is a general procedure that solves for the eigenstates. The main step is mapping the problem from the original occupation basis to a soliton basis which will eliminate some redundancy in the description. In this new basis the Hamiltonian becomes easier to solve, although it may require further mappings to solve completely.

Q=0

To understand solitonic behaviour in this model, the $Q = 0$ part is solved first as only one soliton is present. Any two neighbouring unoccupied sites in the chain form a soliton as they mark the presence of a domain wall. The two types of domains are when the fermions occupy even or odd indexed sites.

Joining up these domains requires the existence of two neighbouring unoccupied sites². To see how this is expressed in the mathematics, the occupation n_i of a configuration at site i at this filling will be given by,

$$n_i = \frac{1}{2} (1 - \cos(\pi i + \phi_i(u))), \quad (7.6)$$

where $\phi_i(u)$ is,

$$\phi_i(u) = \begin{cases} 0, & i < u, \\ \pi, & i \geq u. \end{cases} \quad (7.7)$$

This is a discretised version of the continuum 1D soliton,

$$\phi_i(u) = \arctan(\lambda(i - u)) + \frac{\pi}{2}, \quad (7.8)$$

in the limit that $\lambda \rightarrow \infty$ [82]. The values that u can take define the soliton lattice which will be a set of discrete values rather than the continuous variable of the above equation. To find these values, consider all possible occupation configurations of the fermions on the lattice and express them in this form.

To be concrete, all the states in the $Q = 0$ projected subspace for a 10 site chain are,

$$\begin{aligned} |-\times-\times-\times-\times-\times\rangle, |\times--\times-\times-\times-\times\rangle &\quad |\tilde{1}\rangle, |\tilde{2}\rangle \\ |\times-\times--\times-\times-\times\rangle, |\times-\times-\times--\times-\times\rangle &\rightarrow |\tilde{3}\rangle, |\tilde{4}\rangle \\ |\times-\times-\times-\times-\times-\times\rangle, |\times-\times-\times-\times-\times-\times\rangle &\quad |\tilde{5}\rangle, |\tilde{6}\rangle \end{aligned}$$

where \times indicates an occupied site and $-$ an unoccupied one. The position of the soliton is given by the location of the adjacent empty sites, which can be seen to have moved further along to the right of the chain in each basis state. This gives six possible values of u . The values it can take are $u = \{1, 3, 5, 7, 9, 11\}$. These 6 states are then ordered by their value of u and mapped to a soliton position \tilde{i} where $\tilde{i} = \{1, \dots, L_S\}$.

Figure 7.2 shows the mapping from a occupation configuration to a position on a soliton lattice. Under this relabelling, the Hamiltonian hops the soliton along the soliton lattice states. Although there are many fermions for a given configuration that could hop, many of the configurations they can hop to are projected out by the $U_1 \rightarrow \infty$ limit as they would result in neighbouring fermions. The only fermions that can change site without incurring an infinite energy cost are those either side of a soliton. When a

²In general, two adjacent occupied sites can also join up the domains but this possibility does not survive the infinite U_1 limit.

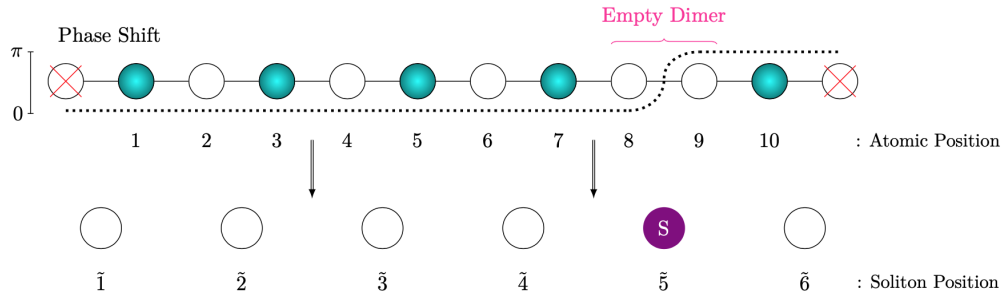


Figure 7.2: Showing how a particular configuration can be uniquely mapped to the position of its soliton. For the atomic lattice, occupied fermionic sites are in blue and open boundary conditions are depicted by the red crosses on the edge sites. The phase shift of the occupation is shown by the overlayed dotted line. The position of the empty dimer is then shown to be at one of six possible places, indicated on the soliton lattice underneath

fermion moves, it will leave a vacancy. As all fermions must already have neighbouring empty states, this creates two adjacent unoccupied sites next to the previous ones. The Hamiltonian on the soliton lattice becomes,

$$H |\tilde{i}\rangle = -t |\tilde{i}-1\rangle - t |\tilde{i}+1\rangle = \epsilon |\tilde{i}\rangle, \quad (7.9)$$

which has solutions of,

$$\epsilon_n = -2t \cos\left(\frac{\pi n}{L+1}\right), \quad |\tilde{i}\rangle = \sqrt{\frac{2}{L+1}} \sin\left(\frac{\pi n}{L+1}\tilde{i}\right), \quad (7.10)$$

for $n \in \{1, 2, \dots, L_S\}$.

Q=-1/2 Eigenstates

Having initially considered the more straightforward problem of one soliton, the same procedure is repeated but for two solitons in the system. Firstly, the allowed states in the projected subspace need to be found. As an example, consider the $L = 9$ case which would have 4 electrons for $Q = -1/2$. Writing out all the electron states is just a combinatorial problem and will form the basis for our eigenstates. This is shown in Figure 7.3

The next step is to understand these basis states in terms of the solitons. The system will now have two solitons, so two sets of empty adjacent sites, which can be seen in some of the configurations. Other configurations, however, have three neighbouring empty sites and some appear to only have one soliton.

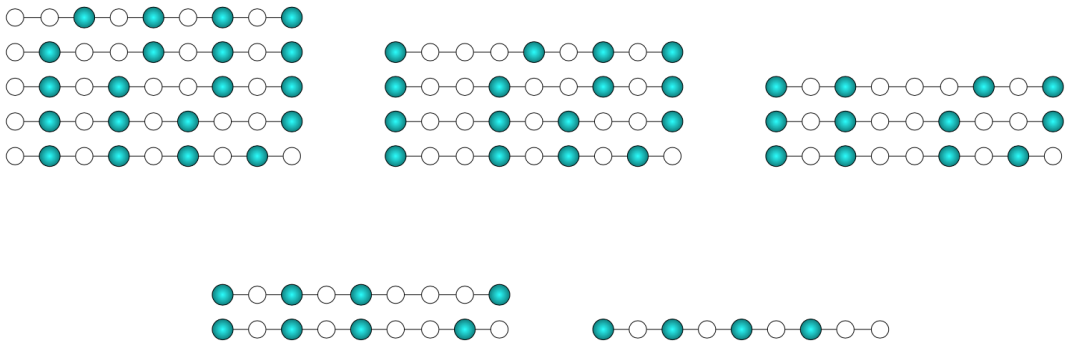


Figure 7.3: Configurations in the $Q = -1/2$ subspace in the limit $U_1 \rightarrow 0$. The blue, filled circles represent a fermion occupying that site.

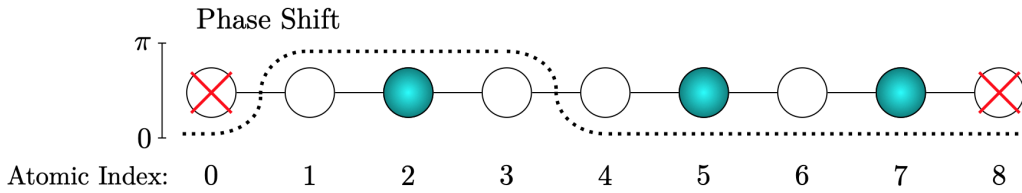


Figure 7.4: For a given configuration in the $Q = -1/2$ subspace, the phase shift that corresponds to the specific occupation is shown.

The open boundary conditions provide two more empty sites which explain the configurations that seem to only have one soliton - the other one is hiding at the edge.

This will be described by an occupation of,

$$n_i = \frac{1}{2} \left(1 - \cos(\pi i + \phi_i(u) + \phi_i(v)) \right), \quad (7.11)$$

where $\phi_i(u), \phi_i(v)$ have the same form as before. Figure 7.4 demonstrates how this phase shifting works for a specific state. Now the possible values of u, v that correspond to the configurations need to be found. The position of one of the solitons describes the location of two empty sites when the empty site on the right of the pair has an odd atomic index. The other soliton describes the empty sites for the right site having an even atomic index. Looking back to the one soliton case, the right site of the pair always lands on an odd atomic site so this parity does not have to be considered in the previous case. Writing the values explicitly for the 9 site case, $u = \{1, 3, 5, 7\}, v = \{2, 4, 6, 8\}$, where $u < v$.

The occupation labelling can therefore be replaced by $|\tilde{u}, \tilde{v}\rangle$ where $\tilde{u}, \tilde{v} \in \{1, 2, \dots, L_S\}$, u is the odd

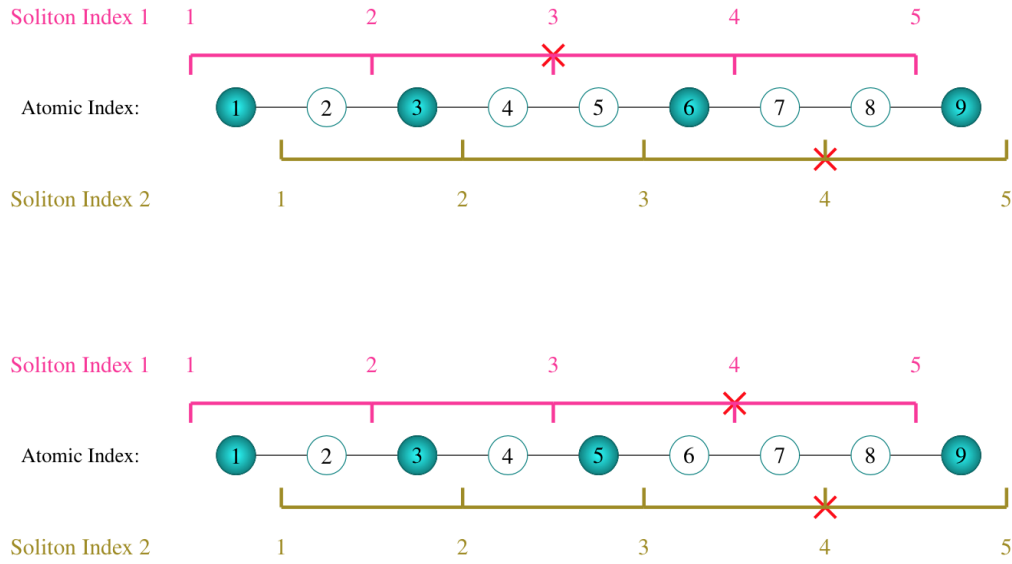


Figure 7.5: Showing how the mapping to the soliton basis occurs in the case of two separate solitons and for three neighbouring unoccupied sites

indexed soliton and v is the even one. Figure 7.5 shows the mapping for two more states. When mapping all the allowed configurations in the subspace, a restriction arises that $u \leq v$. This can be confirmed through trying to construct a state that contradicts this restriction, with the rules laid out for u, v . Any state that has $u > v$ will have to contain adjacent fermions to have the right filling.

The next hurdle is to find how the Hamiltonian acts on the soliton representation. Similarly to the previous case, only fermions that are next to a soliton will be able to hop. However, when there are two solitons in the system this means that there is a maximum of four fermions that can move. Figure 7.6 displays how the hopping of the fermions also moves the domain walls.

The Hamiltonian in terms of the soliton indices becomes,

$$H |u, v\rangle = -t |u-1, v\rangle - t |u+1, v\rangle - t |u, v+1\rangle - t |u, v-1\rangle, \quad \text{where } u \leq v. \quad (7.12)$$

The restriction on the indices carries over to the Hamiltonian so the number of states that can hop to depends on the current state. There is, however, a nice geometric way to visualise the possible hoppings. Figure 7.7 shows these connections.

The problem will be easier to solve when mapped to a 2D square lattice hopping problem. This

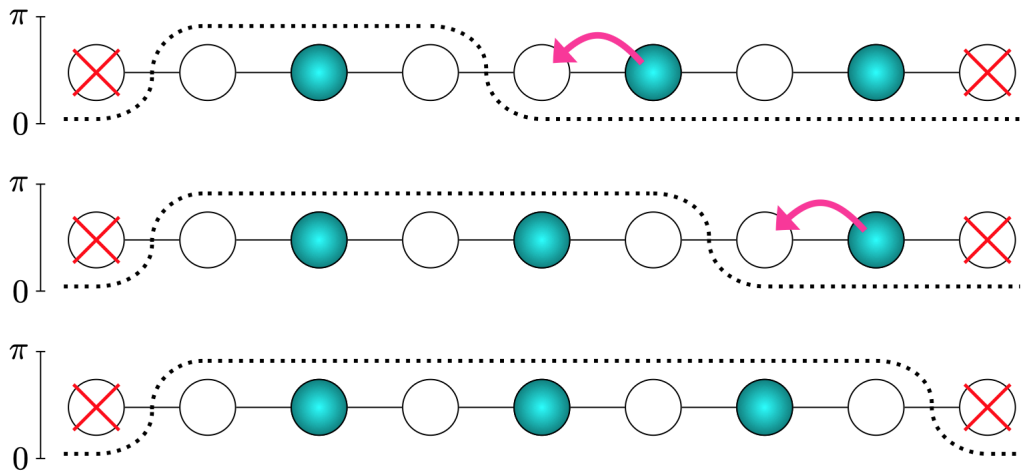


Figure 7.6: Configurations that differ by the movement of one fermion also have adjacent solitons.

$$\begin{array}{c}
 |1,1\rangle - |1,2\rangle - |1,3\rangle - |1,4\rangle - |1,5\rangle \\
 |2,2\rangle - |2,3\rangle - |2,4\rangle - |2,5\rangle \\
 |3,3\rangle - |3,4\rangle - |3,5\rangle \\
 |4,4\rangle - |4,5\rangle \\
 |5,5\rangle
 \end{array}$$

Figure 7.7: The possible hoppings between the different configurations of the $Q = -1/2$ filling are demonstrated for $L_S = 5$. The states connected with a line can hop to each other and gain an energy t in the process.

mapping is suitable as there are two ‘independent’ indices that hop both forwards and backwards, but with an extra constraint on where the hopping can occur. Solving a hopping Hamiltonian on a finite 2D square lattice is simple. Having arrived upon these solutions, the task is to understand what restrictions on the 2D problem will give the solutions to the original restricted hopping problem.

2D Finite Square Lattice

Continuing to use $L_S = 5$, more states have to be introduced to match this problem up with a 2D square lattice. These additional sites are shown in red below.

$$\begin{array}{ccccccc}
 |1,0\rangle & - |1,1\rangle & - |1,2\rangle & - |1,3\rangle & - |1,4\rangle & - |1,5\rangle & \\
 |2,0\rangle & - |2,1\rangle & - |2,2\rangle & - |2,3\rangle & - |2,4\rangle & - |2,5\rangle & \\
 |3,0\rangle & - |3,1\rangle & - |3,2\rangle & - |3,3\rangle & - |3,4\rangle & - |3,5\rangle & \\
 |4,0\rangle & - |4,1\rangle & - |4,2\rangle & - |4,3\rangle & - |4,4\rangle & - |4,5\rangle & \\
 |5,0\rangle & - |5,1\rangle & - |5,2\rangle & - |5,3\rangle & - |5,4\rangle & - |5,5\rangle & \\
 |6,0\rangle & - |6,1\rangle & - |6,2\rangle & - |6,3\rangle & - |6,4\rangle & - |6,5\rangle &
 \end{array}
 \quad
 \begin{array}{ccccccc}
 0 & |1,1\rangle & - |1,2\rangle & - |1,3\rangle & - |1,4\rangle & - |1,5\rangle & \\
 |2,0\rangle & 0 & |2,2\rangle & - |2,3\rangle & - |2,4\rangle & - |2,5\rangle & \\
 |3,0\rangle & - |3,1\rangle & 0 & |3,3\rangle & - |3,4\rangle & - |3,5\rangle & \\
 |4,0\rangle & - |4,1\rangle & - |4,2\rangle & 0 & |4,4\rangle & - |4,5\rangle & \\
 |5,0\rangle & - |5,1\rangle & - |5,2\rangle & - |5,3\rangle & 0 & |5,5\rangle & \\
 |6,0\rangle & - |6,1\rangle & - |6,2\rangle & - |6,3\rangle & - |6,4\rangle & 0 &
 \end{array}$$

Requiring a state to be zero will stop any neighbouring state from being able to hop to that state. If all of the states along the diagonal of the square lattice are zero, then there becomes two disconnected sublattices. In each of the disconnected copies, the connection between the states are identical to the original problem. Therefore finding a solution to one particle moving on a square lattice such that there is no hopping through the diagonal will solve the original problem.

To clean up notation, we define $\psi_{xy} \equiv |x, y+1\rangle$ where the second index is shifted by one in order to make the main diagonal in the matrix of states above correspond to ψ_{xx} . The generic square matrix problem is solved by utilising the open boundary conditions which mean that $\psi_{0y} = \psi_{7y} = 0$ and $\psi_{x0} = \psi_{x7} = 0$. The square lattice wavefunction and eigenvalues will be given by

$$\psi_{xy}^{(n,m)} = \sqrt{\frac{2}{D+1}} \sin(k_x x) \sin(k_y y), \quad \epsilon^{(n,m)} = -2t(\cos(k_x) + \cos(k_y)) \quad (7.13)$$

$$\text{where } k_x = \frac{\pi n}{D+1}, k_y = \frac{\pi m}{D+1}, \quad \text{for } n, m, x, y \in \{1, 2, \dots, D\}, \quad (7.14)$$

where $D = L_S + 1$ is the length of the square lattice. Requiring $\psi_{xx} = 0$ for all x will ensure the

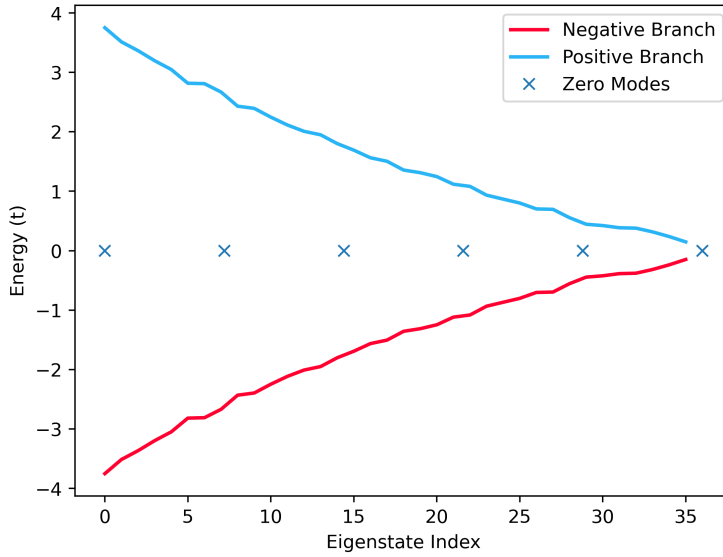


Figure 7.8: The different energies that can occur in the $Q = -1/2$ filling are shown for a chain of 23 sites. The eigenstate index labels the combinations (n, m) that produce distinct energies with there being a positive and negative energy pair for each non-zero combination. The zero modes have been overlaid and do not correspond to an eigenstate index.

diagonal is always zero. This condition will be satisfied when the solution is antisymmetrised in the position index,

$$\begin{aligned} \phi_{xy}^{(n,m)} &= \psi_{xy}^{(n,m)} - \psi_{yx}^{(n,m)} \\ &= \sqrt{\frac{2}{D+1}} \left[\sin\left(\frac{\pi n}{D+1}x\right) \sin\left(\frac{\pi m}{D+1}y\right) - \sin\left(\frac{\pi m}{D+1}x\right) \sin\left(\frac{\pi n}{D+1}y\right) \right]. \end{aligned} \quad (7.15)$$

To ensure there is no double counting arising from the two disconnected copies, we arbitrarily choose $x < y$ and $n < m$. This is the same reason that the normalisation stays the same despite the factor of $1/\sqrt{2}$ that normally is required. That factor would be needed if the solution was being normalised on the full square lattice, but the number of sites in the restricted problem is half the number of sites that contribute to the normalisation - cancelling the factors of two. Appendix F shows more details of this antisymmetrisation. The eigenvalues will be,

$$\epsilon^{(n,m)} = -2t \left(\cos\left(\frac{\pi n}{D+1}\right) + \cos\left(\frac{\pi m}{D+1}\right) \right). \quad (7.16)$$

The form of the dispersion is shown in Figure 7.8 for $N = 23$. This shows that for each non-zero

energy state there are positive and negative energy pairs. There are also zero-energy modes, the number of which grow linearly with the size of the system. Inserting two solitons into the system can lower the energy in comparison to the frozen state due to the hybridisation of the configurations.

The eigenstates of the 1D Wigner chain at $Q = -1/2$ have been found in terms of the configurations of the fermions on the chain. Although two mappings were used to find these coefficients, the mapping has always been one to one and the relationship between the representations are,

$$\phi_{12} = |1, 1\rangle = |-- \times - \times - \times - \times\rangle. \quad (7.17)$$

An eigenstate for a given (n, m) is a linear combination of all $\phi_{xy}^{(n,m)}$ that have $x < y$. The value of $\phi_{12}^{(n,m)}$ describes the coefficient of the $|1, 1\rangle$ term for a given eigenvalue. The rest of the eigenstates are given by every value of n, m that have $n < m$. In a compact form the general eigenstates are,

$$|Q = -1/2, (n, m)\rangle = \sum_{0 < x < y \leq L_S} \phi_{xy}^{(n,m)} |x, y-1\rangle. \quad (7.18)$$

Using $\sin(x) = (-1)^n \sin(x - \pi n)$ for integer n it can be shown that,

$$\phi_{L_S L_S + 1}^{(n,m)} = (-1)^{n+m+1} \phi_{12}^{(n,m)}. \quad (7.19)$$

This relation means that for any eigenstate, the probability of the soliton being either end of the wire is the same because $\psi_{12} = |1, 1\rangle$ and $\psi_{L_S L_S + 1} = |L_S, L_S\rangle$. This will turn out to be useful in the conductance calculation. The next task is to apply the Keldysh formalism to calculate conductance.

7.1.2 Attaching Contacts

To find the conductance, a connection to the contacts must be made. For a wire between two reservoirs, the only sites in the wire that will exchange particles with the reservoirs are the two edges of the finite

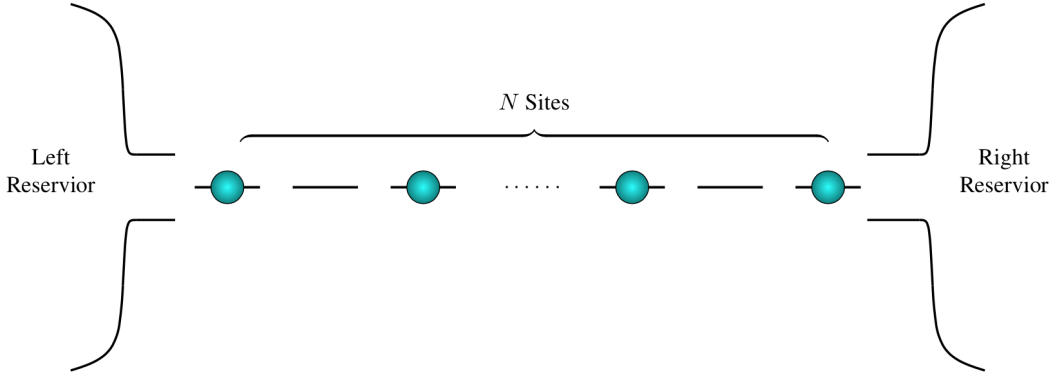


Figure 7.9: The connection of a 1D Wigner chain to reservoirs either side.

system as long as the overlap decays sufficiently quickly. The Hamiltonian for the full system becomes,

$$\begin{aligned} H &= H_{reservoir}^L + H_{wire} + H_{reservoir}^R + H_{tun} \\ &= \sum_k \epsilon_k^L c_{L,k}^\dagger c_{L,k} + \sum_q E_q d_q^\dagger d_q + \sum_k \epsilon_k^R c_{R,k}^\dagger c_{R,k} \\ &\quad - \sum_k V_{1,k}^L (c_{L,k}^\dagger d_1 + d_1^\dagger c_{L,k}) + V_{L,k}^R (c_{R,k}^\dagger d_L + d_L^\dagger c_{R,k}), \end{aligned} \quad (7.20)$$

for operators $c_{\alpha,k}$ that annihilate a fermion in the $\alpha = \{L, R\}$ reservoir with momentum k . The operators d_i annihilate a fermion on site i as before and d_q annihilates the eigenstate q on the wire. Figure 7.9 illustrates the setup of the system.

Comparing this Hamiltonian to the generic one considered in the NEGF formalism, the coupling is now between positions rather than eigenstates. This does not cause much trouble because both the effective action and the current expression contain the trace over the eigenstates which is basis-independent. Therefore the trace can be chosen to be in the position basis which will utilise the sparseness of the coupling.

The form of the self-energy matrix can be calculated through finding the effective action after integrating out the reservoirs. This was found in Section 5.3 to be,

$$S_{eff} = S_{wire} + \int_K dt dt' \sum_{\alpha,k} \text{Tr}_{q,q'} [V_{q,k}^\alpha V_{q',k}^\alpha \bar{\phi}_q(t) g_{\alpha,k}(t, t') \phi_{q'}(t)]. \quad (7.21)$$

Taking the trace in the position basis results in just one term for each reservoir as the coupling in the

Hamiltonian only has non-zero $V_{1,k}^L$ term (i.e. $V_{2,k}^L = 0$). Therefore our effective action becomes,

$$S_{eff} = S_{wire} - e \sum_k \int_K dt dt' (V_{1,k}^L)^2 \bar{\phi}_1(t) g_{L,k}(t, t') \phi_1(t) + (V_{N,k}^R)^2 \bar{\phi}_L(t) g_{R,k}(t, t') \phi_L(t), \quad (7.22)$$

where the number of indices can finally be reduced by letting $V_{1,k}^L \equiv V_{L,k}$.

This defines the matrix structure of the self-energy in position space, $\bar{\phi} \Sigma \phi$, for $\phi = (\phi_1, \phi_2, \dots, \phi_L)^T$ as,

$$\Sigma = \begin{pmatrix} \Sigma_L(k) & 0 & \cdots & 0 \\ 0 & 0 & \cdots & 0 \\ \vdots & \vdots & \ddots & \vdots \\ 0 & 0 & \cdots & \Sigma_R(k) \end{pmatrix} \quad (7.23)$$

where $\Sigma_L(k) = V_{L,k}^2 g_{L,k}$ and $\Sigma_R(k) = V_{R,k}^2 g_{R,k}$.

Conductance Expression

Having found the self-energy matrix, the current expression of the NEGF formalism can be simplified by utilising the sparseness of the self-energy matrix. This gives the current as,

$$J_\alpha = e \sum_k \int_{-\infty}^{\infty} \frac{d\omega}{2\pi} \Delta G_{\alpha\alpha}(\omega) \Sigma_{\alpha,k}^<(\omega) - G_{\alpha\alpha}^<(\omega) \Delta \Sigma_{\alpha,k}(\omega), \quad \text{where } \Delta A \equiv A^r - A^a, \quad (7.24)$$

where α in the Green's function index refers to the first site if $\alpha = L$, or the last site if $\alpha = R$. The indices ($r, a, <$) have their usual meaning as the retarded, advanced and lesser Green's functions respectively. The kinetic equation can be used to get a Landauer type equation where the transmission multiplied by the difference of two Fermi distributions. The kinetic equation is,

$$\mathbf{G}^{\{<, >\}} = \mathbf{G}^r \Sigma^{\{<, >\}} \mathbf{G}^a \implies \mathbf{G}^> - \mathbf{G}^< = \mathbf{G}^r - \mathbf{G}^a = \Delta \mathbf{G} = \mathbf{G}^r \Delta \Sigma \mathbf{G}^a. \quad (7.25)$$

This can then be put into our current equation to give,

$$J_\alpha = \int_{-\infty}^{\infty} \frac{d\omega}{2\pi} (G^r \Delta \Sigma G^a)_{\alpha\alpha} \Sigma_\alpha^< - (G^r \Sigma^< G^a)_{\alpha\alpha} \Delta \Sigma_\alpha, \quad (7.26)$$

where the matrix elements can be calculated. Doing this for each of the reservoir currents gives,

$$\begin{aligned} J_L &= e \sum_k \int_{-\infty}^{\infty} \frac{d\omega}{2\pi} G_{1N}^r \Delta \Sigma_R G_{N1}^a \Sigma_L^< - G_{1N}^r \Sigma_L^< G_{N1}^a \Delta \Sigma_R \\ &= e \sum_k \int_{-\infty}^{\infty} \frac{d\omega}{2\pi} |G_{1N}^r|^2 (\Delta \Sigma_R \Sigma_L^< - \Delta \Sigma_L \Sigma_R^<), \end{aligned} \quad (7.27)$$

$$\begin{aligned} J_R &= e \sum_k \int_{-\infty}^{\infty} \frac{d\omega}{2\pi} G_{N1}^r \Delta \Sigma_L G_{1N}^a \Sigma_R^< - G_{N1}^r \Sigma_R^< G_{1N}^a \Delta \Sigma_L \\ &= e \sum_k \int_{-\infty}^{\infty} \frac{d\omega}{2\pi} |G_{N1}^r|^2 (\Delta \Sigma_L \Sigma_R^< - \Delta \Sigma_R \Sigma_L^<). \end{aligned} \quad (7.28)$$

Spatial invariance means that $G_{1N}^r = G_{N1}^r$, which will be seen more explicitly shortly. It follows that the two currents are equal in magnitude and opposite in direction.

The self-energy contains the Green's function of the reservoirs which are taken to be a Fermi gas. As the reservoirs are much larger than the contacts, which are in equilibrium, which allows the different types of self-energy to be related. The difference between the retarded and advanced functions, $\Delta\Sigma$, is the density of states of the eigenvalues of Σ , because $\Sigma^r = (\Sigma^a)^*$ and $\text{Im}(\Sigma^r) = -\sum_k \pi\delta(\omega - \epsilon_k)$. The self-energy then becomes $\Delta\Sigma_{\alpha,k} = -2\pi i V_{\alpha,k}^2 \delta(\omega - \epsilon_k) \equiv -2i\Gamma_{\alpha,k}$ where the delta function will give the the density of states of a Fermi gas in the α reservoir when the sum over k is performed. From Fermi's golden rule, multiplying the density of states and the coupling matrix elements gives the tunnelling rate, $\Gamma_{\alpha,k}$.

Next, the lesser function is defined as $A^<(t, t') = i \langle a^\dagger(t') a(t) \rangle$. The fermions in the reservoirs are a Fermi gas, so the lesser self-energy can be rewritten as $\Sigma_{k,\alpha}^<(\omega) = -f_\alpha(\omega) \Delta\Sigma_{k,\alpha}(\omega)$ where $f_\alpha(\omega)$ is the Fermi distribution in the α reservoir. This states that the average occupation of electrons in the reservoirs is given by the Fermi distribution multiplied by the density of states. This form is possible because $\langle a_k^\dagger(\omega) a_k(\omega) \rangle = \langle c^\dagger(\omega) c(\omega) \rangle \delta(\omega - \epsilon_k)$. The average $\langle c^\dagger(\omega) c(\omega) \rangle$ is simply given by the Fermi function $f(\omega)$. There will also be a a chemical potential μ_L and μ_R associated to each lead so $\Sigma_\alpha^< = -\Delta\Sigma_\alpha f(\omega - \mu_\alpha)$.

Putting this into Equation 7.28, gives

$$\begin{aligned} J_L &= e \sum_k \int_{-\infty}^{\infty} \frac{d\omega}{2\pi} \Delta\Sigma_{L,k} \Delta\Sigma_{R,k} |G_{1N}^r|^2 (f_L - f_R) \\ &= e^2 V \sum_k 4\Gamma_{L,k} \Gamma_{R,k} \int_{-\infty}^{\infty} \frac{d\omega}{2\pi} |G_{1N}^r(\omega)|^2 f'(\omega - \mu). \end{aligned} \quad (7.29)$$

This assumes linear bias by setting $\mu^L = \mu^R + eV$ (where V here is the applied voltage not the coupling) which results in $f_R \approx f_L + eVf'_L + O(V^2)$. The conductance through a spinless wire connected up reservoirs through single sites is therefore,

$$g = \frac{e^2}{2\pi} \sum_k 4\beta\Gamma_k \int_{-\infty}^{\infty} d\omega |G_{1N}^r(\omega)|^2 \operatorname{sech}^2\left(\frac{\beta}{2}(\omega - \mu)\right). \quad (7.30)$$

From here on, the notation of the retarded Green's function will be dropped as this will be the only type of Green's function that is used. This result is similar to the Landauer formalism with the difference of two Fermi functions providing the voltage through the system. The transmission matrix here is expressed in terms of the probability for the effective excitations to travel from one end of the wire to the other.

Coupled Green's Functions

In the NEGF formalism, G_{ij} was defined with the effective action that took into account the contacts. The ‘coupled’ Green’s functions are related to the uncoupled ones, \mathcal{G}_{ij} , using Dyson’s equation. The uncoupled Green’s functions are the ones that are described in terms of the eigenstates of the isolated system. The specific form of the coupling allows the problem to be simplified. This is because Dyson’s equation involves a matrix of Green’s functions and would in general require a full matrix inversion. The sparseness of the coupling matrix allows the inversion to be performed and G_{1N}^r calculated.

The coupling is $\Sigma_{ij} = \delta_{ij}(\delta_{1i}\Sigma_L + \delta_{iN}\Sigma_R)$. This can be substituted into the Dyson equation for G_{11} and G_{1N} . Assuming that the imaginary singularity of the reservoir Green’s function dominates the real principle part, means that $\Sigma_\alpha^r = -i\Gamma_\alpha$. The real part usually rescales the energy so can be safely ignored. The Dyson’s equation becomes,

$$\mathbf{G} = \mathbf{\mathcal{G}} - i\mathbf{\mathcal{G}}\boldsymbol{\Gamma}\mathbf{G}. \quad (7.31)$$

Denoting $G_{11} \equiv A$, $G_{1N} \equiv B$, $G_{N1} \equiv C$, $G_{NN} \equiv D$, this matrix equation can be explicitly solved. There is translational symmetry in the wire so $\mathcal{G}_{11} = \mathcal{G}_{NN} \equiv a$ and $\mathcal{G}_{1N} = \mathcal{G}_{N1} \equiv b$ which can be explicitly seen from the form of the uncoupled Green’s functions in the next section. The matrix

equation then reduces to,

$$A = a - ia\Gamma_L A - ib\Gamma_R C, \quad B = b - ia\Gamma_L B - ib\Gamma_R D \quad (7.32)$$

$$C = b - ib\Gamma_L A - ia\Gamma_R C, \quad D = a - ib\Gamma_L B - ia\Gamma_R D. \quad (7.33)$$

These two pairs of equations are the same under $\Gamma_L \leftrightarrow \Gamma_R$. Solving simultaneously for A and C ,

$$C(1 + ia\Gamma_R) = b - \frac{ib\Gamma_L}{1 + ia\Gamma_L} (a - ib\Gamma_R C) \implies C((1 + ia\Gamma_R)(1 + ia\Gamma_L) + b^2\Gamma_L\Gamma_R) = b.$$

Therefore,

$$G_{N1} = \frac{\mathcal{G}_{1N}}{1 + 2i\mathcal{G}_{11}(\Gamma_R + \Gamma_L) + (\mathcal{G}_{1N}^2 - \mathcal{G}_{11}^2)\Gamma_L\Gamma_R} = G_{1N}. \quad (7.34)$$

The final answer is invariant under $\Gamma_L \leftrightarrow \Gamma_R$ which shows that $G_{1N} = G_{N1}$.

7.1.3 Conductance

Having discovered how to relate the coupled Green's function that appears in the current formula to the uncoupled Green's functions, our attention turns to calculating the uncoupled Green's functions. This will use the isolated eigenstates that were explicitly calculated in Chapter 7.1.1. The Lehmann representation of a Green's function is,

$$\mathcal{G}_{ij}(\omega) = \frac{1}{Z} \sum_{n,m} \left(e^{-\beta(\epsilon_n - \mu n_e)} + e^{-\beta(\epsilon_m - \mu m_e)} \right) \frac{\langle n | d_j^\dagger | m \rangle \langle m | d_i | n \rangle}{\omega + \epsilon_m - \epsilon_n + i\delta}, \quad (7.35)$$

where the sum n, m is over all possible eigenstates which includes all fillings. This form is simply the definition of Equation 3.16 expressed in terms of the positional operators. The number of fermions in the eigenstates are given by n_e, m_e , for each eigenstate and the partition function is Z .

The calculations will consider low temperatures and $\mu > 0$. For large μ , the system will be forced into the $Q = 1/2$ frozen state. The chemical potential will be set so that the cost in removing a particle from the system will be compensated by the reduction in energy from introducing two solitons into the system. This amounts to setting $\mu + \epsilon_0 \approx 0$ as the minimum energy, ϵ_0 , of the $Q = -1/2$ state. This minimum energy is negative, as can be seen in Figure 7.8. In this regime, the Green's function can be

simplified to,

$$\mathcal{G}_{11}(\omega) = \sum_q \frac{z_q}{\omega - \epsilon_q + i\eta}, \quad \mathcal{G}_{1N}(\omega) = \sum_q \frac{z'_q}{\omega - \epsilon_q + i\delta}, \quad (7.36)$$

where ϵ_q denotes the q th eigenstate for the $Q = -1/2$ filling. Note that when the eigenstates were calculated earlier they were indexed by the tuple of integers (n, m) but now it will be indexed by just one integer q . The coefficients z_q, z'_q is given by

$$z_q = \frac{1}{\bar{Z}} (\psi_{12}^q)^2 (1 + e^{-\beta(\epsilon_q + \mu)}), \quad z'_q = \frac{1}{\bar{Z}} \psi_{LS}^q L_{S+1} \psi_{12}^q (1 + e^{-\beta(\epsilon_q + \mu)}), \quad (7.37)$$

where the reduced partition function Z is,

$$Z = 1 + \sum_q e^{-\beta(\epsilon_q + \mu)}. \quad (7.38)$$

A more lengthy derivation of this form is shown in Appendix F. To briefly understand why this form is obtained, a factor of $e^{\beta\mu L_S}$ is taken out which results in any subspaces with fillings lower than $Q = -1/2$ being exponentially suppressed. This simplification is only possible if the ground state eigenvalue of the $Q = -3/2$ filling is less than twice as large as the ground state of the $Q = -1/2$ filling. This has not been analytically proven but can be shown to be true numerically. The frozen state means that one of the summations in Equation 7.35 can be dropped as there is only one possible state in the larger subspace.

To understand why the coefficients have the form they do in Equation 7.37, the matrix overlaps will now be calculated. Considering \mathcal{G}_{11} first, one of the overlaps is given by,

$$\langle Q = -1/2, q | d_1 | Q = 1/2 \rangle = \langle Q = -1/2, q | - - \times - \times \cdots - \times \rangle = \psi_{12}^q. \quad (7.39)$$

Using Equation 7.18 to express the eigenstates, the overlap is seen to be ψ_{12}^q . The other matrix element in \mathcal{G}_{11} is given by the complex conjugate of the above term leading to a total factor of $(\psi_{12}^q)^2$.

For \mathcal{G}_{1N} , one of the overlaps is the same as Equation 7.39. The other overlap is given by,

$$\langle Q = 1/2 | d_N^\dagger | Q = -1/2, q \rangle = \langle \times - \times \cdots \times - | Q = -1/2, q \rangle = \psi_{L_S L_{S+1}}^q. \quad (7.40)$$

Multiplying these contributions together gives the result of Equation 7.37.

Recalling Equation 7.19 allows the coefficients of the two different Green's functions to be linked. Introducing $z_q = z'_q s_q$, where $s_q = \{1, -1\}$, provides the connection. Consider one term in the Green's function sum, denoted q^* . Then $\mathcal{G}_{11}^2 = \mathcal{G}_{1N}^2$ as $z_q^2 = z'^2$. The coupled Green's function becomes,

$$G_{1N} = \frac{\mathcal{G}_{1N}}{1 + i(\Gamma_L + \Gamma_R)\mathcal{G}_{11}} = \frac{z_{q^*} s_{q^*}}{\omega - \epsilon_{q^*} + i(\Gamma_L + \Gamma_R)z_{q^*}}. \quad (7.41)$$

Only considering one term is reasonable when the chemical potential is near the resonance of ϵ_0 and the eigenstate spacing δ is large³.

Connecting up the reservoirs for a spinless system broadens the peaks and leads to the Green's functions acquiring a finite imaginary part. The quasi-particles of the system now have finite lifetimes, proportional to the tunnelling rate. For very weak couplings to the reservoirs, $\Gamma_L + \Gamma_R \ll \delta$, each of the peaks in the Green's function will be renormalised separately. This is possible as $\Gamma_{L,R}$ is the width of the resonance and each resonance will be δ away from each other. This limit corresponds to a high potential barrier for tunnelling into the system. The full coupled Green's function is then the sum over each renormalised peak,

$$G_{1N}^r = \sum_q \frac{z_q s_q}{\omega - \epsilon_q + i(\Gamma_L + \Gamma_R)z_q}. \quad (7.42)$$

The conductance then becomes,

$$\sum_k 4\Gamma_{L,k}\Gamma_{R,k} \int_{-\infty}^{\infty} d\omega \left| \sum_q \frac{z_q}{\omega - \epsilon_q + i(\Gamma_{L,k} + \Gamma_{R,k})z_q} \right|^2 \beta \operatorname{sech}^2(\beta(\omega - \mu)). \quad (7.43)$$

This expression contains the integral over two sharply peaked distributions - one being the sum of Lorenztians coming from Green's functions and the other is due to the temperature. Taking temperature to be the smallest scale in the system, the temperature peak becomes a delta function and sets all frequencies to be μ . The sum over k is related to the frequency due to the dispersion of the reservoirs. Only the small energy region around μ will contribute in the sum. Therefore setting ω to be the chemical potential reduces the k sum to just only contain one term at k and the coupling becomes $\bar{\Gamma}_\alpha = V_{\alpha,k_F}^2 \nu_{k_F}$ where ν_{k_F} is the density of states at k_F .

³The main reason why so many terms can be ignored is due to the peaked temperature function in Equation 7.30. This peak will only select a certain frequency in the Green's function sum. The criterion for whether terms can be ignored depends on if each peak affects each other, not the relative size of the peaks. When the chemical potential is at resonance with an excited state, the size of the ground state peak will be much larger. Yet, if it is far enough away from the excited state, it will not affect the peak of the excitation.

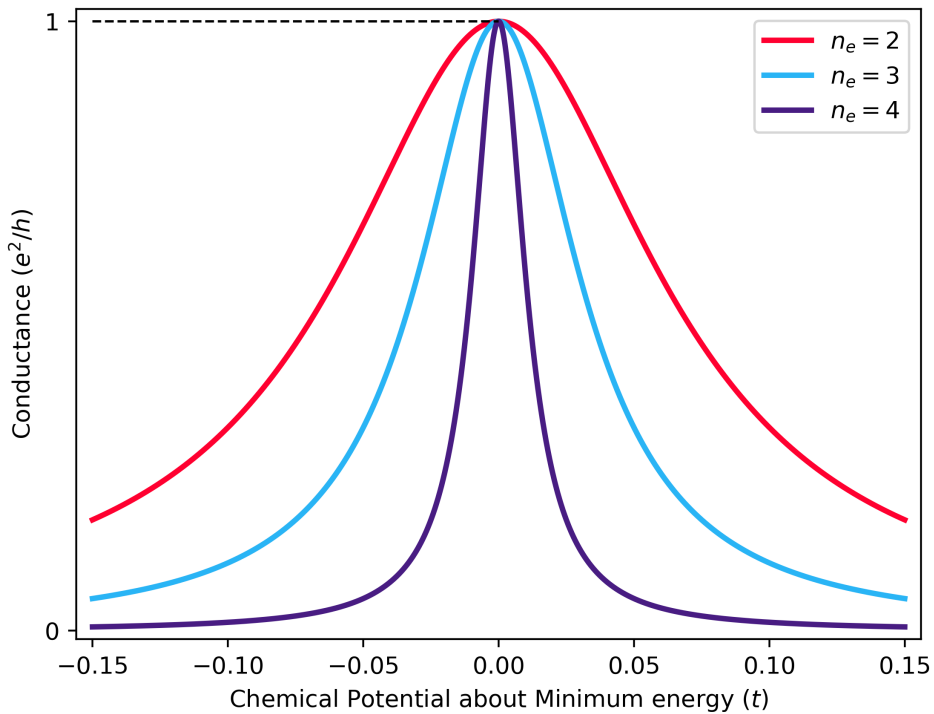


Figure 7.10: The conductance is shown to be peak at e^2/h as the chemical potentials of the reservoirs are changed. The width of the peak is smaller for larger 1D chains in the Wigner crystal regime.

Taking into account the first excited state above ϵ_0 which will be at an energy of $\epsilon_0 + \delta$, the conductance can finally be given as,

$$g = 4\bar{\Gamma}_L\bar{\Gamma}_R \left| \frac{1}{i(\bar{\Gamma}_L + \bar{\Gamma}_R)} + \frac{z_{q'}}{\delta + i(\bar{\Gamma}_L + \bar{\Gamma}_R)z_{q'}} \right|^2 = \frac{4\bar{\Gamma}_L\bar{\Gamma}_R}{(\bar{\Gamma}_L + \bar{\Gamma}_R)^2} + O\left(\frac{\bar{\Gamma}_{L,R}}{\delta}\right). \quad (7.44)$$

This is finally the conductance! It was already assumed that the eigenvalue spacing is much larger than the coupling so higher-order terms will be suppressed. In the case of equal coupling either side of the wire, there is perfect cancellation and the peak of the conductance is not renormalised by the interaction in the wire. The microscopics of the state are relegated to only affecting the width of the resonance.

To get the width of the resonance we let $\mu = \epsilon_0 + \delta\mu$ such that $\delta\mu \ll \delta$. Knowing that all the higher-order terms do not contribute means only the term at resonance needs to be considered. This results in,

$$g = \frac{4\bar{\Gamma}_L\bar{\Gamma}_R z_{q^*}^2}{\delta\mu^2 + z_{q^*}^2(\bar{\Gamma}_L + \bar{\Gamma}_R)^2}. \quad (7.45)$$

The width of the peak depends on the length of the system and Figure 7.10 displays the conductance for different number of sites. Equation 7.37 defines the widths in terms of the wavefunction overlaps. for the ground state, the width decreases as $1/L_S^5$, or $1/L_S^3$ for the excited states, whereas the eigenvalue spacing decreases by $1/L_S^2$. Therefore the infinite length system should have a conductance equal to the quantum of conductance over the range of the band. This result will hold until the chemical potential is such that other fillings apart from $Q = 1/2, -1/2$ are allowed. This result mirrors the result of Maslov-Stone, where the interactions in the system are irrelevant to the conductance.

Altering the coupling to the reservoirs independently provides one method for obtaining fractional conductance peaks. Letting $n\bar{\Gamma}_L = m\bar{\Gamma}_R$ results in,

$$g = \frac{nm}{n^2 + m^2}. \quad (7.46)$$

This result could be found in the original treatment by Meir, Wingreen and Jauho [30]. It is not of much interest here as the fractions are not an expression of the underlying quantum state but as a imposed constraint. There is no requirement for n or m to be an integer when setting the couplings to the reservoirs, therefore changing the parameters of the system will likely affect the precise nature of the coupling. This makes unequal coupling to the reservoirs unlikely to be a cause of the fractional plateaus, especially as experimentally there is no reason to expect unequal coupling.

7.2 Spinful Generalisation

The previous analysis will now be generalised to a spinful case, which will reveal fractional peaks in the conductance. The lack of renormalisation in the prior result is due to the cancellation provided by $\mathcal{G}_{1N}^2 = \mathcal{G}_{11}^2$ for each term. Any system that has a difference between excitations travelling along the chain and staying at the same place will result in different behaviour to the spinless case. A spinful generalisation of the original model will provide this transmission behaviour.

First, the spinful Hamiltonian is defined as,

$$H_{spin} = -t \sum_{\sigma} \sum_i (d_{\sigma,i}^\dagger d_{\sigma,i+1} + d_{\sigma,i+1}^\dagger d_{\sigma,i}) + \sum_i U_0 n_{\uparrow,i} n_{\downarrow,i} + N_i U_1 N_{i+1} \quad (7.47)$$

where $d_{\sigma,i}$ now annihilates an electron of spin σ on site i and N_i is the total number electron operator

$N_i = n_{\uparrow,i} + n_{\downarrow,i}$. Taking the $U_0, U_1 \rightarrow \infty$ limit projects out any states that contain neighbouring spins, regardless of their respective spins. Crucially the hopping term in the Hamiltonian is diagonal in spin space, with no spin flipping terms. The filling parameter Q now refers to the total electrons,

$$Q = N_e + \frac{L}{2}. \quad (7.48)$$

7.2.1 Eigenstates

As before, the eigenstates at $Q = 1/2$ and $Q = -1/2$ need to be solved for in order to find the uncoupled Green's function. Instead of having one frozen state at $Q = 1/2$, there now are 2^{L_S} degenerate configurations of the form $|\sigma_1 - \sigma_2 - \cdots - \sigma_{L_S}\rangle$ that will be orthogonal to each other. All of these spin configurations are eigenstates with zero energy.

The $Q = -1/2$ filling will have 2^{L_S-1} subspaces corresponding to each possible ordering of spins. The infinite repulsion between the electrons prevents two spins from swapping places, so there is a subspace for every ordering rather than just total magnetisation. The eigenstates are given by the spinless eigenstates. To see why, consider all the possible states in the projected subspace for a given spin configuration $\{\sigma_1 \sigma_2 \cdots \sigma_{L_S-1}\}$. The eigenstates will be a linear combination of all of the ways to arrange the electrons on the sites, such that the ordering remains the same,

$$\begin{aligned} |Q = -1/2, \{\sigma_1 \sigma_2 \cdots \sigma_{L_S-1}\}, k\rangle = & a_{1,k} |--\sigma_1 - \sigma_2 - \cdots - \sigma_{L_S-1}\rangle \\ & + a_{2,k} |-\sigma_1 - -\sigma_2 - \cdots - \sigma_{L_S-1}\rangle \\ & \cdots + a_{P,k} |\sigma_1 - \sigma_2 - \cdots - \sigma_{L_S-1} --\rangle, \end{aligned} \quad (7.49)$$

where $P = L_S(L_S + 1)/2$.

This collection of basis states corresponds to the positional configurations of the spinless case for a specific spin configuration and can be mapped to the same soliton representation in the exact same way. The hopping is equal for the different spins, so the Hamiltonian in the soliton basis is the same. Therefore the eigenstates and coefficients for a given spin configuration are exactly the same as in Equation 7.15 and 7.16. As there is no magnetic field, all configurations are equal in energy and the full dispersion is the spinless dispersion with a 2^{L_S-1} degeneracy at each eigenstate corresponding to each possible spin configuration. The coefficients of the above expression will be the same for every spin configuration for

a particle eigenstate but the basis states will be different due to involving a different set of spins.

To recap notation, the occupation representation will be denoted by the string of dashes and σ . The eigenstates of the spinful Hamiltonian will contain the filling, the spin configuration from left to right and an additional counting index labelling the eigenstates for the $Q = -1/2$ filling. The eigenstate index is not needed in the $Q = 1/2$ filling as there is only one state for each spin configuration.

7.2.2 Attaching Spinful Contacts

A crucial change from the spinless case is that there are now extra modes in the reservoir and each mode can hop onto the wire. The total Hamiltonian of the system now becomes,

$$H = \sum_{\sigma} \sum_{k,\alpha} \epsilon_{k,\alpha}^{\sigma} c_{k,\sigma,\alpha}^{\dagger} c_{k,\sigma,\alpha} + \sum_{\sigma,\alpha} V_{k,\alpha}^{\sigma} (c_{k,\sigma,\alpha}^{\dagger} d_{\sigma,\alpha} + d_{\sigma,\alpha}^{\dagger} c_{k,\sigma,\alpha}) + H_{spin}. \quad (7.50)$$

Using Equation 7.21, the effective action can be found,

$$S_{eff} = S_{wire} + e \sum_{k,\sigma} \int_K dt dt' V_{L,\sigma,k}^2 \bar{\phi}_{\sigma,1}(t) g_{L,\sigma,k}(t, t') \phi_{\sigma,1}(t) + V_{R,\sigma,k}^2 \bar{\phi}_{\sigma,L}(t) g_{R,\sigma,k}(t, t') \phi_{L,\sigma}(t),$$

where the Green's functions in the reservoir are now defined for each spin mode. As before, the extra terms in the effective action define the self-energy matrix. Using the vector $\phi = (\phi_{\uparrow}, \phi_{\downarrow})^T$, where ϕ_{σ} is the N dimensional vector that describes the field at each position along the chain for each spin, the self-energy becomes,

$$\Sigma = \begin{pmatrix} \Sigma^{\uparrow\uparrow} & 0 \\ 0 & \Sigma^{\downarrow\downarrow} \end{pmatrix}. \quad (7.51)$$

This is just two copies of the spinless case where $\Sigma^{\sigma\sigma}$ are $N \times N$ matrices with only two non-zero elements at $\Sigma_{11}^{\sigma\sigma} = V_{\sigma,L,k}^2 g_{k,L}^{\sigma}$ and a similarly defined $\Sigma_{NN}^{\sigma\sigma}$.

The current $J_{L,\uparrow}$ will be given by Equation 7.24

$$J_{L,\uparrow} = \int_{-\infty}^{\infty} d\omega (\Delta G)_{11}^{\uparrow\uparrow} (\Sigma_{11}^{\uparrow\uparrow})^< + (\Delta \Sigma)_{11}^{\uparrow\uparrow} (G_{11}^{\uparrow\uparrow})^<, \quad (7.52)$$

where the new spinful coupled Green's functions are,

$$G_{ij}^{\sigma\sigma'} = \frac{1}{Z} \int \mathcal{D}\phi \phi_{\sigma i} \bar{\phi}_{\sigma' j} e^{iS_{eff}}. \quad (7.53)$$

The kinetic equation then is used to express $\Delta\mathbf{G}$ and $\mathbf{G}^<$ in terms of the retarded and advanced Green's function. There is no spin flipping term in the Hamiltonian so the uncoupled Green's function will not have any terms that link together the spin spaces. As the self-energy is also diagonal, the problem decouples into two spin sectors that do not interact with each other. This is what is expected to happen - after all in the Landauer case every channel contributes e^2/h and there are two non-interacting channels. The channels are non-interacting as all interactions are projected out in the $U_0, U_1 \rightarrow \infty$ limit.

The spin space decoupling means that the derivation of the current expression will proceed in the same way as the spinless case. Therefore,

$$J_{L,\uparrow} = \int_{-\infty}^{\infty} (G_{1N}^{\uparrow\uparrow})^r (G_{N1}^{\uparrow\uparrow})^a [\Delta\Sigma_R^{\uparrow\uparrow} (\Sigma_L^{\uparrow\uparrow})^< - (\Sigma_L^{\uparrow\uparrow})^< \Delta\Sigma_R^{\uparrow\uparrow}]. \quad (7.54)$$

The total current, $\bar{I}_L = I_{L,\uparrow} + I_{L,\downarrow}$, in the left reservoir will become,

$$\bar{I}_L = e^2 V \sum_k \int_{-\infty}^{\infty} \frac{d\omega}{2\pi} \left(4\Gamma_{L,k}^{\uparrow} \Gamma_{R,k}^{\uparrow} |(G_{1N}^{\uparrow\uparrow})^r(\omega)|^2 f'_\uparrow(\omega - \mu) + 4\Gamma_{L,k}^{\downarrow} \Gamma_{R,k}^{\downarrow} |(G_{1N}^{\downarrow\downarrow})^r(\omega)|^2 f'_\downarrow(\omega - \mu) \right). \quad (7.55)$$

Solving Dyson's equation for the coupled Green's function also uses the separation of spin spaces. There is then an equation for each spin,

$$\mathbf{G}^{\sigma\sigma} = \mathbf{G}^{\sigma\sigma} + \mathbf{G}^{\sigma\sigma} \Sigma^{\sigma\sigma} \mathbf{G}^{\sigma\sigma} \quad (7.56)$$

where the uncoupled Green's functions in the spinful case become,

$$\mathcal{G}_{ij}^{\sigma\sigma'}(\omega) = \frac{1}{Z} \sum_{n,m} \left(e^{-\beta(\epsilon_n - \mu n_e)} + e^{-\beta(\epsilon_m - \mu m_e)} \right) \frac{\langle n | d_{j\sigma'}^\dagger | m \rangle \langle m | d_{i\sigma} | n \rangle}{\omega + \epsilon_m - \epsilon_n + i\eta}. \quad (7.57)$$

Dyson's equation can be solved in the exact same way as previously. The coupled spinful Green's function becomes,

$$G_{1N}^{\sigma\sigma} = \frac{\mathcal{G}_{1N}^{\sigma\sigma}}{1 + 2i\mathcal{G}_{11}^{\sigma\sigma}(\Gamma_R^\sigma + \Gamma_L^\sigma) + ((\mathcal{G}_{1N}^{\sigma\sigma})^2 - (\mathcal{G}_{11}^{\sigma\sigma})^2)\Gamma_L^\sigma\Gamma_R^\sigma}. \quad (7.58)$$

This looks identical to the previous case and would naively be expected to simply double the previous result. It is in the calculation of the matrix overlaps in the uncoupled Green's function where the difference hides.

7.2.3 Conductance

To calculate $\mathcal{G}_{11}^{\sigma\sigma}$ and $\mathcal{G}_{1N}^{\sigma\sigma}$, only the $Q = -1/2$ and $Q = 1/2$ fillings are considered. This is justified in the same way as before: that the chemical potential is chosen to be equal to the ground state energy of the $Q = -1/2$ filling. The small temperature guarantees that the other fillings are exponentially suppressed. With this simplification, and using the fact that all eigenstates with a $Q = 1/2$ filling are zero energy,

$$\begin{aligned} \mathcal{G}_{11}^{\sigma\sigma'} &= \frac{1}{Z} \sum_{n,m} \frac{1 + e^{-\beta(\epsilon_n + \mu)}}{\omega - \epsilon_n + i\eta} \\ &\quad \times \langle Q = 1/2, m | d_{1\sigma}^\dagger | Q = -1/2, n \rangle \langle Q = -1/2, n | d_{1\sigma'} | Q = 1/2, m \rangle \end{aligned} \quad (7.59)$$

where n, m index the states in the $Q = -1/2$ and $Q = 1/2$ fillings respectively regardless of spin configuration.

The crux of the difference in the spinful case can be found in the matrix overlaps, which depend on the spin structure. Considering the frozen states in the $Q = 1/2$ filling, the sum over all eigenstates is the same as the sum over all configurations $\{\sigma\}$,

$$\sum_m |Q = 1/2, m\rangle = \sum_{\{\sigma\}} |\sigma_1 - \sigma_2 - \dots - \sigma_{L_S}\rangle. \quad (7.60)$$

The smaller filling contains the same eigenstate sum as the spinless case, summed over all spin configurations. There will be half the number of spin configurations in this sum as there is one fewer electron,

$$\sum_n |Q = -1/2, n\rangle = \sum_{\{\sigma\}} \sum_k |Q = -1/2, \{\sigma_1 \sigma_2 \dots \sigma_{L_S-1}\}, k\rangle. \quad (7.61)$$

For a given spin configuration, we act the annihilation operator on the first site,

$$d_{1\sigma'} |Q = 1/2, \{\sigma_1 - \sigma_2 - \dots - \sigma_{L_S}\}\rangle = \delta_{\sigma'\sigma_1} |Q = -1/2, \{- - \sigma_2 - \dots - \sigma_{L_S}\}\rangle, \quad (7.62)$$

giving one of the underlying occupation configurations. This will have a non-zero overlap with the eigenstates in the $|Q = -1/2, \{\sigma_2 \dots \sigma_{L_S}\}\rangle$ subspace. The overlap will be given by ψ_{12}^q .

Applying the creation operator $d_{1\sigma}^\dagger$ in this subspace produces the original state with the coefficient

of the eigenstate expansion,

$$\begin{aligned} d_{1\sigma}^\dagger |Q = -1/2, \sigma_2 \cdots \sigma_{L_S}, q\rangle &= d_{1\sigma}^\dagger (\psi_{12}^q |--\sigma_2 - \cdots - \sigma_{L_S}\rangle + \cdots) \\ &= \psi_{12}^q |\sigma - \sigma_2 - \cdots - \sigma_{L_S}\rangle. \end{aligned} \quad (7.63)$$

All the operators must bring us back to the original state due to the trace, resulting in $\sigma = \sigma'$. The factor of $\delta_{\sigma'\sigma_1}$ means that all configurations with $\sigma' \neq \sigma_1$ do not contribute, halving the number of contributing spin configurations. The Green's function then becomes,

$$G_{11}^{\sigma\sigma'} = \frac{1}{Z} \sum_q \sum_{\{\sigma\}} \frac{1 + e^{-\beta(\epsilon_n + \mu)}}{\omega - \epsilon_n + i\eta} \delta_{\sigma',\sigma_1} (\psi_{12}^q)^2 = \frac{2^{L_S-1}}{Z} \sum_q \frac{1 + e^{-\beta(\epsilon_n + \mu)}}{\omega - \epsilon_n + i\eta} (\psi_{12}^q)^2. \quad (7.64)$$

It is due to the degeneracy of the eigenstates for each spin configuration that the sum can be easily performed.

When considering propagation through the entire chain, the new matrix overlap to consider is,

$$\langle Q = 1/2, m | c_{N\sigma}^\dagger |Q = -1/2, n\rangle \langle Q = -1/2, n | c_{1\sigma} |Q = 1/2, m\rangle, \quad (7.65)$$

Following the above idea, the annihilation operator acts first, annihilating the electron on the end site,

$$c_{1\sigma} |Q = 1/2, \{\sigma_1 - \sigma_2 - \cdots - \sigma_{L_S}\}\rangle = \delta_{\sigma\sigma_1} |Q = -1/2, \{--\sigma_2 - \cdots - \sigma_{L_S}\}\rangle. \quad (7.66)$$

This will only have a non-zero overlap with an eigenstate that has same the spin configuration. This produces the coefficient of this state in the $Q = -1/2$ eigenstate expansion which is ψ_{12}^q , just like the previous case. Acting the creation operator in this subspace gives,

$$\begin{aligned} d_{N\sigma}^\dagger |Q = -1/2, \{\sigma_2 \cdots \sigma_{L_S}\}, q\rangle &= d_{1\sigma}^\dagger (\psi_{12}^q |--\sigma_2 - \cdots - \sigma_{L_S}\rangle + \cdots) \\ &= \psi_{L_S L_S+1}^q |\sigma_2 - \sigma_3 - \cdots - \sigma_{L_S} - \sigma\rangle. \end{aligned} \quad (7.67)$$

The overlap between this state and the original state $|\sigma_1 - \sigma_2 - \cdots - \sigma_{L_S}\rangle$ will only be non-zero if $\sigma_{i+1} = \sigma_i$ for all i . This means only a fully polarised spin chain can have an electron hop off at one end and hop on at the other. All other possibilities are precluded by the orthogonality of spin configurations.

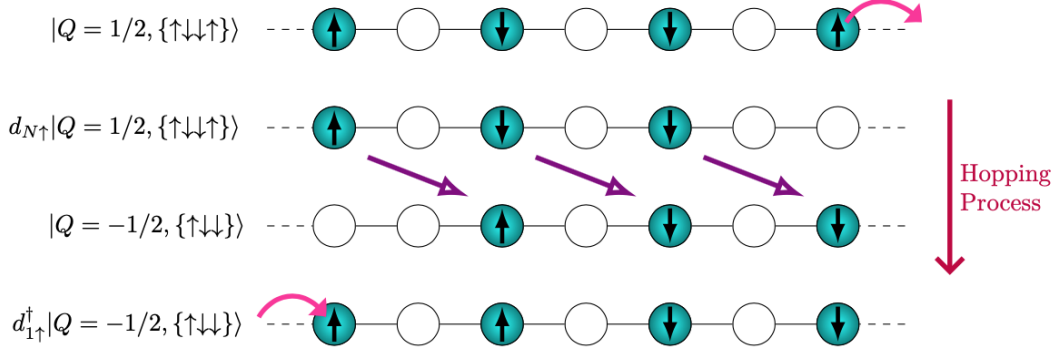


Figure 7.11: Demonstrating how the states change upon application of the creation and annihilation operators in \mathcal{G}_{N1} starting from a given spin configuration. The final state is orthogonal to the starting state, which will result in only spin-polarised states contributing in the sum over spin configurations in the Green's function.

Figure 7.11 shows how a non-polarised spin configuration will result in an orthogonal configuration after acting the operators in the Green's function.

Therefore in the summation over all possible spin configurations in the Green's function not every state contributes equally. Only the polarised configuration has a non-zero overlap,

$$\mathcal{G}_{1N}^{\sigma\sigma} = \frac{1}{Z} \sum_q \frac{1 + e^{-\beta(\epsilon_n + \mu)}}{\omega - \epsilon_n + i\eta} \psi_{12}^q \psi_{L_S L_S+1}^q. \quad (7.68)$$

Thus we have shown the form that the Green's functions take in the spinful case. Using the same form as Equation 7.36 we obtain,

$$\mathcal{G}_{11}^{\sigma\sigma}(\omega) = \frac{A}{Z} \sum_q \frac{z_q}{\omega - \epsilon_q + i\eta}, \quad \mathcal{G}_{1N}^{\sigma\sigma}(\omega) = \frac{1}{Z} \sum_q \frac{z_q s_q}{\omega - \epsilon_q + i\eta}, \quad (7.69)$$

where $A = 2^{L_S-1}$ and $s_q = \{1, -1\}$ as before.

To calculate the precise form of the coupled spinful Green's function, Equation 7.58 is used. Again only one term, q^* , in the sum will contribute. This results in,

$$G_{1N}^{\sigma\sigma} = \frac{z_{q^*} s_{q^*}^*}{\left(\omega - \epsilon_{q^*} - \Gamma_L \Gamma_R z_{q^*}^2 \left(\frac{A^2 - 1}{\omega - \epsilon_{q^*}} \right) \right) + i z_{q^*} A (\Gamma_L + \Gamma_R)}, \quad (7.70)$$

where the $\delta \rightarrow 0$ limit can be safely taken due to the finite imaginary part. The conductance uses the

modulus squared of this expression, which in the zero temperature limit allows us to set $\omega - \epsilon_{q^*} = \delta\mu$ in the expression,

$$|G_{1N}^{\sigma\sigma}|^2 = \frac{4\bar{\Gamma}_L\bar{\Gamma}_R z_{q^*}^2}{\left(\delta\mu - \frac{\bar{\Gamma}_L\bar{\Gamma}_R z_{q^*}^2(A^2-1)}{\delta\mu}\right)^2 + A^2 z_{q^*}^2(\bar{\Gamma}_L + \bar{\Gamma}_R)^2}. \quad (7.71)$$

The term containing $\delta\mu$ is positive definite, so the maximum of the function can be found where this term equals zero, $\delta\mu = \pm z_{q^*}\Gamma\sqrt{A^2 - 1}$. The conductance will therefore split into two upon the addition of spinful channels. The height of this peak is $1/A^2$ for equal coupling to the reservoirs. Exactly at resonance, when $\delta\mu = 0$, this expression tends to zero. For $A = 1$, this term reduces to the spinless result of Equation 7.45.

Calculating the total current requires the contribution from both channels which will behave in the exact same way due to the separation in spin space. For zero temperature and generic coupling, upon substituting back in for A ,

$$g = \frac{I_L^\uparrow + I_L^\downarrow}{V} = \frac{1}{2^{2L_S-4}} \left[\frac{\Gamma_L^\uparrow \Gamma_R^\uparrow}{(\Gamma_L^\uparrow + \Gamma_L^\uparrow)^2} + \frac{\Gamma_L^\downarrow \Gamma_R^\downarrow}{(\Gamma_L^\downarrow + \Gamma_L^\downarrow)^2} \right]. \quad (7.72)$$

Many different fractions can be achieved when tuning the couplings to the reservoirs as there are four parameters to vary. This case is not particularly remarkable, as the fractions arise from the choice of condition, rather than as an expression of the microscopic behaviour.

The more compelling case is when the couplings are equal. Fractional resonant peaks will occur at values of $1/2^{2L_S-3}$. When $L_S = 1$, there is only one site which will either be occupied or unoccupied and this has a conductance of $2e^2/h$, which is to be expected for a system with two channels. The first few fractions in units of e^2/h are $2, 1/2, 1/8, 1/32, 1/128$. The results for different numbers of electrons in the Wigner chain are shown in Figure 7.12.

Adding a magnetic field to the spinful case will lift the degeneracy. This will reduce the coefficient of the \mathcal{G}_{11} term because any configuration that is not spin-polarised will have its energy raised. The sum over all spin configurations in Equation 7.64 will only contain a spin-polarised state, for a strong enough field. Therefore this recovers $\mathcal{G}_{11} = \mathcal{G}_{1N}$ for individual terms in the sum and produces the spinless result. More complex interactions could occur when the energy separation from the magnetic field becomes large enough to cross over the excited state.

Finally, higher order process such as co-tunnelling can be safely ignored. For weak coupling to the reservoirs, these terms are suppressed by Γ^{2p} where p is the integer number of tunnelling events. The

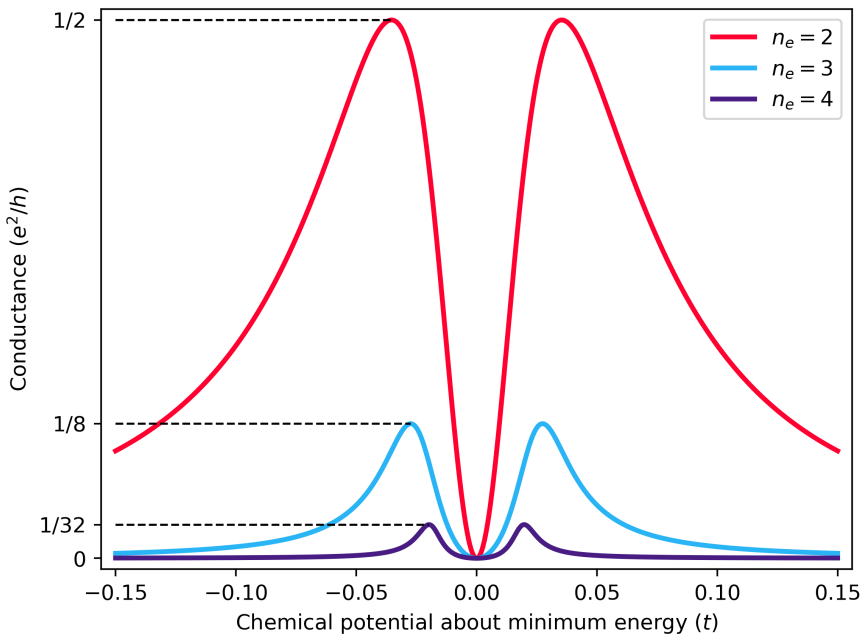


Figure 7.12: The conductance of a spinful Wigner chain upon varying the chemical potential for a different lengths in the system.

number of spin configurations that can contribute to transport, upon allowing higher order processes, does not increase sufficiently quickly to counteract the small coupling. As an example, there are two spin configurations that require four interactions with the reservoir to shift the spin ordering along by two. These correspond to the two antiferromagnetic configurations, which will not compensate the squaring of the coupling.

7.3 Further Work and Conclusions

This thesis set out to analyse the possible origins of fractional conductance in one-dimensional systems. A variety of approaches were explored through a pedagogical lens to provide a solid grounding of the problem and the existing literature that surrounds it. The strongly correlated regime, in which these fractional plateaus reside, is notorious for being hard to study which is why a multi-pronged approach is useful.

Most of the literature has approached this problem, and transport in 1D more generally, by starting with a Luttinger liquid. The ubiquity of this approach is due to the quadratic nature of the action and the

universality of the resulting description, which encapsulates many different models. Under certain conditions with the contacts, this produces fractional plateaus. Luttinger liquid ideas have been successfully applied to describe the fractional plateaus in the fractional quantum Hall effect. Increasingly ingenious combinations of chiral Luttinger liquids and QPCs have resulted in a wealth of understanding and possibilities in this area, with evidence for the fractional statistics of the quasiparticles being observed in recent years [97, 98].

Helical Luttinger liquids were instrumental in reproducing fractional conductance not just in a chiral edge mode of a 2D system, but in a 1D system proper. Shavit and Oreg [58] managed to extend these ideas to a situation where time-reversal symmetry holds. Their results match up to experiment incredibly well, but only for the plateau at $(2/5)e^2/h$. Other fractions are observed which cannot be predicted by this approach. Although Shavit and Oreg's approach gives a convincing partial explanation of this phenomenon, there are clearly other pieces of the puzzle yet to be found.

The concurrent understanding of quantum dots has been developing to describe increasingly complex situations. Much of the research in this field is interested in the limit that there are many electrons crammed onto the dot. The final chapter of this thesis explored the application of these discrete techniques on fractional plateaus. This constitutes a new approach to this problem, with many features that are distinct to finite systems which are quickly washed out with increasing system length.

The fundamental feature that obtains these fractional values of conductance at resonance is a splitting of the state space into states that can support transport and those that cannot. This mechanism could, in theory, generate any fraction. The difficulty is in finding models that have this feature. Both the spinful and spinless cases of a 1D Wigner chain were examined, with the spinless chain containing the exact same amount of configurations that could conduct as ones that could not. The degenerate spinful case did show a difference, where only the polarised configuration could have an electron hopping on at one end and off at the other. The other configurations required higher-order interactions with the reservoirs, which would be negligible for weak tunnelling.

The most obvious way that this work could be extended is through considering the situation where spin symmetry is broken. This would result in both coupled and uncoupled Green's functions no longer being diagonal in spin space. To consider situations where the coupling to the reservoirs is increased would require an understanding of how the co-tunnelling terms contribute. The interaction between the excited states and the lifting of the degeneracy by a magnetic field could also result in interesting

behaviour.

Introducing interactions at longer range would require additional terms in the original Hamiltonian, Including U_2 , which would act on next-nearest neighbours, forms another possible extension. Taking the infinite interaction limit of this new term would result in a Wigner crystal with an electron every three sites. There would be three solitons in the system, of charge $e/3$. The mappings to the 3D square lattice may allow for the eigenstates to be calculated. Generalising this process to a filling of $1/n$ would be possible though by considering the infinite interaction limit of the U_{n-1} term. This will, however, become increasingly unlikely to be a reasonable approximation.

Many more scenarios could be concocted and analysed in the same way, with a microscopic model being required. The number of transport channels in both the wire and contacts are crucial quantities in determining the conductance behaviour. This chapter has only considered the case where each contact was directly connected to the transport channel. This could be generalised by considering channels in the wire that are not connected to the contacts.

APPENDIX A

FUNCTIONALS

A.1 Functional Calculus

Functionals, written as $F[x(t)]$, describe a mapping from a function $x(t)$ to a scalar. This is often implemented by an integration over the variables that the function depend on. Before understanding why functionals are useful in quantum theory, we will deal with how to mathematically deal with the calculus of functionals. All of this introduction follows Altland and Simons' book [28].

A.1.1 Functional Derivatives

Derivatives of functionals describe how the scalar result of the functional changes upon modifying the underlying function [99]. A way of perturbing a given function, $x(t)$ is by using a delta function acting at a generic point t' . As functionals contain an integration, the delta functions are well defined and provide a small bump in the original function. The functional derivative is defined as,

$$\frac{\delta F[x(t)]}{\delta x(t')} = \lim_{\epsilon \rightarrow 0} \frac{F[x(t) + \epsilon \delta(t - t')] - F[x(t)]}{\epsilon}. \quad (\text{A.1})$$

To actually perform any functional derivatives, we simply rely on the following result that can be seen from the definition,

$$\frac{\delta x(t)}{\delta x(t')} = \delta(t - t'). \quad (\text{A.2})$$

Using this relation and both the chain and product rules, which survive the transition to functional differ-

entiation, any functional derivative can be computed. As a prescient example, if $G[x(t)] = e^{\int dt x(t)a(t)}$ then,

$$\frac{\delta G}{\delta a(t')} = e^{\int dt x(t)a(t)} \frac{\delta}{\delta a(t')} \int dt a(t)x(t) = e^{\int dt x(t)a(t)} \int dt x(t)\delta(t - t') = x(t')G[x(t)]. \quad (\text{A.3})$$

Note that taking the functional derivative with respect to t' produces a function that depends on t' , as we have obtained a description of how large the change in the functional is when perturbing the original function at the point t' . Therefore the total change to the functional upon perturbing by a generic function would require an integral over all t' . To linear order for a generic perturbation $g(t)$,

$$\delta F[x(t) + \epsilon g(t)] = \epsilon \int dt' \frac{\delta F[x(t)]}{\delta x(t')} g(t') + O(\epsilon^2). \quad (\text{A.4})$$

Higher orders of functional differentiation are introduced in a similar way but must be with respect to a different variable. The change of a function when it is perturbed in two different places will depend on the location of both t' and t'' , and both must therefore be integrated over. The second order term in the above expansion will therefore be,

$$\frac{1}{2!} \int \int dt dt' \frac{\delta^2 F[x(t)]}{\delta x(t') \delta x(t'')} h(t'') g(t'), \quad (\text{A.5})$$

with the n th order functional derivative requiring n different variables to be integrated over. With this knowledge, any functional can be expanded in a functional Taylor series, except instead of being around a point, it will be around a specific function.

A.1.2 Functional Gaussian Integration

Much like in the calculus of functions, functional integration is a lot harder than calculating derivatives. There is only a small class of functionals that can be integrated and the proof of how they are integrated then comes from considering a continuum generalisation of multi-dimensional Gaussian integration. As such, it is worth a recap of how to integrate Gaussian functions. For N independent copies of a Gaussian multiplied together, each one can be performed separately to give,

$$\int_{-\infty}^{\infty} \prod_{i=1}^N dx_i e^{-x_i A_i x_i} = \prod_{i=1}^N \sqrt{\frac{\pi}{A_i}}. \quad (\text{A.6})$$

Each A_i must be positive in order to ensure convergence of the integral. This can be transformed into a more general matrix form by considering x_i as vectors. The product over exponentials becomes a sum in the exponents, and the components A_i can be interpreted as the diagonal elements of a matrix A_{ij} . A generic form can be found through performing a unitary transformation on the diagonal basis, mixing up the eigenvectors x_i . A unitary transformation is chosen as the Jacobian will be equal to unity and therefore not affect the measure $\prod dx_i$. The product of all A_i on the right hand side of Equation A.6, then becomes the determinant of the matrix A_{ij} which is basis independent. This gives the more general result of,

$$\int_{-\infty}^{\infty} \left(\prod_{i=1}^N dx_i \right) e^{-\sum_{ij} x_i A_{ij} x_j} = (\pi)^{N/2} \frac{1}{\sqrt{\det(A)}}. \quad (\text{A.7})$$

Another generalisation is possible by adding a linear term,

$$\int_{-\infty}^{\infty} \left(\prod_{i=1}^N dx_i \right) e^{-\sum_{ij} x_i A_{ij} x_j + \sum_i J_i x_i} = (\pi)^{N/2} \frac{1}{\sqrt{\det(A)}} e^{\sum_{ij} J_i A_{ij}^{-1} J_j / 4} \quad (\text{A.8})$$

where A_{ij}^{-1} is the ij th component of the matrix inverse of matrix \mathbf{A} . This can be shown through a linear transformation on the vectors, essentially completing the square in a multi-dimensional case. Functional integration comes from letting $N \rightarrow \infty$, because then i goes from an index of different x components to a variable, producing a function, $x(i)$. Each point is separately integrated from $-\infty$ to ∞ which means that all possible $x(i)$ are considered.

The main equation of functional integration is,

$$\begin{aligned} & \int \mathcal{D}x(t) \exp \left(-\frac{1}{2} \int dt dt' x(t) A(t, t') v(t') + \int dt J(t) v(t) \right) \\ & \propto (\det A)^{-1/2} \exp \left(\frac{1}{2} \int dt dt' j(t) A^{-1}(t, t') j(t') \right), \end{aligned} \quad (\text{A.9})$$

where A^{-1} must now satisfy,

$$\int dt' A(t, t') A^{-1}(t', t'') = \delta(t - t''). \quad (\text{A.10})$$

The measure $\mathcal{D}x(t)$ is a compact way to write the infinite product of dx_i integrations. The first issue is that both $\pi^{N/2}$ and the determinant diverge in the infinite dimensional limit, which is why functional

APPENDIX A. FUNCTIONALS

averages need to be introduced. The average of a quantity is defined as

$$\langle(\cdots)\rangle = \frac{1}{\mathcal{Z}} \int \mathcal{D}x(t) (\cdots) e^{iS[x(t)]}, \quad \mathcal{Z} = \int \mathcal{D}x(t) e^{iS[x(t)]} \quad (\text{A.11})$$

where (\cdots) is any combination of the functions $x(t)$. The functional, $S[x(t)]$, defines the weighting of this average. The partition function, \mathcal{Z} provides the same coefficients that diverge as the functional integral in the numerator - resulting in a finite answer.

If the functional is quadratic (which includes the possibility of having a linear term as well) in the fields, then the main functional integration formula can be used to calculate any average. Here is where we introduce the main machinery of functional QFT, differentiating with source fields that get set to zero. For a functional S_0 , the average of two functions is defined as,

$$\langle x(t_1)x(t_2) \rangle = \frac{1}{\mathcal{Z}} \int \mathcal{D}x(t) x(t_1)x(t_2) e^{iS_0[x(t)]}, \quad S_0[x(t)] = \frac{1}{2} \int \int dt dt' x(t) A(t, t') x(t'). \quad (\text{A.12})$$

This average can be found by considering it as the average of a modified functional. A new source field is introduced that linearly and locally couples to the field,

$$S'[x(t), J(t)] = S_0[x(t)] + \int dt x(t) J(t). \quad (\text{A.13})$$

For $J(t) = 0$, it is clear that the two functionals match. The average over the original functional can then be rewritten using Equation A.3,

$$\langle x(t_1)x(t_2) \rangle = -\frac{1}{\mathcal{Z}} \int \mathcal{D}x(t) \left. \frac{\delta^2}{\delta J(t_1)J(t_2)} e^{iS'[x(t), J(t)]} \right|_{J=0}. \quad (\text{A.14})$$

The functional with the source field can be integrated using Equation A.9. The diverging constants will be cancelled out by \mathcal{Z} to give

$$\begin{aligned} \langle x(t_1)x(t_2) \rangle &= -\frac{\delta^2}{\delta J(t_1)J(t_2)} \exp\left(\frac{i}{2} \int dt dt' J(t) A^{-1}(t, t') J(t')\right) \Big|_{J=0} \\ &= A^{-1}(t_1, t_2) \end{aligned} \quad (\text{A.15})$$

where we have used $A^{-1}(t_1, t_2) = A^{-1}(t_2, t_1)$ to collect terms.

Any average over an odd number of fields for a purely quadratic action will result in zero because performing the functional derivative will always produce terms with a factor of the source field that will be set to zero. Averages over an even number of fields can be performed in a similar way and is a demonstration of Wick's theorem,

$$\langle x(t_1) \cdots x(t_{2n}) \rangle = \sum_{\substack{\text{pairings of} \\ \{t_1, \dots, t_{2n}\}}} A^{-1}(t_{k_1}, t_{k_2}) \cdots A^{-1}(t_{k_{2n-1}}, t_{k_{2n}}) \quad (\text{A.16})$$

Finally, it must be acknowledged that so far we had been considering real functions. The complex Gaussian integral has a similar form to Equation A.9, but the square roots on both the π and the determinant disappear. This is because both real and imaginary parts have to be integrated, essentially doubling N .

A.1.3 Beyond Quadratic Functionals

This seems like a very limited formalism as only averages that use functionals that are quadratic in their functions can be calculated. If higher order terms in the function exist in the functional, their effect can be calculated perturbatively. Defining a new functional to average over,

$$S[x(t)] = S_0[x(t)] + \lambda \int dt x(t)^4, \quad (\text{A.17})$$

which is the prototypical ϕ^4 action of QFT [27]. When λ is small, this means that the exponential of this functional present in the average definition can be expanded to give,

$$\langle x(t_1)x(t_2) \rangle = \frac{1}{Z} \int \mathcal{D}x(t) x(t_1)x(t_2) e^{S_0[x(t)]} \left(1 + \lambda \int dt x(t)^4 + \dots \right) \quad (\text{A.18})$$

$$= \langle x(t_1)x(t_2) \rangle_{S_0} + \lambda \left\langle x(t_1) \int dt x(t)^4 x(t_2) \right\rangle_{S_0} + \dots \quad (\text{A.19})$$

This brings the averages back to being over a quadratic functional and so the previous results can be used. Terms that arise from the expansion of the exponential can be calculated using Equation A.16. This transforms the problem into a combinatorial one, where the number of ways that the functions can be paired up is investigated. The Feynman diagram formalism is exactly this problem and all results from it can be derived in this functional way as mentioned in Chapter 3.

Another approximate way to deal with more complicated functionals is to find a stationary configuration and find the functional Taylor series. Expanding around this configuration allows the quadratic terms in this expansion to be considered. This is the basis of the semiclassical approximation which is one of the major strengths of the functional formalism.

A.2 Functional Integrals are Quantum Averages

Quantum mechanics is all about finding averages. Normally these take the form familiar from linear algebra - a weighted sum over eigenstates. Through some clever manipulations we can express these quantum averages as a functional integral. As the first example of re-expressing a quantum problem in terms of functionals, consider a particle moving through a potential, described by the Hamiltonian, $H = P^2/2m + V(x)$.

The aim is to know the probability that the particle will be at a given point, knowing its original position. This is encapsulated in the matrix overlap of $\langle q_f | U | q_i \rangle$, where U is the usual quantum mechanical evolution operator. To tackle this integral, the operator is split up into N time chunks, a process known aptly as time slicing [28]. Letting $t = N\Delta t$ gives us a parameter that is small compared to the eigenvalues of the operator, it can be expanded as,

$$\langle q_f | \exp(-iHt/\hbar) | q_i \rangle = \langle q_f | \exp(-iH\Delta t/\hbar) \cdots \exp(-iH\Delta t/\hbar) | q_i \rangle. \quad (\text{A.20})$$

Using the Baker–Campbell–Hausdorff (BCH) relation $e^A e^B = e^{A+B} e^{O([A,B])}$, the exponential of the Hamiltonian can be split in the following way,

$$e^{-i\Delta t H/\hbar} \approx e^{-iT\Delta t/\hbar} e^{-iV\Delta t/\hbar}, \quad (\text{A.21})$$

as the commutators in the BCH relation will contain higher powers of \hbar . Denoting the states at each of

the time evolution as $\{|q_i\rangle\}$ with $|q_0\rangle$ being the initial state, the probability for one time slice becomes,

$$\begin{aligned} P &= \langle q_N | e^{-iT\Delta t \hbar} e^{-iV\Delta t / \hbar} \dots e^{-iT\Delta t / \hbar} | q_0 \rangle e^{-iV(q_0)\Delta t / \hbar} \\ &= \int dp_0 \langle q_N | e^{-iT\Delta t \hbar} e^{-iV\Delta t / \hbar} \dots e^{-iT\Delta t / \hbar} | p_0 \rangle \langle p_0 | q_0 \rangle e^{-iV(q_0)\Delta t / \hbar} \\ &= \int dp_0 \langle q_N | e^{-iT\Delta t \hbar} e^{-iV\Delta t / \hbar} \dots | p_0 \rangle e^{-iT(p_0)\Delta t / \hbar} e^{ip_0 q_0 / \hbar} e^{-iV(q_0)\Delta t / \hbar} \\ &= \int dp_0 \int \frac{dq_1}{2\pi} \langle q_N | e^{-iT\Delta t \hbar} e^{-iV\Delta t / \hbar} \dots | q_1 \rangle e^{-ip_0 q_1 / \hbar} e^{ip_0 q_0 / \hbar} e^{-iT(p_0)\Delta t / \hbar} e^{-iV(q_0)\Delta t / \hbar}. \end{aligned}$$

Continuing on in this fashion gives the matrix element as,

$$P = \int \prod_{n=1}^{N-1} \frac{dq_n}{2\pi} \prod_{n=0}^N dp_n \exp \left(-\frac{i\Delta t}{\hbar} \sum_{n=0}^{N-1} V(q_n) + T(p_n) - p_n \frac{q_{n+1} - q_n}{\Delta t} \right). \quad (\text{A.22})$$

This integral is a $(2N - 1)$ dimensional integral over position and momentum at each of these time slices. In the continuum limit, where $N \rightarrow \infty$ and $\Delta t \rightarrow 0$ such that t is finite, these integrals become the functional integrals of the previous section. There are now boundary conditions on the fields where the initial and final states are set by the specific matrix overlap we are calculating.

Expressing the quantum average in terms of a functional integral considers all possible ways that the particle could travel from the initial to final point, with each path weighted by this functional. To understand what the functional that weights the average corresponds to, the field $p(t)$ is integrated out by using equation A.9,

$$P = \int \mathcal{D}p \mathcal{D}x \exp \left(\frac{i}{\hbar} \int_0^t p \dot{q} - \mathcal{H}(x, p) dt \right) = \int \mathcal{D}x \exp \left(\frac{i}{\hbar} \int_0^t \mathcal{L}(x, \dot{x}) dt \right). \quad (\text{A.23})$$

The averages can now be seen to be weighted by the action. The use of functional integrals is not limited to just single particle quantum mechanics, so their implementation in QFT will now be looked into.

A.2.1 Functional Integrals in Quantum Field Theory

In many high-energy physics QFT books, the coherent state field integral is not discussed as the fundamental starting point of the Lagrangian is preferred. In condensed matter however, a microscopic second quantised description of the problem is the fundamental description.

In QFT, there no longer is a dynamical position operator that evolves in time. Instead a field of

APPENDIX A. FUNCTIONALS

operators is present in both space and time that obey the equal time commutation relations. In this second quantised form, it is natural to use the creation and annihilation operators to describe a given Hamiltonian. This is a convenient way to represent the many body quantum state that must be confronted in condensed matter, especially the statistical properties of fermions and bosons.

In the calculation of the quantum mechanical average, the eigenstates of both position and momentum operators were used to act the Hamiltonian on a state. It turns out that eigenstates of the annihilation operator can be found and the same procedure performed on a second quantised Hamiltonian. The eigenstates are called coherent states and are given as the infinite sum of creation operators,

$$a_i |\phi\rangle = \phi_i |\phi\rangle, \quad |\phi\rangle = \exp\left(\sum_i \phi_i a_i^\dagger\right) |0\rangle, \quad \langle\phi| a_i^\dagger = \langle\phi| \bar{\phi}_i \quad (\text{A.24})$$

for bosonic annihilation operator a_i . The eigenvalue ϕ_i can be any, possibly complex, number. It turns out that different coherent states are not orthogonal and form an over-complete basis where the resolution of unity becomes,

$$\mathbb{1} = \int \prod_i \frac{d\bar{\phi}_i d\phi_i}{\pi} e^{-\sum_i \bar{\phi}_i \phi_i} |\phi\rangle \langle\phi|. \quad (\text{A.25})$$

This has the same measure as a complex functional integral when $i \rightarrow \infty$, which corresponds to a bosonic operator at every point in space - exactly the quantum field!

The quantity of interest in field theory is the weighted average of eigenstates. For a normal ordered Hamiltonian $H(a_i^\dagger, a_i)$ with number operator $N = \sum_i a_i^\dagger a_i$, the average is given by a sum over the eigenstates $|n\rangle$ of the Hamiltonian. This can be time sliced, but in imaginary time,

$$\sum_n \langle n| e^{-\beta(H-\mu N)} |n\rangle = \sum_n \langle n| e^{-\delta\tau(H-\mu N)} \dots e^{-\delta\tau(H-\mu N)} |n\rangle. \quad (\text{A.26})$$

The details of the change to imaginary time are explored in Chapter 2. Upon inserting a resolution of identity in between each slice, an expression for this average (which is the partition function in disguise) becomes,

$$\mathcal{Z} = \int \mathcal{D}\bar{\phi} \mathcal{D}\phi e^{-S[\bar{\phi}, \phi]}, \quad S[\bar{\phi}, \phi] = \int_0^\beta d\tau \bar{\psi} \partial_\tau \psi + H(\bar{\psi}, \psi) - \mu N(\bar{\psi}, \psi). \quad (\text{A.27})$$

The requirements of the eigenstate to still be $\langle n|$, enforced by the trace, after the full evolution gives a periodicity to the fields $\psi(0) = \psi(\beta)$. The measures over $\bar{\phi}$ and ϕ are combined into just one throughout

this thesis.

Fermions have a similar description to this bosonic one introduced, but they require the introduction of Grassmann numbers, η . These new strange objects have the fermionic property of anticommuting with themselves, $\eta_i \eta_j = -\eta_j \eta_i$. This means that $\eta_i^2 = 0$ which is exactly Pauli's exclusion principle. A field of these numbers can be created. All the coherent state structure of Equation A.24 will persist when Grassmann numbers are used instead of the complex ones. The representation of the coherent state as the exponential of the creation operators multiplied by a number will still work as all terms higher than η^2 cancel. There are some slight subtleties in that the measure no longer contains the factor of π . The functional integral over these Grassmann fields are now proportional to $\det(\mathbf{A})$ instead of the inverse square root found in Equation A.9.

A final point to make about this construction is that the average of functions as defined in Equation A.12 is inherently time ordered. All of the structure of going from a time-ordered formulation to a real-time one is required after averages have been calculated.

Therefore we have managed to describe both finite temperature averages and matrix overlaps as a functional integral over classical fields. The fields manage to sweep a few subtleties about time ordering and rigorous mathematical definition under the rug, but come with the benefit of being much clearer in the symmetries of the system. It is easier to find a transformation under which something is invariant, than a commuting operator.

APPENDIX A. FUNCTIONALS

APPENDIX B

DYSON'S EXPANSION

To find the expression for the time evolution of a time-dependent Hamiltonian, Schrödinger's equation must be solved [27]. Using the evolution operators results in,

$$i \frac{dU(t, t_r)}{dt} = H(t)U(t, t_r), \quad \rightarrow U(t, t_r) = U(t_r, t_r) - i \int_{t_r}^t dt_1 H(t_1)U(t_1, t_r). \quad (\text{B.1})$$

When no time evolution occurs, the state must not change which implies that $U(t, t) = 1$. The problem can be solved by inserting $U(t, t_r)$ into the right hand side iteratively,

$$U(t, t_r) = 1 - i \int_{t_r}^t dt_1 H(t_1) \left(1 - i \int_{t_r}^{t_1} dt_2 H(t_2)U(t_2, t_r) \right). \quad (\text{B.2})$$

This is an infinite sum so we can express it as such,

$$U(t, t_r) = \sum_{n=0}^{\infty} (-i)^n \int_{t_r}^t dt_1 \int_{t_r}^{t_1} \cdots \int_{t_r}^{t_{n-1}} dt_n H(t_1) \cdots H(t_n). \quad (\text{B.3})$$

There are n integrals at the n th order of summation. It is crucial to remember in this derivation that the Hamiltonian is a fully fledged operator whose order cannot be swapped carelessly. The set of t_n is also ordered so that $t \geq t_1 \geq t_2 \cdots \geq t_n \geq t_r$. This is due to the iterative nature of the procedure requiring intermediate times and those intermediate times appearing as the integration limits. This dependence however is difficult to implement and we can re-express this chain of conditional integrals with all the integrals having the same limits. To see how to obtain the same limits on the integral consider the term

at second order,

$$O^{(2)}(t, t_r) = - \int_{t_r}^t dt_1 \int_{t_r}^{t_1} dt_2 H(t_1)H(t_2), \quad \text{where } t_1 \geq t_2. \quad (\text{B.4})$$

Let's introduce a notation for ordering our operators called the time ordering operator \mathcal{T} . It is a tool that ensures that operators at earlier times act first and are therefore on the right side of the equation. This can be explicitly formulated by using Heaviside functions $\Theta(x)$,

$$\mathcal{T}\{A(t_1)B(t_2)\} = \theta(t_1 - t_2)A(t_1)B(t_2) \pm \theta(t_2 - t_1)B(t_2)A(t_1), \quad (\text{B.5})$$

where the \pm refers to the sign produced by the commutation relations of bosons or fermions. The second order term is re-written using this operator,

$$\mathcal{T}\left\{\int_{t_r}^t dt_1 \int_{t_r}^t dt_2 H(t_1)H(t_2)\right\} = 2O^{(2)}(t, t_r) \quad (\text{B.6})$$

which allows the limits on the integral to be the same as the Heaviside function enforces these limits now.

The factor of two must be introduced as the time ordering operator does not specify which time will be smaller. There are two ways of ordering t_1 and t_2 , so if we want to obtain just one of the ways then the division by two must occur. This logic continues to the m th order, where there are $m!$ ways of ordering m times. Each term in the sum can be then be formulate in terms of a time-ordered expression. This leads to the final result,

$$U(t, t_r) = \mathcal{T}\left\{\sum_{n=0}^{\infty} \frac{1}{n!} \int_{t_r}^t dt_1 \cdots dt_n H(t_1) \cdots H(t_n)\right\} = \mathcal{T} \exp\left(-i \int_{t_r}^t d\tau H(\tau)\right). \quad (\text{B.7})$$

The time-ordering that pervades quantum field theory arises due to the time evolution operator being expressed in this way.

APPENDIX C

CALCULATING THE JACOBIAN

The Jacobian is calculated from Equation 4.11, which can be rearranged into

$$\ln(J_\eta) = -\text{Tr}(\ln(1 + g_\eta \alpha_\eta)) = -\text{Tr}\left(\sum_n \frac{(g_\eta \alpha_\eta)^2}{n}\right) \quad (\text{C.1})$$

where $\alpha_\eta = \partial_\eta \theta(x, t)$ has been introduced. The focus of this appendix is concerned with showing that all terms in the sum where $n \neq 2$ do not contribute. Following this, the $n = 2$ term will be calculated to provide the final result of Equation 4.13.

To get to this loop cancellation theorem [42], we first need to examine the Green's functions calculated at finite temperature. The Green's function of the Tomonaga-Luttinger model can be found through taking a Fourier transform of Equation 4.6 and performing a Wick rotation into imaginary time,

$$g_\eta(k, \omega_n) = \frac{1}{i\omega_n - \eta v_F k}. \quad (\text{C.2})$$

Fourier transforming back into position space gives,

$$g_\eta(x - x', \omega_n) = \frac{i}{\nu_F} e^{-\frac{\eta \omega_n}{\nu_F} (x - x')} \quad (\text{C.3})$$

The sum over the Matsubara frequencies, $\omega_n = 2\pi T(n + 1/2)$, can be taken explicitly without having

to deal with contour integrals. This gives the Green's function in imaginary time,

$$g_\eta(x - x', \tau - \tau') = \frac{1}{2\beta v_F} \frac{1}{\sin\left(\frac{\pi}{\beta}((\tau - \tau') + \frac{i\eta}{v_F}(x - x'))\right)}. \quad (\text{C.4})$$

C.1 Loop Cancellation

The actual trace over of the n th term in the sum, where translational and temporal invariance is assumed, is given by,

$$\begin{aligned} \text{Tr}(\alpha_\eta g_\eta)^n &= \int \prod_{i=1}^n dx_i d\tau_i \prod_{i=1}^n \alpha_\eta(x_i, t_i) \\ &\times g_\eta(x_1 - x_2; t_1 - t_2) g_\eta(x_2 - x_3; t_2 - t_3) \cdots g_\eta(x_n - x_1; t_n - t_1). \end{aligned} \quad (\text{C.5})$$

The convolution of all of the Green's functions is defined as Γ . This function is proportional to the product of all of the sine terms,

$$\Gamma(s_1, s_2, \dots, s_n) \propto \prod_{i=1}^n \frac{s_i}{s_i - s_{i+1}}, \quad \text{where } s_i = \exp\left(\frac{2i\pi}{\beta}(\tau + ix/v_F)\right). \quad (\text{C.6})$$

To see why this rewriting is possible, notice that Equation C.4 can be expressed as,

$$g_\eta(x_1, x_2, \tau_1, \tau_2) \propto \frac{\sqrt{s_1 s_2}}{s_1 - s_2} \quad (\text{C.7})$$

from which it is easier to see how Equation C.6 is obtained. Any antisymmetric part of this function¹ will vanish upon the integration over all space and time from the trace. Therefore all our attention is turned to calculating the symmetric part which can be split into,

$$\prod_{i=1}^n \frac{s_i}{s_i - s_{i+1}} = \frac{\mathcal{A}_n(s_1, s_2 \dots s_n)}{\prod_{1 \leq i < j \leq n} (s_i - s_j)} \prod_{i=1}^n s_i. \quad (\text{C.8})$$

The numerator of the left hand side can be seen to be symmetric, and the denominator has been formed into an antisymmetric form, at the cost of introducing another polynomial \mathcal{A} . This polynomial must be antisymmetric in order for the full expression to be symmetric. As an example of what values it

¹Here symmetric is defined with respect to interchange of the variables of this multi-variable polynomial.

should take, consider the $n = 4$ term,

$$\begin{aligned}\Gamma_4 &= \frac{s_1 s_2 s_3 s_4}{(s_1 - s_2)(s_2 - s_3)(s_3 - s_4)(s_4 - s_1)} \\ &= \frac{s_1 s_2 s_3 s_4}{(s_1 - s_2)(s_1 - s_3)(s_1 - s_4)(s_2 - s_3)(s_2 - s_4)(s_3 - s_4)} \times -(s_1 - s_3)(s_2 - s_4),\end{aligned}$$

where the final term is \mathcal{A}_4 . By counting the powers of the right hand side of Equation C.8, the order of the polynomial must be $n(n - 3)/2$. This comes from the fact that there are $n(n - 1)/2$ ways of having $i < j$ (in a calculation to one performed in Chapter 7) and the order from the numerator will be just n . Note that negative orders are allowed as $1/(s_1 - s_2)$ is antisymmetric, so they can be simply view as inverses.

The minimum order of an antisymmetric polynomial must be $n(n - 1)/2$ as the powers of each variable must be different in each term of the polynomial. For $n = 3$, one of the terms will be $s_1^0 s_2^1 s_3^2$. The full polynomial will be the sum of the different ways of distributing the exponents on these three terms. These are the only terms allowed as if the powers were the same on any two terms, there would be a symmetry upon swapping the variables.

Combining these two pieces of information, the required order of the polynomial by power counting is smaller than the minimum possible order for it to be antisymmetric if $n > 2$. Therefore there is no way to create a symmetric contribution to Γ for all $n > 2$. These higher order terms can contribute in an antisymmetric way, but this will be exactly zero upon performing the trace. The $n = 0$ term is just a constant so can be ignored. The $n = 1$ term is related to the total electric charge, because the Green's function is like a density operator, $\langle c_k c_k^\dagger \rangle$. This is coupled to the introduced field, θ , which acts like an electromagnetic field A . This means the first order of the expansion gives the total charge, which must be zero due to electronegativity requirements.

C.2 The RPA Term

The only term that needs to be calculated is the $n = 2$ term, which corresponds to a polarisation term. Therefore the RPA approximation of normal materials is exact in the Tomonaga-Luttinger model! This

term in the expansion of Equation C.1 is, for $\xi \equiv (x, t)$,

$$\begin{aligned} -\frac{1}{2} \text{Tr}(\alpha_\eta^2 g_\eta^2) &= -\frac{1}{2} \int d\xi_1 d\xi_2 \alpha_\eta(\xi_1) g_\eta(\xi_1 - \xi_2) \alpha_\eta(\xi_2) g_\eta(\xi_2 - \xi_1) \\ &= -\frac{1}{2} \sum_{\epsilon_n} \int \frac{dk}{2\pi} \alpha_\eta(k, \epsilon_n) \alpha_\eta(-k, -\epsilon_n) \sum_{\omega_n} \int \frac{dp}{2\pi} g_\eta(p + k, \epsilon_n + \omega_n) g_\eta(p, \omega_n). \end{aligned} \quad (\text{C.9})$$

Both ω_n, ϵ_n are fermionic Matsubara frequencies. The sum over ω_n can be performed by considering a contour integral with a function that has poles at each of the fermionic Matsubara frequencies multiplied into the integrand. The contour along the imaginary axis is again deformed to include the two poles of the Green's function,

$$\frac{1}{2\pi i} \oint dz \frac{\beta}{e^{\beta z} + 1} \frac{1}{z + i\epsilon_n - \eta v_F(p+k)} \frac{1}{z - \eta v_F p} = \frac{1}{i\epsilon_n - \eta v_F k} (f(p) - f(p+k)), \quad (\text{C.10})$$

where $f(p)$ is the Fermi function at momentum p .

At low temperatures the integral over p will give either $\pm k$, dependent on the sign of η as both Fermi functions can be assumed to be a step function. The remaining term is simply $g_\eta(\epsilon_n, k)$ so we have shown that the convolution of two Green's functions produces the Green's function multiplied by $\pm k$. The whole expression is,

$$\ln(J_\eta) = - \sum_{\epsilon_n} \int \frac{dk}{2\pi} \alpha_\eta(\epsilon_n, k) \alpha_\eta(-\epsilon_n, -k) \frac{\eta k}{4\pi} g_\eta(\epsilon_n, k) \quad (\text{C.11})$$

$$= -\frac{i\eta}{4\pi} \int d\xi_1 d\xi_2 \alpha_\eta(\xi_1) \partial_x(g_\eta(\xi_1 - \xi_2) \alpha_\eta(\xi_2)). \quad (\text{C.12})$$

The Green's function is the inverse of the kernel in the action, $g_\eta = \partial_\eta^{-1}$. This will cancel with the ∂_η in the definition of α . This gives the final result as stated in the main thesis.

APPENDIX D

RENORMALISATION GROUP

The renormalisation group (RG) is a technique to extract the desired information from equations that cannot be exactly solved - allowing us to go from a complex microscopic theory to a macroscopic one. The idea behind it is that the description of a system at one specific scale can be related to the description at another scale with changed parameters. Usually in condensed matter physics we are interested in long wavelength degrees of freedom, so we want a procedure that integrates out the short wavelengths iteratively and focuses in on the low-energy behaviour. For a theory to be renormalisable, the structure of the Hamiltonian (or action) must be the same up to parameters changing, following this coarse graining procedure. Observing how these parameters change iteratively provides insight into whether microscopic interactions affect the long wavelength behaviour, helping to define relevant models.

If the parameter associated with an interaction strength grows under repeated action of the RG, then the interaction will dominate the low-energy behaviour [28, 100]. Although this can be performed in real space, performing this coarse graining in momentum space allows the procedure to be done in infinitesimal steps.

The particular way that RG will be implemented in this thesis will be the perturbative functional integral way. The first step is to split the field up into fast and slow modes, which are chosen to occur at Λ' . Beginning with a generic field $\theta(r)$,

$$\begin{aligned}\theta(r, t) &= \frac{1}{\beta L} \sum_{\omega} e^{iqr} e^{i\omega t} \theta(q, \omega) = \frac{1}{\beta L} \sum_{\omega < \Lambda'} e^{iqr} e^{i\omega t} \theta \theta(q, \omega) + \frac{1}{\beta L} \sum_{\Lambda' < \omega < \Lambda} e^{iqr} e^{i\omega t} \theta \theta(q, \omega) \quad (\text{D.1}) \\ &= \theta^s(r, t) + \theta^f(r, t),\end{aligned}$$

where θ^s are defined as the ‘slow’ modes and θ^f are the ‘fast’ modes. Λ is an ultraviolet cutoff beyond which contributions to the field are ignored. This is often the bandwidth in many fermionic problems. Another way of parameterising the frequency is by a scaling parameter b such that $\Lambda' = \Lambda/b$. Letting $b = 1 + \delta l$, defines an infinitesimally small portion of fast modes.

The next step is to integrate over all the fast modes to find a new effective action. The form of this new action is compared to the original action and must contain the same types of terms. If extra terms are generated by the integrating out of the fast modes then the procedure cannot be iterated and the theory is not renormalisable. Splitting the action of the system into parts containing the slow and fast modes separately and a mixed term,

$$Z[\theta] = \int \mathcal{D}\theta e^{-S[\theta]} = \int \mathcal{D}\theta^s e^{-S_s[\theta^s]} \int \mathcal{D}\theta^f e^{-S_f[\theta^f] - S_m[\theta^f, \theta^s]} \quad (\text{D.2})$$

$$= \int \mathcal{D}\theta^s e^{-S'[\theta^s]}, \quad (\text{D.3})$$

defines a new action $S'[\theta]$ that is given by the original slow modes of the action multiplied by functional integral over the fast modes. Defining this as an average with respect to the fast mode action, the new renormalised action becomes,

$$\begin{aligned} e^{-S'[\theta^s]} &= e^{-S_s[\theta^s]} \frac{\int \mathcal{D}\theta^f e^{-S_m[\theta^f, \theta^s]} e^{-S_f[\theta^f]}}{\int \mathcal{D}\theta^f e^{-S_f[\theta^f]}} \int \mathcal{D}\theta^f e^{-S_f[\theta^f]} \\ &= e^{-S_s[\theta^s]} \langle e^{-S_m[\theta^f, \theta^s]} \rangle_{S_f} Z_f[\theta^f]. \end{aligned} \quad (\text{D.4})$$

The partition function of the fast variables will be independent of the slow variables and will be cancelled in any calculations of the correlation functions. If this average can be calculated then we can follow the couplings in the action and determine how the system behaves at low energy. It is not always possible to calculate this average exactly, so the average must be perturbatively calculated.

Suppose there is a coupling in the action of the mixed term $S[\theta^f, \theta^s] = \lambda S[\theta^f, \theta^s]$, where λ is small. An expansion about this parameter can be performed to first order in λ . If the term is small enough, the resulting term can be re-exponentiated,

$$\langle e^{-\lambda S_m[\theta^f, \theta^s]} \rangle_{S_f} \approx 1 - \lambda \left\langle S_m[\theta^f, \theta^s] \right\rangle_{S_f} \approx e^{-\lambda \langle S_m[\theta^f, \theta^s] \rangle_{S_f}}. \quad (\text{D.5})$$

The final step is to rescale the frequencies in the effective action so that the cutoff momenta is the same regardless of scale $\omega' = s\omega$. This will rescale the fields by $\theta'(\omega') = \zeta^{-1}\theta^s(\omega'/s)$, and ζ is chosen appropriately. This allows us to compare the new action to the old one.

The new action is characterised by coupling constants changing, which in this case would be λ . Iterating the procedure leads to the RG flow equations which describe how λ changes with ω . An example of this technique in action is shown in Appendix E.

APPENDIX E

RG CALCULATIONS

Most of the calculations in this section appear in many other resources, notably Giamarchi's book [32]. They are written out here in a reasonable amount of detail for anyone masochistic enough to want to know the details. One of the difficulties of RG calculations in Luttinger liquids is that, despite their ubiquity within the literature, each author has their own choice of scaling of the fields. This leads to extra factors floating around in the calculation and can make switching between different literature confusing.

E.1 Weak Local Impurity

The effect of a point-like impurity at $x = 0$ ($V(x) = V_0\delta(x)$) to the Lagrangian will be

$$\begin{aligned}\mathcal{L}_{imp} &= V_0\rho(x = 0, t) = V_0 (\psi_L^\dagger + \psi_R^\dagger)(\psi_L + \psi_R) \Big|_{x=0} \\ &= V_0 \left(\rho_0 - \frac{1}{\pi} \partial_x \theta + 2 \cos(2\theta) \right) \Big|_{x=0},\end{aligned}\tag{E.1}$$

where the fermionic operators have been bosonised between lines. The first two terms can be absorbed into a redefinition of the Luttinger parameters. The cosine term, however, cannot be incorporated. This non-quadratic term only exists at one point, with the fields being quadratic at all other points in the system. Therefore an effective description can be obtained by integrating out these fields, which is done by introducing a new variable that only depends on time. Illustrating this technique, we use the action of

APPENDIX E. RG CALCULATIONS

a infinite spinless Luttinger liquid with an impurity at the origin

$$S = \frac{1}{2\pi K\nu} \int dx d\tau \left((\partial_\tau \theta)^2 + (\nu \partial_x \theta)^2 \right) + 2V_0 \int d\tau \cos(2\theta(x=0, \tau)). \quad (\text{E.2})$$

A Lagrange multiplier λ can be introduced that sets $\theta(x=0, t^*) = \theta_0(t^*)$ for a specific point in time t^* . Doing this for all times introduces the function $\lambda(t)$. This function can also be introduced by multiplying the measure by delta functions that enforce that the $\theta(x, t)$ field is equal to $\theta_0(t)$ at all points in time, then taking the Fourier transform. Now the quadratic fields can be integrated out by first Fourier transforming the quadratic part of the action,

$$e^{-S_{eff}} = \int \mathcal{D}\theta \mathcal{D}\lambda \exp \left(-\frac{1}{2\pi K\nu} \int \frac{d\omega dq}{4\pi^2} (\omega^2 + \nu^2 q^2) |\theta(q, \omega)|^2 + i \int d\tau \lambda(\tau) [\theta_0(\tau) - \theta(x=0, \tau)] \right). \quad (\text{E.3})$$

All these calculations will be at zero temperature to make calculations easier but can be generalised to finite temperatures by using Matsubara sums. The θ functional integral can be performed after taking the Fourier transform of the Lagrange multiplier term,

$$\begin{aligned} e^{-S_{eff}} &= \int \mathcal{D}\theta \mathcal{D}\lambda \exp \left(-\frac{1}{2\pi K\nu} \int \frac{d\omega dq}{4\pi^2} (\omega^2 + \nu^2 q^2) |\theta(q, \omega)|^2 \right. \\ &\quad \left. + i \int \frac{d\omega}{2\pi} \lambda(\omega) \left[\theta_0(-\omega) - \int \frac{dq}{2\pi} \theta(q, -\omega) \right] \right) \\ &= A \int \mathcal{D}\lambda \exp \left(-\frac{1}{4} \int \frac{dq d\omega}{4\pi^2} \frac{K\pi\nu\lambda(\omega)\lambda(-\omega)}{\omega^2 + \nu^2 q^2} + i \int \frac{d\omega}{2\pi} \lambda(\omega) \theta_0(-\omega) \right). \end{aligned}$$

Extra factors of $1/2$ are appearing as the functional integrals are complex and the $\lambda(\omega)\theta(-\omega)$ term is being split up into $\lambda(\omega)\theta(-\omega) + \lambda(-\omega)\theta(\omega)$. This gets it into the form of the usual functional integration, but at the cost of introducing a half.

The q integration in the first term can be performed. Finally the λ functional integral can be evaluated to give the effective action, where all quadratic fields have been integrated out,

$$\begin{aligned} e^{-S_{eff}} &= \int \mathcal{D}\lambda \exp \left(-\frac{1}{4} \int \frac{d\omega}{2\pi} \frac{K\pi}{2|\omega|} \lambda(\omega)\lambda(-\omega) + i \int \frac{d\omega}{2\pi} \lambda(\omega) \theta_0(-\omega) \right) \\ &= \exp \left(-\frac{1}{8} \int \frac{d\omega}{2\pi} \frac{|\omega|}{K\pi} |\theta_0(\omega)|^2 \right). \end{aligned}$$

Combining this with the impurity term and redefining the fields, $2\theta_0 \rightarrow \theta$ give the action,

$$S = \frac{1}{32\pi} \int_{|\omega| < \Lambda} \frac{d\omega}{2\pi} \frac{|\omega|}{K} |\theta(\omega)|^2 + 2V_0 \int d\tau \cos(\theta(\tau)) , \quad (\text{E.4})$$

where an ultraviolet cutoff corresponding to bandwidth has been included to prevent divergences. As a small note, inserting this bandwidth means that the bosonisation form with the cutoff should have been used throughout this calculation. However, this amounts to the introduction of some factors of $\sqrt{2\pi\alpha}$ which can be absorbed into definitions of K and V_0 .

Following the procedure outlined in Appendix D, the fields are split into slow and fast modes $\theta(\tau) = \theta_f(\tau) + \theta_s(\tau)$ with fast modes being defined as the modes that lie between $\Lambda/b < |\omega| < \Lambda$. As the quadratic part of the integral is already expressed in the frequency basis, it can simply be split into slow and fast modes by having two terms with the integral limits 0 to Λ' and Λ' to Λ . The mixed term of this problem arises from the cosine term, so this is the average that needs to be considered

$$\langle S_{mixed} \rangle_f = 2V_0 \langle \cos(2\theta_s + 2\theta_f) \rangle_f = V_0 (e^{2i\theta_s} \langle e^{2i\theta_f} \rangle_f + e^{-2i\theta_s} \langle e^{-2i\theta_f} \rangle_f) . \quad (\text{E.5})$$

Performing this average is possible when armed with the following identity,

$$\langle e^{i\theta} \rangle = e^{-\frac{1}{2}\langle \theta^2 \rangle} , \quad (\text{E.6})$$

which results in the average becoming,

$$\langle S_{mixed} \rangle_f = 2V_0 \cos(\theta_s(x=0, \tau)) e^{-2\langle \theta_f(x=0, \tau)^2 \rangle_f} . \quad (\text{E.7})$$

The average of $\theta(\tau)^2$ defines the Green's function of the action evaluated at the same point. The average is over the quadratic part of the action which is invariant over space, therefore it does not matter where it is evaluated. There is no issue with the diverging nature of the Green's function as the average is over an infinitesimal slice of ω . The average of the Green's function is evaluated in frequency and momentum space by translating the limits on the energy integral to be on the momentum integral.

APPENDIX E. RG CALCULATIONS

This avoids doing a more difficult integral. This gives,

$$\langle \theta_f^2(x, \tau) \rangle_f = \int_{\Lambda'/\nu}^{\Lambda/\nu} \frac{dq}{2\pi} \int \frac{d\omega}{2\pi} \frac{\pi\nu K}{\omega^2 + \nu^2 q^2} e^{i\omega\tau} = \frac{K}{2} \ln\left(\frac{\Lambda}{\Lambda'}\right). \quad (\text{E.8})$$

Putting this all back into the original action results in,

$$S = \frac{1}{32\pi} \int_{|\omega| < \Lambda'} d\omega \frac{|\omega|}{K} |\theta_s(\omega)|^2 + 2V_0 e^{K \ln(\Lambda/\Lambda')} \int d\tau \cos(\theta_s(\tau)). \quad (\text{E.9})$$

This has the same form as our original action in Equation E.4, up to the integration limits in the first term and a multiplicative factor in the second term. To bring the original cutoff to same value, the energy is rescaled by $\omega' = b\omega$ and correspondingly $\tau' = \tau/b$. As our interest is in how the impurity term changes, we elect to leave the cosine term to be invariant under this transformation by rescaling the fields by $\theta'(\tau') = \theta(\tau)$ which enforces that $\theta'(\omega') = \theta(\omega)/b$. The action after performing one iteration of the RG is therefore,

$$S = \frac{1}{8\pi^2} \int_{|\omega| < \Lambda} d\omega \frac{|\omega|}{K} |\theta(\omega)|^2 + V_0 b^{1-K} \int d\tau \cos(\theta(\tau)). \quad (\text{E.10})$$

Comparing this to the original action, the RG flow equation for the impurity strength is

$$V(b) = b^{1-K} V_0. \quad (\text{E.11})$$

E.2 Weak Link

The opposite limit to a small barrier is a weak link between two separated Luttinger liquids. Hopping between the systems now becomes the small parameter in our RG calculations. Two separate Luttinger liquids can be described by having a term of the form $\delta(\theta(x=0, \tau))$ essentially ensuring that there are no particles at $x=0$ as $\partial_x \theta$ is the density. The phase ϕ over this disconnect will be continuous so the dual action is used instead,

$$S_L = \frac{K}{2\pi\nu} \int_{-\infty}^0 dx \int d\tau \left((\partial_\tau \phi_1)^2 - v^2 (\partial_x \phi_1)^2 \right) + \frac{K}{2\pi\nu} \int_0^\infty dx \int d\tau \left((\partial_\tau \phi_2)^2 + v^2 (\partial_x \phi_2)^2 \right), \quad (\text{E.12})$$

where $\phi_1(x) = \phi(x < 0)$, $\phi_2(x) = \phi(x > 0)$. To get things moving between the two wires, a hopping term is introduced,

$$\delta H = -t(\psi_L^\dagger(x=0)\psi_R(x=0) + h.c.). \quad (\text{E.13})$$

When bosonising this term, we can use the fact that the density field will be pinned at $x = 0$ due to the discontinuity. Therefore instead of $\psi_\eta = e^{i(\phi-\eta\theta)}$, the θ field can be completely ignored to give $e^{i\phi}$. Using this for each respective side, the hopping term becomes,

$$S = -2t \int dx d\tau \cos(\phi_1(x=0,\tau) - \phi_2(x=0,\tau)). \quad (\text{E.14})$$

The argument of the cosine term does not match up to the action, therefore a rotation to new fields are needed. This can be done with,

$$\tilde{\phi}_1 = \frac{1}{2\sqrt{2}}(\phi_1 + \phi_2), \quad \tilde{\phi}_2 = \frac{1}{2\sqrt{2}}(\phi_2 - \phi_1), \quad (\text{E.15})$$

where the cross terms $\tilde{\phi}_1\tilde{\phi}_2$ in the new action will cancel out. The new action is,

$$S = \frac{4K}{\pi\nu} \int dx d\tau (\partial_\tau \tilde{\phi}_1)^2 + \nu^2 (\partial_x \tilde{\phi}_1)^2 \quad (\text{E.16})$$

$$+ \frac{4K}{\pi\nu} \int dx d\tau (\partial_\tau \tilde{\phi}_2)^2 + \nu^2 (\partial_x \tilde{\phi}_2)^2 - 2t \int dx d\tau \cos(2\sqrt{2}\phi_2). \quad (\text{E.17})$$

Only $\tilde{\phi}_2$ needs to be considered as the other field is the usual term. The remaining action is simply the dual of Equation E.2, where $\theta \rightarrow \tilde{\phi}$ and $K \rightarrow 1/K$. The result of the weak impurity in Equation E.11 can therefore be transformed to its dual to solve the weak tunnelling problem,

$$t = b^{1-\frac{1}{K}} t_0. \quad (\text{E.18})$$

Although the use of the dual mapping seems like cheating, it can be shown by employing the exact same process as earlier that the same result is achieved.

E.3 Global Sine-Gordon

When the cosine term is not local, the analysis is actually a lot simpler because the effective action for the integrated out fields is not needed. Using the spin sector of the spinful Luttinger liquid as a prototypical case,

$$S_\sigma = \frac{1}{2\pi\nu_\sigma K_\sigma} \int dx d\tau (\partial_t \theta_\sigma)^2 + \nu_\sigma^2 (\partial_x \theta_\sigma)^2 + \int dx dt 2g_{1\perp} \cos(2\sqrt{2}\theta_\sigma). \quad (\text{E.19})$$

The RG calculation can be started straight away. Equation E.7 is obtained in the exact same way except the average for the full Green's function is found rather than at a specific point,

$$\langle S_{mixed} \rangle_f = 2g_{1\perp} \cos(\theta_s(x, \tau)) e^{-4\langle \theta_f(x, \tau)^2 \rangle_f}. \quad (\text{E.20})$$

where the $2\sqrt{2}$ factor in the cosine results in the factor of 4 instead of 1/2. Equation E.8 describes the average over the fast modes again. The rescaling of the slow modes of the field now have to occur for both energy and momentum, which results in a factor of 2 cropping up. This results in an RG equation of,

$$g = g_{1\perp}(2 - 2K_\sigma). \quad (\text{E.21})$$

When the cosine term has a combination of different θ fields, the RG equation for that can be found by relating the Luttinger parameters and performing a rotation to the new ones, much like in the analysis of the weak link case. For the Shavit and Oreg paper, the action is,

$$S = S_\rho[\theta_\rho] + S_\sigma[\theta_\sigma] + 2\lambda \int dx d\tau \cos(\sqrt{2}(n-m)\theta_\rho + \sqrt{2}(n+m)\theta_\sigma), \quad (\text{E.22})$$

where the rotation of the original chiral fields is performed by using Equation 6.38.

The average over the mixed term now contains and average over the fast modes of θ_ρ and θ_σ . In this case,

$$\begin{aligned} \langle S_{mixed}[\theta_\rho, \theta_\sigma] \rangle_f &= e^{-\sqrt{2}i(n-m)\theta_\rho^s + \sqrt{2}i\theta_\sigma^s(n+m)} \left\langle e^{\sqrt{2}i(n-m)\theta_\rho^f} \right\rangle_{S_\rho^f} \left\langle e^{\sqrt{2}i(n+m)\theta_\rho^f} \right\rangle_{S_\sigma^f} + \text{h.c.} \\ &= 2 \cos(\sqrt{2}(n-m)\theta_\rho^s + \sqrt{2}(n+m)\theta_\sigma^s) e^{-\frac{K_\rho}{2}(n-m)^2 \ln(\Lambda/\Lambda')} e^{-\frac{K_\sigma}{2}(n+m)^2 \ln(\Lambda/\Lambda')}. \end{aligned} \quad (\text{E.23})$$

APPENDIX F

FINITE CALCULATIONS

F.1 Finding the $Q = -1/2$ Eigenstates

To expand on the process by which the $Q = -1/2$ eigenstates are found, we start with the matrix of wavefunctions on the square lattice for $L_S = 5$,

$$\psi = \begin{bmatrix} \psi_{11} & \psi_{12} & \psi_{13} & \psi_{14} & \psi_{15} & \psi_{16} \\ \psi_{21} & \psi_{22} & \psi_{23} & \psi_{24} & \psi_{25} & \psi_{26} \\ \psi_{31} & \psi_{32} & \psi_{33} & \psi_{34} & \psi_{35} & \psi_{36} \\ \psi_{41} & \psi_{42} & \psi_{43} & \psi_{44} & \psi_{45} & \psi_{46} \\ \psi_{51} & \psi_{52} & \psi_{53} & \psi_{54} & \psi_{55} & \psi_{56} \\ \psi_{61} & \psi_{62} & \psi_{63} & \psi_{64} & \psi_{65} & \psi_{66} \end{bmatrix}. \quad (\text{F.1})$$

The generic square lattice hopping problem is described by,

$$H\psi_{xy} = -t(\psi_{x+1y} + \psi_{x-1y} + \psi_{xy+1} + \psi_{xy-1}), \quad \psi_{0y} = \psi_{7y} = \psi_{x0} = \psi_{x7} = 0. \quad (\text{F.2})$$

The following wavefunctions can be seen to solve this equation,

$$\psi_{xy}^{(n,m)} = A \sin(k_x x) \sin(k_y y), \quad \epsilon^{(n,m)} = -2t(\cos(k_x) + \cos(k_y)) \quad (\text{F.3})$$

$$\text{where } k_x = \frac{\pi n}{D+1}, k_y = \frac{\pi m}{D+1}, \quad \text{for } n, m \in \{1, 2, \dots, D\},$$

APPENDIX F. FINITE CALCULATIONS

where D corresponds to the size of the finite 2D square lattice which is one site longer than the soliton chain, $L_S + 1 = D$. There must be $D \times D$ eigenvalues, as we are in a $D \times D$ size vector space. We can form a matrix of the different eigenvectors, which themselves are matrices,

$$\Psi = \begin{bmatrix} \psi^{(1,1)} & \psi^{(1,2)} & \psi^{(1,3)} & \psi^{(1,4)} & \psi^{(1,5)} & \psi^{(1,6)} \\ \psi^{(2,1)} & \psi^{(2,2)} & \psi^{(2,3)} & \psi^{(2,4)} & \psi^{(2,5)} & \psi^{(2,6)} \\ \psi^{(3,1)} & \psi^{(3,2)} & \psi^{(3,3)} & \psi^{(3,4)} & \psi^{(3,5)} & \psi^{(3,6)} \\ \psi^{(4,1)} & \psi^{(4,2)} & \psi^{(4,3)} & \psi^{(4,4)} & \psi^{(4,5)} & \psi^{(4,6)} \\ \psi^{(5,1)} & \psi^{(5,2)} & \psi^{(5,3)} & \psi^{(5,4)} & \psi^{(5,5)} & \psi^{(5,6)} \\ \psi^{(6,1)} & \psi^{(6,2)} & \psi^{(6,3)} & \psi^{(6,4)} & \psi^{(6,5)} & \psi^{(6,6)} \end{bmatrix}. \quad (\text{F.4})$$

This may seem like a redundant step but the reason for doing this is to re-express the antisymmetrisation of the position indices in terms of the eigenstates. This antisymmetrisation is given by,

$$\phi_{xy}^{(n,m)} = \psi_{xy}^{(n,m)} - \psi_{yx}^{(n,m)}. \quad (\text{F.5})$$

The explicit form of $\psi_{xy}^{(n,m)}$ in Equation F.3 can be seen to have a symmetry upon the interchange of $x \leftrightarrow y$ and $n \leftrightarrow m$. The antisymmetrised solutions can now be expressed as $\phi_{xy}^{(n,m)} = \psi_{xy}^{(n,m)} - \psi_{xy}^{(m,n)}$.

This will cause the diagonals in n, m to be zero,

$$\Phi = \begin{bmatrix} \phi^{(1,1)} & \phi^{(1,2)} & \phi^{(1,3)} & \phi^{(1,4)} & \phi^{(1,5)} & \phi^{(1,6)} \\ \phi^{(2,1)} & \phi^{(2,2)} & \phi^{(2,3)} & \phi^{(2,4)} & \phi^{(2,5)} & \phi^{(2,6)} \\ \phi^{(3,1)} & \phi^{(3,2)} & \phi^{(3,3)} & \phi^{(3,4)} & \phi^{(3,5)} & \phi^{(3,6)} \\ \phi^{(4,1)} & \phi^{(4,2)} & \phi^{(4,3)} & \phi^{(4,4)} & \phi^{(4,5)} & \phi^{(4,6)} \\ \phi^{(5,1)} & \phi^{(5,2)} & \phi^{(5,3)} & \phi^{(5,4)} & \phi^{(5,5)} & \phi^{(5,6)} \\ \phi^{(6,1)} & \phi^{(6,2)} & \phi^{(6,3)} & \phi^{(6,4)} & \phi^{(6,5)} & \phi^{(6,6)} \end{bmatrix} = \begin{bmatrix} 0 & \phi^{(1,2)} & \phi^{(1,3)} & \phi^{(1,4)} & \phi^{(1,5)} & \phi^{(1,6)} \\ \phi^{(2,1)} & 0 & \phi^{(2,3)} & \phi^{(2,4)} & \phi^{(2,5)} & \phi^{(2,6)} \\ \phi^{(3,1)} & \phi^{(3,2)} & 0 & \phi^{(3,4)} & \phi^{(3,5)} & \phi^{(3,6)} \\ \phi^{(4,1)} & \phi^{(4,2)} & \phi^{(4,3)} & 0 & \phi^{(4,5)} & \phi^{(4,6)} \\ \phi^{(5,1)} & \phi^{(5,2)} & \phi^{(5,3)} & \phi^{(5,4)} & 0 & \phi^{(5,6)} \\ \phi^{(6,1)} & \phi^{(6,2)} & \phi^{(6,3)} & \phi^{(6,4)} & \phi^{(6,5)} & 0 \end{bmatrix}. \quad (\text{F.6})$$

Using the same symmetry of the square lattice solutions, the off-diagonal solutions can be shown to be related, $\phi_{xy}^{(n,m)} = -\phi_{xy}^{(m,n)}$. This means that there are $5 \times 4 \times \dots \times 1$ independent eigenvectors. This is exactly the size of the state space of our restricted problem. Therefore choosing the side where $n < m$, gives the solutions in the main text in Equation 7.15.

F.2 Green's Function Simplifications

Having obtained a description of the eigenfunctions, the Green's function can be calculated in certain limits such that only some of the n particle subspaces need to be taken into account. The other subspaces will be exponentially suppressed in the summation. From the Lehmann representation where n, m are full eigenstates of the system,

$$\mathcal{G}_{ij}(\omega) = \frac{1}{Z} \sum_{n,m} \left(e^{-\beta(\epsilon_n - \mu n_e)} + e^{-\beta(\epsilon_m - \mu m_e)} \right) \frac{\langle n | c_j^\dagger | m \rangle \langle m | c_i | n \rangle}{\omega + \epsilon_m - \epsilon_n + i\eta}. \quad (\text{F.7})$$

The total fermions in the system is a good quantum number as the uncoupled Green's function is for the isolated system. Therefore the eigenstates can be split up into the n_e particle subspaces and the q_{n_e} eigenstates in that subspace, $|n_e, q_{n_e}\rangle$ where each subspace will have a different dimension. These eigenstates will have an energy $\epsilon_{q_{n_e}}$. The summation in the Green's function can be split into these parts, where n must be in the subspace with one extra particle than m ,

$$\begin{aligned} \mathcal{G}_{ij}(\omega) = & \frac{1}{Z} \left(\sum_{q_M, q_{M-1}} \frac{e^{-\beta(\epsilon_{q_M} - \mu M)} + e^{-\beta(\epsilon_{q_{M-1}} - \mu(M-1))}}{\omega - \epsilon_{q_{M-1}} + \epsilon_{q_M} + i\eta} A_{ij}(q_M, q_{M-1}) \right. \\ & \left. + \sum_{q_{M-1}, q_{M-2}} \frac{e^{-\beta(\epsilon_{q_{M-1}} - \mu(M-1))} + e^{-\beta(\epsilon_{q_{M-2}} - \mu(M-2))}}{\omega - \epsilon_{q_{M-2}} + \epsilon_{q_{M-1}} + i\eta} A_{ij}(q_{M-1}, q_{M-2}) + \dots \right), \end{aligned} \quad (\text{F.8})$$

where $M = L_S$ is largest number of fermions that the system can have in the projected subspace and

$$A_{ij}(q_N, q_{N-1}) = \langle N, q_N | c_j^\dagger | N-1, q_{N-1} \rangle \langle N-1, q_{N-1} | c_i | N, q_N \rangle. \quad (\text{F.9})$$

Upon factorising $e^{\beta\mu M}$, all terms apart from the frozen state will depend on higher orders of $e^{-\beta\mu}$ which for large μ and low temperatures will exponentially decay. In the spinless case, there is only one possible frozen state for the M fermion subspace, denoted q^* , which will have zero energy. Therefore the sum over these states can be dropped.

Now consider what happens when μ is reduced such that the filling below the $Q = 1/2$ frozen state is energetically accessible. The minima of the $Q = -1/2$ state is denoted ϵ_0 , which occurs at k^* . This value was found to be negative earlier as the system gains energy when hybridising the solitons in the

APPENDIX F. FINITE CALCULATIONS

$Q = -1/2$ state. Before setting $\mu = -\epsilon_0$, consider the previous expansion,

$$\begin{aligned}\mathcal{G}_{ij}(\omega) &= \frac{e^{\beta\mu M}}{\mathcal{Z}} \left(\sum_{q_{M-1}} \frac{1 + e^{-\beta(\epsilon_{q_{M-1}} + \mu)}}{\omega + \epsilon_{q^*} - \epsilon_{q_{M-1}} + i\eta} A_{ij}(q^*, q_{M-1}) \right. \\ &\quad \left. + e^{-\beta\mu} \sum_{q_{M-1}, q_{M-2}} \frac{e^{-\beta\epsilon_{q_{M-1}}} + e^{-\beta(\epsilon_{q_{M-2}} + \mu)}}{\omega + \epsilon_{q_{M-1}} - \epsilon_{q_{M-2}} + i\eta} A_{ij}(q_{M-1}, q_{M-2}) + \dots \right).\end{aligned}\quad (\text{F.10})$$

Taking $\mu = -\epsilon_0$ results in the other states becoming exponentially suppressed if $|\epsilon_1| < 2|\epsilon_0|$, with ϵ_1 being the minima of the $Q = -3/2$ state. This condition can be numerically shown to be satisfied. This agrees with intuition as, although there are more states to hybridise with in a lower filling, the band will not double in size. This now means that any term that contains $\epsilon_{q_{M-2}}$ or higher orders can be discarded. The next simplification is to consider other states in the q_{M-1} subspace. If the distance between successive eigenvalues is δ , the state above ϵ_0 will be given by $\epsilon_0 + \delta$. Terms in the sum over all q_{M-1} , will have the form $e^{-\beta(\epsilon_0 + \delta + \mu)}$. Assuming that $e^{-\beta\delta}$ is small, any higher-energy states in the $Q = -1/2$ will be zero due to the rapid decaying of the exponential.

Putting together those simplifications, the Green's function becomes,

$$\mathcal{G}_{ij}(\omega) = \frac{e^{\beta\mu M}}{\mathcal{Z}} \left(\frac{2A_{ij}(q^*, k^*)}{\omega - \epsilon_0 + i\eta} + \sum_{q_{M-1} \neq k^*} \frac{A_{ij}(q^*, q_{M-1})}{\omega - \epsilon_{q_{M-1}} + i\eta} + \sum_{q_{M-2}} \frac{B_{k^*, q_{M-2}}}{\omega + \epsilon_0 - \epsilon_{q_{M-2}} + i\eta} \right). \quad (\text{F.11})$$

This can be simplified further by ignoring the summation over the $M-2, M-1$ fermion subspaces, which will not be exponentially suppressed in the Green's function but correspond to peaks at further distances away from $\omega \sim \epsilon_0$. Currently because these are the uncoupled Green's functions, the peaks are all delta functions due to the infinitesimal η . However, upon including the coupling to the leads Γ , each term obtains a finite imaginary width. This on its own is not enough to justify ignoring these terms, but the fact that the conductance is given by the square of the Green's function evaluated at the chemical potential means that peaks far away from the chemical potential will not affect behaviour.

The width of the peaks is given by Γ and the spacing between them is δ , so if $\Gamma \ll \delta$ then each peak will not affect the other. The remaining sums in Equation F.11 will pick up a factor of Γ^2/δ^2 and can therefore be ignored. The starting point of calculation in Chapter 7.1.3 is obtained by remembering that the temperature delta function in the conductance means that only one peak will contribute if the peaks are well separated.

BIBLIOGRAPHY

- [1] D. Laws. 13 sextillion & counting: the long & winding road to the most frequently manufactured human artifact in history. *CHM Blogs*, accessed on 08/09/2022.
- [2] R. Sender, S. Fuchs, and R. Milo. Revised estimates for the number of human and bacteria cells in the body. *PLoS Biology*, 14(8):e1002533, 2016.
- [3] N.W. Ashcroft and N.D. Mermin. *Solid State Physics*. Saunders College Publishing, 1976.
- [4] H. Bruus and K. Flensberg. *Many-body quantum theory in condensed matter physics: an introduction*. Oxford University Press, 2004.
- [5] D. Ferry and S. M. Goodnick. *Transport in nanostructures*. Cambridge University Press, 1999.
- [6] Y. Imry. *Introduction to mesoscopic physics*. Oxford University Press, 2002.
- [7] S. Datta. *Electronic transport in mesoscopic systems*. Cambridge University Press, 1997.
- [8] T. Ihn. Diffusive quantum transport. In *Semiconductor Nanostructures: Quantum states and electronic transport*. Oxford University Press, 2009.
- [9] K.-F. Berggren, T. J. Thornton, D. J. Newson, and M. Pepper. Magnetic depopulation of 1D subbands in a narrow 2D electron gas in a GaAs:AlGaAs heterojunction. *Physical Review Letters*, 57:1769–1772, 1986.
- [10] L. Pfeiffer and K.W. West. The role of MBE in recent quantum Hall effect physics discoveries. *Physica E: Low-dimensional Systems and Nanostructures*, 20(1):57–64, 2003.
- [11] T. Ando, A. B. Fowler, and F. Stern. Electronic properties of two-dimensional systems. *Reviews of Modern Physics*, 54:437–672, 1982.
- [12] C. P. Umbach, C. Van Haesendonck, R. B. Laibowitz, S. Washburn, and R. A. Webb. Direct observation of ensemble averaging of the Aharonov-Bohm effect in normal-metal loops. *Physical Review Letters*, 56:386–389, 1986.
- [13] H. van Houten, B. J. van Wees, and C. W. J. Beenakker. Quantum and classical ballistic transport in constricted two-dimensional electron gases. In H. Heinrich, G. Bauer, and F. Kuchar, editors, *Physics and Technology of Submicron Structures*, pages 198–207. Springer Berlin Heidelberg, 1988.
- [14] H. Van Houten and C.W.J. Beenakker. Quantum point contacts. *Physics Today*, 49(7), 1996.
- [15] B. J. van Wees, H. van Houten, C. W. J. Beenakker, J. G. Williamson, L. P. Kouwenhoven, D. van der Marel, and C. T. Foxon. Quantized conductance of point contacts in a two-dimensional electron gas. *Physical Review Letters*, 60:848–850, 1988.

BIBLIOGRAPHY

- [16] S. Kumar, M. Pepper, H. Montagu, D. Ritchie, I. Farrer, J. Griffiths, and G. Jones. Engineering electron wavefunctions in asymmetrically confined quasi one-dimensional structures. *Applied Physics Letters*, 118(12):124002, 2021.
- [17] S. Kumar and M. Pepper. Interactions and non-magnetic fractional quantization in one-dimension. *Applied Physics Letters*, 119(11):110502, 2021.
- [18] S. Kumar, M. Pepper, S. N. Holmes, H. Montagu, Y. Gul, D. A. Ritchie, and I. Farrer. Zero-magnetic field fractional quantum states. *Physical Review Letters*, 122:086803, 2019.
- [19] Y. Gul, S.N. Holmes, M. Myronov, S. Kumar, and M. Pepper. Self-organised fractional quantisation in a hole quantum wire. *Journal of Physics: Condensed Matter*, 30(9):09LT01, 2018.
- [20] D. C. Tsui, H. L. Stormer, and A. C. Gossard. Two-dimensional magnetotransport in the extreme quantum limit. *Physical Review Letters*, 48:1559–1562, 1982.
- [21] R. B. Laughlin. Anomalous quantum Hall effect: An incompressible quantum fluid with fractionally charged excitations. *Physical Review Letters*, 50:1395–1398, 1983.
- [22] R. L. Willett. The quantum Hall effect at 5/2 filling factor. *Reports on Progress in Physics*, 76(7):076501, 2013.
- [23] A.P. Micolich. What lurks below the last plateau: experimental studies of the $0.7 \times 2e2/h$ conductance anomaly in one-dimensional systems. *Journal of Physics: Condensed Matter*, 23(44):443201, 2011.
- [24] G. D. Mahan. *Many-particle physics*. Plenum Press New York, 1981.
- [25] J. Rammer. *Quantum Field Theory of Non-equilibrium States*. Cambridge University Press, 2007.
- [26] M. Gell-Mann and F. Low. Bound states in quantum field theory. *Physical Review*, 84:350–354, 1951.
- [27] M. E. Peskin and D.V. Schroeder. *An Introduction to quantum field theory*. Addison-Wesley, Reading, USA, 1995.
- [28] A. Altland and B. D. Simons. *Condensed matter field theory*. Cambridge University Press, 2010.
- [29] J. Rammer and H. Smith. Quantum field-theoretical methods in transport theory of metals. *Reviews of modern physics*, 58(2):323, 1986.
- [30] A.-P. Jauho, N. S. Wingreen, and Y. Meir. Time-dependent transport in interacting and noninteracting resonant-tunneling systems. *Physical Review B*, 50(8):5528, 1994.
- [31] M. Rother, W. Wegscheider, R.A. Deutschmann, M. Bichler, and G Abstreiter. Evidence of Luttinger liquid behavior in GaAs/AlGaAs quantum wires. *Physica E: Low-dimensional Systems and Nanostructures*, 6(1):551–554, 2000.
- [32] T. Giamarchi. *Quantum physics in one dimension*, volume 121. Clarendon Press, 2003.
- [33] S. Tomonaga. Remarks on Bloch's Method of Sound Waves applied to Many-Fermion Problems. *Progress of Theoretical Physics*, 5(4):544–569, 1950.
- [34] J. M. Luttinger. An exactly soluble model of a many-fermion system. *Journal of Mathematical Physics*, 4(9):1154–1162, 1963.

- [35] F. D. M. Haldane. 'Luttinger liquid theory' of one-dimensional quantum fluids. I. properties of the Luttinger model and their extension to the general 1D interacting spinless Fermi gas. *Journal of Physics C: Solid State Physics*, 14(19):2585–2609, 1981.
- [36] G. Gruner. *Density waves in solids*. CRC Press, 2018.
- [37] S.A. Kivelson. Electron fractionalization. *Synthetic Metals*, 125(1):99–106, 2001.
- [38] D.K.K. Lee and Y. Chen. Functional bosonisation of the Tomonaga-Luttinger model. *Journal of Physics A: Mathematical and General*, 21(22):4155–4171, November 1988.
- [39] J. Voit. One-dimensional Fermi liquids. *Reports on Progress in Physics*, 58(9):977–1116, 1995.
- [40] M. A. Cazalilla. Bosonizing one-dimensional cold atomic gases. *Journal of Physics B: Atomic, Molecular and Optical Physics*, 37(7):S1–S47, 2004.
- [41] J. von Delft and H. Schoeller. Bosonization for beginners - refermionization for experts. *Annalen der Physik*, 7(4):225–305, November 1998.
- [42] A. Grishin, I. V. Yurkevich, and I. V. Lerner. Functional integral bosonization for an impurity in a Luttinger liquid. *Physical Review B*, 69:165108, 2004.
- [43] R. Shankar. *Quantum Field Theory and Condensed Matter: An Introduction*. Cambridge University Press, 2017.
- [44] M. Bockrath, D. H. Cobden, J. Lu, A. G Rinzler, R. E. Smalley, L. Balents, and P. L. McEuen. Luttinger-liquid behaviour in carbon nanotubes. *Nature*, 397(6720):598–601, 1999.
- [45] C. Blumenstein, J. Schäfer, S. Mietke, S. Meyer, A. Dollinger, M. Lochner, X.Y. Cui, L. Patthey, R. Matzdorf, and R. Claessen. Atomically controlled quantum chains hosting a Tomonaga–Luttinger liquid. *Nature Physics*, 7(10):776–780, 2011.
- [46] A. M. Chang. Chiral Luttinger liquids at the fractional quantum Hall edge. *Reviews of Modern Physics*, 75:1449–1505, 2003.
- [47] R. Landauer. Spatial variation of currents and fields due to localized scatterers in metallic conduction. *IBM Journal of Research and Development*, 1(3):223–231, 1957.
- [48] J. Frenkel. On the electrical resistance of contacts between solid conductors. *Physical Review*, 36:1604–1618, 1930.
- [49] M. Di Ventra. *Electrical Transport in Nanoscale Systems*. Cambridge University Press, 2008.
- [50] R.I. Lesovik, L.I. Glazman, D.E. Khmelnitskii, and R. Shekhter. Reflectionless quantum transport and fundamental ballistic-resistance steps in microscopic constrictions. *Soviet Physics: JETP Letters*, 48:238–241, 1988.
- [51] M. Büttiker. Absence of backscattering in the quantum Hall effect in multiprobe conductors. *Physical Review B*, 38:9375–9389, 1988.
- [52] Y. Meir and N. S. Wingreen. Landauer formula for the current through an interacting electron region. *Physical Review Letters*, 68(16):2512, 1992.
- [53] N. S. Wingreen, A.-P. Jauho, and Y. Meir. Time-dependent transport through a mesoscopic structure. *Physical Review B*, 48:8487–8490, 1993.

BIBLIOGRAPHY

- [54] N. Sedlmayr, I.V. Yurkevich, and I. V. Lerner. Tunnelling density of states at Coulomb-blockade peaks. *EPL (Europhysics Letters)*, 76(1):109, 2006.
- [55] P. P. Aseev, D. Loss, and J. Klinovaja. Conductance of fractional Luttinger liquids at finite temperatures. *Physical Review B*, 98(4):045416, 2018.
- [56] V. Kagalovsky, I. V. Lerner, and I. V. Yurkevich. Local impurity in a multichannel Luttinger liquid. *Physical Review B*, 95(20):205122, 2017.
- [57] Y. Oreg, E. Sela, and A. Stern. Fractional helical liquids in quantum wires. *Physical Review B*, 89:115402, 2014.
- [58] G. Shavit and Y. Oreg. Fractional conductance in strongly interacting 1D systems. *Physical Review Letters*, 123:036803, 2019.
- [59] R. Shankar. Solvable model of a metal-insulator transition. *International Journal of Modern Physics B*, 04(15n16):2371–2394, 1990.
- [60] D. L. Maslov and M. Stone. Landauer conductance of Luttinger liquids with leads. *Physical Review B*, 52(8):R5539, 1995.
- [61] V. V. Ponomarenko. Renormalization of the one-dimensional conductance in the Luttinger-liquid model. *Physical Review B*, 52:R8666–R8667, 1995.
- [62] I. Safi and H. J. Schulz. Transport in an inhomogeneous interacting one-dimensional system. *Physical Review B*, 52:R17040–R17043, 1995.
- [63] A. Kawabata. On the renormalization of conductance in Tomonaga-Luttinger liquid. *Journal of the Physical Society of Japan*, 65(1):30–32, 1996.
- [64] R. Egger and H. Grabert. Electroneutrality and the Friedel sum rule in a Luttinger liquid. *Physical Review Letters*, 79(18):3463, 1997.
- [65] R. Egger and H. Grabert. Applying voltage sources to a Luttinger liquid with arbitrary transmission. *Physical Review B*, 58:10761–10768, 1998.
- [66] X. G. Wen. Chiral Luttinger liquid and the edge excitations in the fractional quantum Hall states. *Physical Review B*, 41:12838–12844, 1990.
- [67] M.P. A. Fisher and Leonid I. Glazman. Transport in a one-dimensional Luttinger liquid. In Lydia L. Sohn, Leo P. Kouwenhoven, and Gerd Schön, editors, *Mesoscopic Electron Transport*, pages 331–373. Springer Netherlands, Dordrecht, 1997.
- [68] C. L. Kane and Matthew P. A. Fisher. Contacts and edge-state equilibration in the fractional quantum Hall effect. *Physical Review B*, 52:17393–17405, 1995.
- [69] C. Chamon and E. Fradkin. Distinct universal conductances in tunneling to quantum Hall states: The role of contacts. *Physical Review B*, 56:2012–2025, 1997.
- [70] J. M. Leinaas, M. Horsdal, and T. H. Hansson. Sharp fractional charges in Luttinger liquids. *Physical Review B*, 80:115327, 2009.
- [71] C. L. Kane and M. P. A. Fisher. Transmission through barriers and resonant tunneling in an interacting one-dimensional electron gas. *Physical Review B*, 46:15233–15262, 1992.

- [72] A. Furusaki and N. Nagaosa. Tunneling through a barrier in a Tomonaga-Luttinger liquid connected to reservoirs. *Physical Review B*, 54:R5239–R5242, 1996.
- [73] E. Cornfeld, I. Neder, and E. Sela. Fractional shot noise in partially gapped Tomonaga-Luttinger liquids. *Physical Review B*, 91:115427, 2015.
- [74] J. Klinovaja and D. Loss. Giant spin-orbit interaction due to rotating magnetic fields in graphene nanoribbons. *Physical Review X*, 3:011008, 2013.
- [75] P. P. Aseev, J. Klinovaja, and D. Loss. Finite-temperature conductance of strongly interacting quantum wire with a nuclear spin order. *Physical Review B*, 95:125440, 2017.
- [76] B. Braunecker, P. Simon, and D. Loss. Nuclear magnetism and electron order in interacting one-dimensional conductors. *Physical Review B*, 80:165119, 2009.
- [77] T. Meng, L. Fritz, D. Schuricht, and D. Loss. Low-energy properties of fractional helical Luttinger liquids. *Physical Review B*, 89:045111, 2014.
- [78] C.-H. Hsu, F. Ronetti, P. Stano, J. Klinovaja, and D. Loss. Universal conductance dips and fractional excitations in a two-subband quantum wire. *Physical Review Research*, 2:043208, 2020.
- [79] A. Luther and V. J. Emery. Backward scattering in the one-dimensional electron gas. *Physical Review Letters*, 33:589–592, 1974.
- [80] I.V. Krive and A.S. Rozhavskii. Fractional charge in quantum field theory and solid-state physics. *Soviet Physics Uspekhi*, 30(5):370, 1987.
- [81] R. Jackiw and C. Rebbi. Solitons with fermion number $\frac{1}{2}$. *Physical Review D*, 13:3398–3409, 1976.
- [82] R. Rajaraman. Solitons and instantons - an introduction to solitons and instantons in quantum field theory., 1987.
- [83] W. P. Su, J. R. Schrieffer, and A. J. Heeger. Solitons in polyacetylene. *Physical Review Letters*, 42:1698–1701, 1979.
- [84] J. Goldstone and F. Wilczek. Fractional quantum numbers on solitons. *Physical Review Letters*, 47:986–989, 1981.
- [85] V. V. Ponomarenko and N. Nagaosa. Fractional charge in transport through a 1d correlated insulator of finite length. *Physical Review Letters*, 83:1822–1825, 1999.
- [86] I. V. Krive, A. S. Rozhavsky, E. R. Mucciolo, and L. E. Oxman. Electron transport through a mesoscopic metal-CDW-metal junction. *Physical Review B*, 61:12835–12841, 2000.
- [87] S. T. Carr, B. N. Narozhny, and A. A. Nersesyan. Spinful fermionic ladders at incommensurate filling: Phase diagram, local perturbations, and ionic potentials. *Annals of Physics*, 339:22–80, 2013.
- [88] Y. V. Nazarov and Y. M. Blanter. *Quantum Transport: Introduction to Nanoscience*. Cambridge University Press, 2009.
- [89] I. Shapir, A. Hamo, S. Pecker, C. P. Moca, Ö. Legeza, G. Zarand, and S. Ilani. Imaging the electronic Wigner crystal in one dimension. *Science*, 364(6443):870–875, 2019.

BIBLIOGRAPHY

- [90] N. T. Ziani, F. Cavaliere, K. G. Becerra, and M. Sassetti. A short review of one-dimensional Wigner crystallization. *Crystals*, 11(1), 2021.
- [91] J. S. Meyer, K. A. Matveev, and A. I. Larkin. Transition from a one-dimensional to a quasi-one-dimensional state in interacting quantum wires. *Physical review letters*, 98(12):126404, 2007.
- [92] J.S. Meyer and K.A Matveev. Wigner crystal physics in quantum wires. *Journal of Physics: Condensed Matter*, 21(2):023203, 2008.
- [93] W. K. Hew, K. J. Thomas, M. Pepper, I. Farrer, D. Anderson, G. A. C. Jones, and D. A. Ritchie. Incipient formation of an electron lattice in a weakly confined quantum wire. *Physical Review Letters*, 102:056804, 2009.
- [94] S.-C. Ho, H.-J. Chang, C.-H. Chang, S.-T. Lo, G Creeth, S Kumar, I Farrer, D Ritchie, J Griffiths, G Jones, M Pepper, and T.-M. Chen. Imaging the zigzag Wigner crystal in confinement-tunable quantum wires. *Physical Review Letters*, 121:106801, 2018.
- [95] Y. Weiss, M. Goldstein, and R. Berkovits. Finite doping of a one-dimensional charge density wave: Solitons vs Luttinger liquid charge density. *Physical Review B*, 77(20):205128, 2008.
- [96] A.-M. Visuri, P. Törmä, and T. Giamarchi. Impurity and soliton dynamics in a Fermi gas with nearest-neighbor interactions. *Physical Review A*, 95(6):063605, 2017.
- [97] D.E. Feldman and B.I. Halperin. Fractional charge and fractional statistics in the quantum Hall effects. *Reports on Progress in Physics*, 84(7):076501, 2021.
- [98] James Nakamura, Shuang Liang, Geoffrey C Gardner, and Michael J Manfra. Direct observation of anyonic braiding statistics. *Nature Physics*, 16(9):931–936, 2020.
- [99] T. Lancaster and S. J. Blundell. *Quantum Field Theory for the Gifted Amateur*. Oxford University Press, 2014.
- [100] J. Cardy. *Scaling and renormalization in statistical physics*, volume 5. Cambridge University Press, 1996.